A Meta-analysis Informed Investigation into the Quantification of the NAD Metabolome in Mammalian Tissues

Dassine Azouaoui

A thesis submitted in partial fulfillment of the requirements for the master's degree in biochemistry

Supervisor: Dr. Keir Menzies

Department of Biochemistry, Microbiology and Immunology
Faculty of Medicine
University of Ottawa

Abstract

This study investigates the *in vivo* effect of nicotinamide riboside (NR), a nicotinamide adenine dinucleotide (NAD) precursor, on the NAD metabolome of mouse tissues. In order to build a strong basis for this work, pre-analytical and analytical procedures used to measure NAD-related metabolites were examined and an LC-MS-based method was developed to study the NAD metabolome. The meta-analysis of published NAD(P)(H) quantification results from rodents and humans showed important discrepancies between studies regardless of the quantification method. Thereafter, a targeted NAD metabolomics protocol, including the preparation of yeast-derived stable isotope internal controls, was developed and used to confirm that NR oral supplementation increased the concentrations of most NAD-related metabolites in mouse liver and skeletal muscle with an important accumulation of degradation metabolites. Ultimately, this study provides new insight into the kinetics of oral NR supplementation and highlights the need for standardization in NAD quantification methods.

Keywords: nicotinamide adenine dinucleotide, NAD^+, nicotinamide riboside, metabolism, quantification methods, metabolomics, LC-MS.

Acknowledgements

First and foremost, I would like to express my sincerest gratitude to my supervisor, Dr. Keir Menzies. Thank you for giving me the opportunity to join your lab and believing in me at every step of my master's program. I could not have undertaken this journey without your endless support and constant encouragement. I am extremely grateful for your invaluable guidance throughout this research.

I would like to extend my sincere thanks to my thesis advisor committee members: Dr. Julie St-Pierre and Dr. Michael De Lisio for their support and insightful comments. Additionally, this endeavor would not have been possible without the generous financial support from the Metabolomics Advanced Training and International Exchange Program (MATRIX) funded by the Collaborative Research and Training Experience (CREATE) from the Natural Sciences and Engineering Research Council of Canada (NSERC).

I would also like to express my deepest gratitude to all my colleagues from the Menzies lab in particular Dr. Alex Green, as well as my collaborators from the Metabolomics Core facility, Dr. David Patten and Dr. Shama Naz, the McGill Goodman Cancer Research Center Metabolomics Core, the MATRIX program, the Slack lab, and the Baetz lab. Thanks should also go to the uOttawa librarians, Animal Care and Veterinary Service (ACVS) staff, and the Graduate and Postdoctoral Studies Office (GradMed) employees who have always been a great support.

Lastly, I'd like to acknowledge my family and friends for their moral support and encouragement. I would also like to thank my son, who has given me the strength and motivation to persevere despite the challenges.

Remerciements

Tout d'abord, je tiens à exprimer ma plus sincère gratitude à mon superviseur, le Dr Keir Menzies. Merci de m'avoir donné l'opportunité de rejoindre votre laboratoire et d'avoir cru en moi à chaque étape de mon programme de maîtrise. Je n'aurais pas pu entreprendre ce projet sans votre soutien indéfectible et vos encouragements constants. Je vous suis extrêmement reconnaissante pour vos précieux conseils tout au long de ce projet.

Je voudrais aussi remercier les membres de mon comité de thèse : Dre Julie St-Pierre et Dr Michael De Lisio pour leur soutien et leurs commentaires éclairés. De plus, cette entreprise n'aurait pas été possible sans le généreux soutien financier du programme de formation avancée et d'échange international en métabolomique (MATRIX) financé par le programme de Formation Orientée vers la Nouveauté, la Collaboration et l'Expérience en Recherche (FONCER) du Conseil de recherches en sciences naturelles et en génie du Canada (CRSNG).

Je tiens également à exprimer ma plus profonde gratitude à tous mes collègues du laboratoire Menzies, en particulier le Dr Alex Green, ainsi qu'à mes collaborateurs de la plateforme métabolomique de l'Université d'Ottawa, le Dr David Patten et le Dr Shama Naz, la plateforme métabolomique de l'Institut du cancer Rosalind et Morris Goodman (Université McGill), le programme MATRIX, le laboratoire Slack, ainsi que le laboratoire Baetz. Des remerciements doivent également être adressés aux bibliothécaires de l'Université d'Ottawa, au personnel du service animalier et vétérinaire, et aux employés du bureau des études supérieures et postdoctorales (GradMed) qui ont toujours été d'un grand soutien.

Enfin, je tiens à remercier ma famille et mes amis pour leur soutien moral et leurs encouragements. Je tiens également à remercier mon fils, qui m'a donné la force et la motivation pour persévérer malgré les défis.

Table of Contents

List of figures

List of tables

List of abbreviations

3-HAA	3-Hydroxylanthranilic acid
3-HK	3-Hydroxy-L-kynurenine
5-HTP	5-Hydroxy-L-tryptophan
ACMS	Aminocarboxymuconate semialdehyde
ACMSD	Aminocarboxymuconate semialdehyde decarboxylase
ADPR	ADP-Ribose
AFMID	Kynurenine-formamidase (Arylformamidase)
AMS	2-Aminomuconate semialdehyde
ATP	Adenosine triphosphate
BAT	Brown adipose tissue
cADPR	Cyclic ADP-Ribose
ELISA	Enzyme-linked immunosorbent assay
ESI	Electro-spray ionization
ETC	Electron transport chain
GC-MS	Gas chromatography-Mass spectrometry
HAAO	3-Hydroxyanthranilate 3,4-dioxygenase
HILIC-Z	Hydrophilic interaction liquid chromatography-zwitterioni
HPLC	High-performance liquid chromatography
IDO	Indolamine 2,3-dioxygenase
ISTD	Internal standard
KMO	Kynurenine 3-monooxygenase
KYNU	Kynureninase
LC-MS	Liquid chromatography-Mass spectrometry
L-Kyn	L-Kynurenine
L-Tryp	Tryptophan
m/z	Mass-over-charge ratio
Me2Py	N1-methyl-2-pyridone-5-carboxamide
Me4Py	N1-methyl-4-pyridone-3-carboxamide
MeNAM	1-Methylnicotinamide
MRS	Magnetic Resonance Spectrometry
NA	Nicotinic acid
NAAD	Nicotinic acid adenine dinucleotide
NAD^+	Nicotinamide adenine dinucleotide
NADH	Reduced nicotinamide adenine dinucleotide
NADP	Nicotinamide adenine dinucleotide phosphate
NADPH	Reduced nicotinamide adenine dinucleotide phosphate
NADS	NAD synthase
NAM	Nicotinamide
NAMN	Nicotinic acid mononucleotide
NAMPT	Nicotinamide phosphoribosyltransferase
NAPRT	Nicotinic acid phosphoribosyltransferase
NMN	Nicotinamide mononucleotide
NMNAT	Nicotinamide mononucleotide adenylyltransferase
NMR	Nuclear magnetic resonance spectroscopy

NR	Nicotinamide riboside
NRK	Nicotinamide riboside kinase
NSM	NAD standards mix
NUA	Nicotinuric Acid
PARP	Poly-ADP polymerases
PBMC	Peripheral blood mononuclear cell
PEEK	Polyetheretherketone
PRBC	Packed red blood cells
QPRT	Quinolinate phosphoribosyltransferase
Q-TOF	Quadrupole-Time of Flight
QUIN	Quinolinic acid
RBC	Red blood cells
RPE	Retinal pigmented epithelium
RT	Retention time
TCA	Tricarboxylic Acid
TDO	Tryptophan 2,3-dioxygenase
UV	Ultra-violet
WAT	White adipose tissue

Chapter 1: Introduction

1.1. A Brief History of NAD

Nicotinamide adenine dinucleotide (NAD^+) is a widespread redox co-enzyme involved in hundreds of cellular reactions in prokaryotic and eukaryotic organisms. In the early 1900s, Arthur Harden and William J. Young demonstrated that alcoholic fermentation in yeast requires the presence of an enzymatic catalyst, presumably a protein, and a thermostable substance called "coferment" or "cozymase" (1). The "coferment" fraction contained NAD^+ along with other components. However, NAD^+ wasn't purified until 1929 by Hans von Euler-Chelpin. With the help of Karl Myrbäck, they uncovered the chemical components of the NAD^+ molecule: adenine, a reducing sugar, and phosphoric acid (2). In 1936, Otto Warburg and Walter Christian studied the reversible reduction and oxidation of the pyridine nucleotides: diphosphopyridine nucleotide (or NAD^+) and triphosphopyridine nucleotide ($NADP^+$) and revealed the mechanism of action of these redox co-enzymes (3).

During the pellagra epidemic in the United States of America (1906–1940), the physician and epidemiologist Joseph Goldberger identified the disease as a nutritional deficiency that could be treated by a "pellagra-preventive factor" or "PP factor" present in meat and milk (4). To prove his theory, Goldberger used humans and an animal model of pellagra in dogs (black tongue model). However, some of his human experiments were considered unethical and he failed to identify the PP factor. Ultimately, it was Conrad Elvehjem who isolated and identified the PP factor as nicotinic acid (NA) and nicotinamide (NAM) in 1937 after studying the black tongue model in dogs (5, 6). This prepared the groundwork for treating pellagra in humans using NA, a nutrient that was renamed niacin to avoid confusion with nicotine.

The following decades will witness important discoveries regarding NAD^+ and niacin metabolism. In 1948, Athur Kornberg discovered the NAM salvage pathway by uncovering the reversible conversion of nicotinamide mononucleotide (NMN) to NAD^+ using the energy from adenosine triphosphate (ATP) hydrolysis into inorganic pyrophosphate and transfer of an adenylyl group to NMN (7). Ten years later, Preiss and Handler discovered the metabolic pathway synthesizing NAD^+ from NA. They identified the metabolic intermediates and the three main enzymes of the aptly named “Preiss-Handler" pathway (8, 9). Later on, the observation that diets including foods with low NA content like milk were not inducing pellagra led to the conclusion that the amino acid tryptophan could also prevent pellagra. Tryptophan was thought to be metabolized *in vivo* into either NA, NAM, or other metabolites like NAD^+ after its conversion into kynurenines intermediates (10, 11). This pathway was named the *de novo* pathway and shared the last steps of the Preiss-Handler pathway.

In addition to its role as a redox co-enzyme, NAD^+ is also a substrate to different enzymes like Poly-ADP polymerases (PARPs) that were discovered by Chambon *et al.* In 1963 (12, 13). At the time, they presumed that PARPs were DNA-dependent poly-adenylic acid synthetases that used ATP to produce a polyA chain like other known nuclear enzymes, but in 1966, they identified the substrate as NAD and the product of the reaction as a polymer of ADP-ribose (13). After the characterization of the PARP family, their role in DNA damage repair (14, 15) and cell death (16–18) raised a lot of interest in the 1980s and 1990s. In 2000, Imai *et al*. showed that NAD^+ can also be broken down by sirtuins, which are protein deacetylases shown to have a beneficial effect on metabolism and lifespan (19). The role of NAD^+ in signaling pathways is still under study and other NAD^+-consuming enzymes have been uncovered. Additionally, basic concepts on NAD+ metabolism are still evolving such as the discovery of the mammalian mitochondrial

NAD^+ transporter SLC25A51 in 2020 (20). Altogether, the recent discoveries about the various roles of NAD^+ and its metabolites have revitalized the interest in this molecule and led to the development of NAD^+-boosting therapies as well as sensitive techniques to study the NAD^+ metabolome.

1.2. NAD^+ Metabolism in mammals

1.2.1. NAD^+ Biosynthesis

NAD^+ can be synthesized through three different pathways depending on the availability of the biosynthetic enzymes and NAD^+ precursors in each tissue or cell type (Fig. 1):

a. De novo NAD^+ synthesis

The amino acid L-Tryptophan (Trp) is converted through the kynurenine pathway to α-amino-β-carboxymuconate-ε-semialdehyde (ACMS), which can undergo either enzymatic decarboxylation by the ACMS decarboxylase (ACMSD) followed by spontaneous cyclization to quinolinic acid or further metabolic reactions leading to complete oxidation via the tricarboxylic acid (TCA) cycle. The total oxidation of ACMS in the TCA cycle being more favorable than the spontaneous non-enzymatic reaction leading to NAD^+ biosynthesis explains why tryptophan is not considered a good NAD^+ precursor in most tissues (21, 22). When the ACMS decarboxylase is saturated, quinolinic acid is formed and converted by the QPRT (quinolinate phosphoribosyltransferase) to nicotinic acid mononucleotide (NAMN). The consecutive conversion of NAMN to nicotinic acid adenine dinucleotide (NAAD) is catalyzed by one of the NMN adenylyltransferases (NMNAT 1–3). The final step is the amidation of NAAD to form NAD^+ by the NAD synthase enzyme. This last enzyme also catalyzes the final step of the Preiss-Handler pathway (described below). Ultimately, *de novo* synthesis is a minor mechanism governing the NAD^+ metabolome, occurring mainly in the liver, kidney, and neurons (10, 23–25).

b. Preiss-Handler pathway

The conversion of nicotinic acid (NA) to NAD^+ by the Preiss-Handler pathway was initially discovered in erythrocytes and liver samples (8, 9) but it is also present in other tissues such as heart, intestine, and kidneys (26). The nicotinic acid phosphoribosyltransferase (NAPRT) enzyme catalyzes the conversion of NA to NAMN. The next 2 steps required for the biosynthesis of NAD^+ are catalyzed by NMNATs and the NAD synthase, which are reactions shared by the *de novo* pathway (8, 9) (Figure 1).

c. Nicotinamide salvage pathway

The salvage pathway is responsible for most of NAD^+ biosynthesis and is the predominant NAD^+ biosynthetic pathway in most tissues, including liver, kidney, skeletal muscle, and adipose tissue (25). The nicotinamide (NAM) derived from NAD^+-consuming reactions or diet is converted through this pathway to nicotinamide mononucleotide (NMN) via NAMPT (NAM phosphoribosyltransferase) and then to NAD^+ by the NMN adenylyltransferases (NMNAT 1–3). Nicotinamide Riboside (NR) can enter the salvage pathway after phosphorylation to NMN by the NR Kinases (NRK 1–2). This last reaction occurs mainly in the liver, heart, skeletal muscle, and neurons (27, 28).

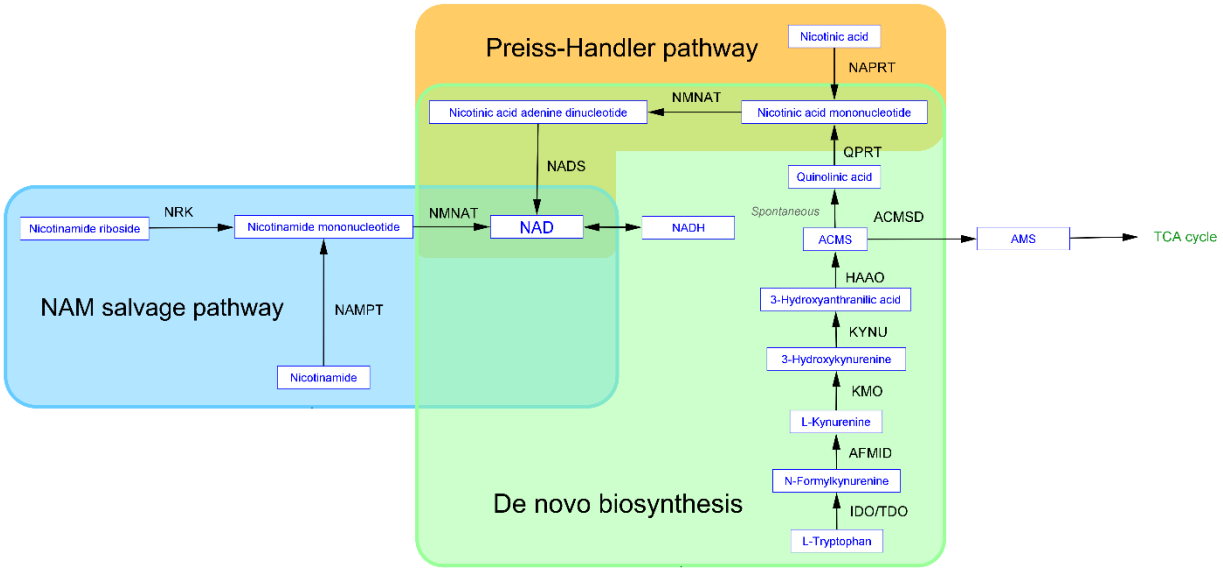

Figure 1: NAD$^+$ biosynthetic pathways. The *de novo* biosynthesis from Tryptophan (Green) shares the last enzymatic steps with the Preiss-Handler pathway (Orange). The NAM salvage pathway (Blue) allows NAD$^+$ biosynthesis from NMN, NAM, or NR. NAD: Nicotinamide adenine dinucleotide, IDO: Indolamine 2,3-dioxygenase, TDO: Tryptophan 2,3-dioxygenase, AFMID: Kynurenine-formamidase (Arylformamidase), KMO: Kynurenine 3-monooxygenase, KYNU: Kynureninase, HAAO: 3-hydroxyanthranilate 3,4-dioxygenase, ACMS: Aminocarboxymuconate semialdehyde, ACMSD: Aminocarboxymuconate semialdehyde decarboxylase, AMS: 2-aminomuconate semialdehyde, QPRT: Quinolinate phosphoribosyltransferase, NAPRT: Nicotinic acid phosphoribosyltransferase, NMNAT: Nicotinamide mononucleotide adenylyltransferase, NADS: NAD synthase, NAMPT: Nicotinamide phosphoribosyltransferase, NRK: Nicotinamide riboside kinase.

1.2.2. NAD$^+$ catabolism and phosphorylation

NAD$^+$ can be cleaved to NAM by a variety of signaling enzymes such as PARPs, Sirtuins (protein deacetylases), cyclic ADP-Ribose (cADPR) synthases (29), and SARM1 (Sterile Alpha and TIR Motif Containing 1) (30). PARPs transfer ADP-ribose moieties onto target proteins and are mainly involved in nuclear functions like DNA maintenance and repair, chromatin structure, and regulation of transcription (31), while sirtuins transfer moieties such as acetyl groups from donor proteins to positively influence mitochondrial biogenesis, cellular metabolism, and cell survival (32, 33). cADPR synthases like CD38 are primarily known as transmembrane ectoenzymes producing cADPR, a second messenger involved in calcium mobilization, insulin

signaling, inflammatory responses, and cell cycle control (34). Similar functions have been attributed to other NAD^+ degradation metabolites, including ADP-Ribose and NAADP (nicotinic acid adenine dinucleotide phosphate) (35). All the aforementioned enzymes also produce NAM. Similarly, NAD^+ cleavage by SARM1 leads to the formation of NAM and cADP-Ribose or ADP-Ribose. In 2021, it was shown that SARM1 can also catalyze the exchange of the nicotinamide group on NADP with nicotinic acid to generate NAADP, which acts as a second messenger involved in calcium signaling (36, 37).

While NAD^+ is mainly intracellular, extracellular NAD^+ has been measured by various studies (38, 39). NAD^+ can be released into the extracellular space after cell lysis or through cell membrane channels such as connexins (e.g., Cx43) (40, 41), which could mediate the bidirectional transport of NAD^+ (42). Additionally, it has been shown that NAD^+ can be released by stressed cells to serve as a neurotransmitter (43, 44). Extracellular NAD^+ can be degraded by the aforementioned cADPR synthases CD38 or CD157 to form NAM and cADPR or ADPR, while CD38 and CD73 can convert NMN into NAM or NR, respectively. NR may also, in turn, be hydrolyzed into NAM by CD157 (45). All of these by-products can then re-enter surrounding cells to produce intracellular NAD^+. Excess cellular NAM, which was not converted into NAD^+, can be methylated to form 1-methyl NAM (meNAM), which can be further oxidized to the degradation products N1-methyl-2-pyridone-5-carboxamide (Me2Py) and N1-methyl-4-pyridone-3-carboxamide (Me4Py). Ultimately, these catabolites can be cleared from the body via urine (46, 47).

NAD^+ can also be phosphorylated by NAD kinases (NADKs) to produce $NADP^+$ (48) which is reduced to NADPH by various enzymes such as the rate-limiting enzyme of the pentose phosphate pathway (PPP), glucose-6-phosphate dehydrogenase, in the cytosol (49) and the

mitochondrial nicotinamide nucleotide transhydrogenase (NNT) (50). Further, maintaining an optimal NADPH/$NADP^+$ ratio is essential for cellular antioxidant responses and glutathione reduction (49, 51).

1.2.3. Whole-body NAD^+ metabolism

The complexity of the NAD^+ metabolome arises from its implication in various cellular functions and the differences in NAD^+ metabolism at the subcellular, tissue/organ and systemic levels. On a whole-body level, the liver represents a major hub for NAD^+ metabolites due to its role in first-pass metabolism, in addition to its high expression of NAD^+ biosynthetic enzymes, especially enzymes of the *de novo* pathway, which are reported to be mainly in the liver and kidney (10, 23, 25). The liver can use various NAD^+ precursors to produce NAD^+, whereas many organs rely on NA or NAM for NAD^+ synthesis (25, 52). Skeletal muscle has been shown to use intact NR when administered intra-venously (52, 53). However, when administered orally, the hepatic first-pass metabolization of NR reduces its bioavailability for use by other tissues. Instead, the liver releases NAM into the circulation, which is taken up by most tissues to sustain NAD^+ synthesis (52).

The variable tissue-specific turnover of NAD^+ metabolites complicates the study of NAD metabolism *in vivo*, however, this has been partially circumvented by analysis using isotopes of NAD^+ precursors (52). Despite the permanent consumption of NAD^+, the homeostasis of the cellular NAD^+ pool is maintained by the tight regulation of NAD^+ anabolism and catabolism fluxes, along with the transport of NAD^+ and its precursors between the different tissues and the intracellular compartments. However, under pathological conditions such as renal failure, some NAD^+ catabolites can accumulate such as nicotinamide (NAM), Methyl nicotinamide (MeNAM),

4-pyridone 3/5-carboxamide ribonucleoside triphosphate (4PyTP), 4Py-riboside and 2Py-riboside, which may inhibit essential cellular reactions (46, 47).

1.3. Role of NAD(P) in cellular metabolism and signaling pathways

Along with NAD(H), NADP(H) is also essential for the maintenance of cellular redox balance. While the NAD^+/NADH flux is mainly involved in oxidative processes, the NADP/NADPH flux is primarily used in reductive reactions. Specifically, NAD(H) is essential in various metabolic pathways like glycolysis, the TCA cycle, and mitochondrial oxidative phosphorylation (54) while NADPH is necessary for the biosynthesis of lipids, nucleotides, and amino acids (55).

As has been briefly discussed above, beyond the role of NAD^+ as a co-enzyme, NAD^+ is an important substrate for a limited number of enzymes. Sirtuins are a family of seven enzymes that exist in various sub-cellular compartments and have differing roles. Because of their NAD^+ dependency and their beneficial role in mitochondrial metabolism and transcriptional regulation, sirtuins are primarily known as energy sensors controlling gene expression in response to metabolic cues provided by the flux in the NAD^+/NADH ratio (24, 56, 57). Most importantly, many sirtuins promote cell survival and healthy aging when NAD^+ levels are abundant (33, 58, 59). The Poly-ADPRibosyl transferase (PARP) family of 17 enzymes also have various cellular localizations and functions. Nuclear PARPs are mainly involved in DNA damage detection and repair (60). They also play an important role in chromatin structure and regulation of mitosis (61), cellular differentiation and proliferation (62), telomere maintenance (63), and cell death (64–66). Concerning the role of PARPs in mitochondrial regulation, they mainly promote mitochondrial dysfunction (67, 68) but evidence shows that mild PARP activation might have a positive impact on mitochondrial activity (69, 70). cADPR synthases, such as the ubiquitous transmembrane

receptor CD38, possess enzymatic activities that can cleave NAD^+ and NADP to form the second messengers cADPR and NAADP, respectively. These in turn control calcium mobilization, hormone secretion, cell proliferation, and cell death pathways (34). It has also been postulated that CD38 might act as a modulator of intracellular NAD^+ levels with its NADase activity and high affinity for NAD^+ (71).

Unlike PARPs and cADPR synthases, sirtuins have a lower affinity for NAD^+, which explains their NAD^+ sensing function and their inhibition due to NAD^+ depletion following PARPs' and/or cADPR synthases' hyper-activation. The intricate regulatory interactions between the various NAD^+ consuming enzymes and their individual cellular compartment locations are still to be fully understood, but it seems that activation of Sirtuins may have a positive effect on cell survival and metabolic adaptation, while PARPs and cADPR synthases, as well as other NAD^+-consuming enzyme such as SARM1, may promote inflammation and cell death, often in situations of metabolic or genotoxic stress. NAD^+ availability and the interplay between these enzymes certainly affect cellular adaptation to various physio-pathological situations. The observed decline in NAD^+ content during aging and age-related diseases such as diabetes, neurodegeneration, and cancer, has led to the development of various therapeutic strategies to restore NAD^+ homeostasis (29, 72, 73).

1.4. NAD^+-boosting therapies

Compelling evidence shows that NAD^+ replenishment can improve a broad range of pathological conditions, including neurodegenerative disorders (74–76), metabolic syndrome and type 2 diabetes (77, 78), cardiovascular diseases (79), muscular dystrophies (80), mitochondrial myopathies (81), and acute kidney injury (82). Recent studies have also pointed to the role of NAD^+ metabolism in the regulation of innate immunity (83, 84). Moreover, supplementation with

NAD^+ precursors has been shown to extend lifespan in animal models (85, 86). Three major strategies are currently used to increase NAD^+ levels: supplementation with NAD^+ precursors, stimulation of NAD^+ biosynthetic enzymes, and inhibition of NAD^+-consuming enzymes.

1.4.1. NAD^+ precursors

The first medical application of the NAD^+ precursors was the treatment of pellagra with niacin (Vitamin B3) (87). The term niacin usually points to nicotinic acid but can also include nicotinamide despite their different chemical structures and metabolic origins. NA and NAM were used to treat or improve dyslipidemia, cardiovascular diseases, kidney injuries, and mitochondrial diseases in humans (81, 88). However, their utilization to increase NAD^+ levels beyond their physiological norms in humans has been limited by their side effects, including an intense skin flushing reaction for NA (89) and reversible liver toxicity for NAM (90, 91). To evade these potential side effects, new NAD^+ precursors have been studied like Nicotinamide Riboside (NR) and Nicotinamide Mononucleotide (NMN). Currently, only Nicotinamide Riboside (NR) has been confirmed to be safe and effective by 24 completed and 29 ongoing clinical trials and is commercially available under the name Niagen® (92–96). NMN also seems to be an effective NAD^+ precursor, but it was verified only by two clinical trials (97, 98), while 8 other clinical trials are still ongoing (99). However, some human studies have shown minor to no effect of NR supplementation on body composition, lipid metabolism, or insulin sensitivity in overweight subjects (93, 100, 101). Dihydronicotinamide riboside (NRH), a reduced form of NR, was also developed to offer a stability and oral bioavailability than NR (102). Thus, further studies of the NAD^+ metabolome and the effect of NAD^+ precursor are necessary to determine the short- and long-term effects of these therapies on humans.

1.4.2. PARP inhibitors

PARP inhibitors have been shown to increase NAD^+ levels *in vitro* and *in vivo* (103, 104) and, due to their negative effect on PARP DNA repair activities, they are currently being used in the treatment of ovarian and breast cancers. In 2014, olaparib (AZD2281) was the first PARP inhibitor to be FDA approved as a treatment of BCRA1/2 mutant cancers (105). Rucaparib (AG014699) was approved by the FDA in 2015(106). Other molecules are in the late phases of clinical trials like niraparib (MK4827) (107) and veliparib (ABT-888) (108). Multiple studies have also shown that these drugs increase intracellular NAD^+ levels (56, 109). However, their general use as NAD^+ boosters is limited due to important toxic effects including gastro-intestinal symptoms and anemia for all previously cited PARP inhibitors (105, 106, 110) and leucopenia and thrombocytopenia for niraparib (107), talazoparib (111) and veliparib (108).

1.4.3. NAMPT activators

Several members of the P7C3 class of neuroprotective agents act as nicotinamide phosphoribosyl transferase (NAMPT) activators and are being developed and optimized to improve their specificity and bioavailability, along with their pro-neurogenic and neuroprotective effects (112, 113). SBI-797812 was also identified as an NAMPT activator that binds the enzyme active site, increases NAMPT affinity for ATP, inhibits negative feedback by NAD^+, and stimulates NAMPT activity toward NMN synthesis, which promotes NAD^+ formation by the NMNAT enzymes (114).

1.4.4. CD38 inhibitors

The cADPR synthase enzyme CD38 is an important regulator of intra- and extra-cellular NAD^+ homeostasis and plays a critical role in age-related NAD^+ decline and diet-induced obesity (115, 116). Different therapeutic strategies targeting CD38 have been developed and tested *in vivo*

or *ex vivo*, including small molecule inhibitors like the NAD^+ analogue arabinosyl-2'-fluoro-2'-deoxynicotinamide mononucleotide (Ara-F-NMN phosphoester/C48) (117) and the non-covalent inhibitor Luteolinidin (118), which were effective at preserving the NAD(P) pool by inhibiting the NADase activity of CD38.

1.5. NAD(P) quantification methods

Initial methods for NAD(H) and NADP(H) quantification relied on the spectrophotometric or fluorometric properties of these metabolites. NAD(P)H and $NAD(P)^+$ have a common absorbance peak at 260 nm, while the NAD(P)H spectrum exhibits a second absorption peak at 340 nm that can be used to measure the reduced forms concentrations independently from the oxidized forms (119) (Supp. Fig. 1a). Additionally, unlike NAD^+ and $NADP^+$, which are not fluorescent, NADH and NADPH are intrinsically fluorescent, with similar excitation peaks at 340 nm and emission peaks at 445 nm (120) (Supp. Fig. 1b).

Later on, the direct measurement of $NAD(P)^+$ was made possible with the cyanide addition reaction, in which hydrogen cyanide reacts with $NAD(P)^+$, and not NAD(P)H, at pH 10 to form a cyanide adduct with an absorption peak at 325 nm (121). Given that fluorometric methods were found to be more sensitive than colorimetric methods (122, 123), various fluorescence-based methods have been developed using strong alkali (124) and/or specific dehydrogenase enzymes (125), or additives like phenazine methosulfate (126). However, fluorometric methods also lack specificity and are affected by interferences and photosensitivity (127). The need for higher specificity and sensitivity led to the development of enzyme cycling methods coupled with spectrophotometric or fluorometric detection. In the case of NAD(H), enzyme coupling begins with NADH quantification followed by that of NAD^+ by enzymatically cycling NAD^+ to NADH and performing a second measurement of total NADH (first measurement of [NADH] – second

measurement of total [NADH] = [NAD^+]) (Supp. Fig. 2). Enzyme cycling assays have therefore been the most frequently used methods to quantify pyridine nucleotides in mammalian tissues since the 1960s. However, they are limited by substrate saturation, enzyme stability and enzyme kinetics, and the presence of interfering substances in the samples like enzyme inhibitors (128). Moreover, measuring the reduced (NADH and NADPH) and oxidized (NAD^+ and $NADP^+$) nucleotides by enzyme cycling methods requires the initial separation of the reduced and/or phosphorylated forms (129–131). Beyond these assays, bioluminescence (129, 130) and polarography (132) have been sparingly used to quantify NAD^+ and its metabolites, but they suffer from many disadvantages including interferences from other ions and complex molecules in the tissue samples.

The increased requirement for high sensitivity and resolution in the quantification of NAD^+ and, eventually, the simultaneous study of its metabolites led to the development of new methods like high-performance liquid chromatography (HPLC) and mass spectrometry (MS). HPLC was naturally a good candidate as it could simultaneously separate different metabolites with high resolution and was appropriate for separating polar thermolabile compounds. HPLC columns were coupled with ultraviolet-visible or fluorometric detectors for the identification and quantification of the metabolites (132). The separation was further improved by using differential extraction methods (133–135), various elution modes and elution buffers (133, 136), or ion-pairing reagents (134).

High-resolution separation of HPLC and the specific and sensitive identification of the metabolites with mass spectrometry has the added benefit of the simultaneous study of a large number of metabolites present in tissue samples (137). Despite these advantages, liquid chromatography-mass spectrometry (LC-MS) remains expensive and complex to implement. The

choice of chromatography, MS instrumentation, and insufficient standardization for the absolute quantification of metabolites, are major hurdles to LC-MS quantification methods. Along with the cost of running LC-MS experiments, these hurdles explain why enzyme cycling assays persist in recent studies. Magnetic Resonance Spectrometry (MRS) has also been used to quantify NAD^+ in tissues (138). These assays rely on the presence of 1H and 31P in the tissues and offer many advantages like the possibility of non-invasive measurements, high reproducibility, and precise quantification. However, it suffers from low sensitivity and resolution in comparison to LC-MS methods (139, 140).

1.6. Hypothesis and research objectives

Rationale:

Despite the latest advances in NAD^+ metabolism, many questions need to be resolved to allow the translation of recent pre-clinical results into feasible clinical applications. With the complexity of the NAD^+ metabolome and the rapid interconversion and metabolism of its metabolites in different tissues, it is important to assess the entire NAD^+ metabolome at different timepoints in tissues of interest following NAD^+-driven interventions. In addition to the biological aspects, it is important to optimize technical procedures for the determination of NAD^+-related metabolites to obtain accurate and reproducible quantification results. Currently, the ideal method for the quantification of the NAD^+ metabolome is LC-MS, which combines mass spectrometry coupled with liquid chromatography, thereby benefiting from the high sensitivity of mass spectrometry and the resolutive separation of the chromatography, allowing for the simultaneous determination of a large number of metabolites in tissue samples (141, 142).

The main goals of this work are first, to perform a meta-analysis of all quantitative NAD(P)(H) measurements in rodents and humans, and second, to develop and optimize a targeted

LC-MS-based method for NAD^+ metabolomics including the preparation of a ^{13}C-labeled yeast standard for internal quality control. Finally, this method will be used to study changes in the NAD^+ metabolome in mouse tissues at different timepoints following supplementation with NR. A preliminary analysis using an enzyme cycling method will be used to identify the effect of NR on NAD^+ and NADH levels in various mouse tissues. Subsequently, the NAD^+ metabolomics method will be applied to the study of the entire NAD^+ metabolome in mouse liver, which is the main transit point for oral NR and a central hub for whole-body NAD^+ metabolism, and skeletal muscle, which will represent the target tissue and allow us to determine whether oral NR supplementation is sufficient to produce changes in the muscle NAD^+ metabolome.

Hypothesis: Oral NR supplementation increases NAD^+-related metabolite levels in mouse liver and skeletal muscle.

Research objectives:

- Perform a systematic review of literature to summarize pre-analytical and analytical conditions for NAD^+ metabolome analyses, along with a meta-analysis of NAD(P)(H) measures, in all tissues and mammalian species including rodents and humans.
- Optimize an LC-MS-based metabolomics method to accurately measure NAD^+-related metabolites in mouse tissues and develop a reproducible protocol for the preparation of yeast-derived stable isotope labeled internal standards.
- Determine changes in the NAD^+ metabolome in mouse tissues under anesthesia versus post-necropsy.
- Determine changes in the NAD^+ metabolome in mouse tissues after acute and chronic NR administration.

Chapter 2: Meta-analysis of NAD(P) quantification in mammalian tissues

2.1. Introduction

Nicotinamide adenine dinucleotide plays a dual role as a reduction-oxidation (redox) co-enzyme, in its oxidized ($NAD(P)^+$) and reduced (NAD(P)H) forms, and as a co-substrate ($NAD(P)^+$) for enzymes involved in deacylation (32), mono- and poly-ADP-ribosylation (13, 143), and the creation of adenine-based second messengers (34, 144–146). The $NAD(P)^+$/NAD(P)H ratio is an important indicator of the intracellular redox state and plays a critical role in the regulation of key metabolic pathways (54, 147). For example, NAD^+ is essential for glycolysis, along with the tricarboxylic acid (TCA) cycle, to provide reducing equivalents during the generation of adenosine triphosphate (ATP), the main source of energy for the cell (54, 147). When NAD^+ is limited it can also be regenerated from NADH by the fermentation of pyruvate to produce lactate in mammalian cells, thereby maintaining cellular redox balance[25]. NAD^+ and NADH can also be phosphorylated to NADP and NADPH, respectively, by NAD^+ Kinases (NADKs) (48, 148). NADPH is essential for reductive biosynthesis, signal transduction, cellular antioxidant responses, and particularly, glutathione reduction (35, 49, 51). In the cytosol, $NADP^+$ is reduced to NADPH by the glucose-6-phosphate dehydrogenase and 6-phosphogluconate dehydrogenase of the pentose phsophate pathway (PPP), amongst other reactions (49). Whereas in the mitochondria, NADPH production is sustained by various reactions, including those reliant on nicotinamide nucleotide transhydrogenase (NNT) and isocitrate dehygronases (IDH2) enzyme activity (50). As a result, NAD(P)(H) status has been shown to affect cell signaling and metabolism, energy homeostasis, mitochondrial biogenesis, oxidative stress responses and DNA maintenance and repair (25, 149, 150). Further, since the progression of age-related diseases, such as obesity (151), non-alcoholic fatty liver disease (152, 153), neurodegeneration (154), mitochondrial (81) and

cardiovascular (79) diseases, and muscle atrophy or dystrophy (80), has been linked to alterations in NAD^+-related metabolites, approaches aimed at maintaining NAD^+ homeostasis are currently under investigation.

Beyond common redox transitions, $NADP^+$ can be consumed by exchanging its nicotinamide group with nicotinic acid in a reaction catalyzed by cADPR synthases, such as CD38, to form the second messenger NAADP, which is involved in calcium mobilization, hormone secretion, and immune cell proliferation (34, 146, 155). NAD^+ can also be consumed when acting as a co-substrate to form nicotinamide (NAM), which can be used as a substrate to regenerate NAD^+ via the NAM salvage pathway. NAM can also be methylated to form 1-methyl NAM (meNAM), which can be further oxidized to the degradation products N1-methyl-2-pyridone-5-carboxamide (2py) and N1-methyl-4-pyridone-3-carboxamide (4py). Ultimately, the methylated catabolites can be cleared from the body via urine (46, 156). The NAD^+ pool can also be reduced by consumption of $NADP^+$ via a base-exchange reaction for the formation of the second messenger NAADP(35). Maintaining the pool of NAD^+ therefore requires biosynthesis via the Preiss-Handler pathway (starting with the common vitamin B3 molecule niacin (NA; nicotinic acid)), the *de novo* biosynthesis pathway (starting with the amino acid tryptophan (Trp)) or regeneration from the conversion of NAM via the salvage pathway to NMN then to NAD^+. Finally, the salvage pathway is also important for the biosynthesis of NAD^+ from nicotinamide riboside (NR), an alternative form of vitamin B3 found in foods, following its phosphorylation by nicotinamide riboside kinase to NMN and then conversion to NAD^+ via the salvage pathway.

Understanding the dynamics of the NAD^+ metabolome has therefore become essential and ultimately requires rigorous metabolite quantification in order to better understand the flux of NAD^+ metabolites during normal physiology, or with disease progression or healthy aging. A clear

picture of these changes is essential for linking alterations in the NAD^+ metabolome to downstream enzymatic or redox reactions, which hold the key to changes in tissue phenotypes. Given the substantial amount of previously reported quantitative data on NAD^+ metabolites in mammals, including a growing number of reports in humans, it is essential and timely to summarize these changes during health and disease. Numerous studies have examined components of the NAD^+ metabolome in rodents and humans under different metabolic states, ages, and diseases, yet rely on different methods for sample preparation or quantification. Sample preparation is important for metabolites involved in redox reactions due to potential degradation and inter-conversions under certain conditions (157, 158). For quantification, liquid chromatography coupled to mass spectrometry (LC-MS) and magnetic resonance spectrometry (MRS) are thought to be sensitive and specific methods (142, 159, 160), while enzyme cycling assays are the more common. Quantitative LC-MS methods require a comprehensive inclusion of quality controls for individual metabolites being measured and for the overall matrix effect of the samples, an effect that explains varying mass spectrometric responses for a given analyte when measured in different solutions. Without these controls, LC-MS is at best semi-quantitative. In this study, we identified considerable variability in NAD(P)(H) measures across rodent and human studies, emphasizing the need for proper methods reporting and for standardized sample processing and analytical protocols. Overall, comparable NAD(P)(H) datasets across studies is needed for meaningful interpretation of the existing and future data in the field of NAD^+ biology.

This study provides 1) a meta-analysis of the observed physiological NAD(P)(H) metabolite levels, in different tissues from mice, rats, and humans; 2) a summary of the effects of tissue sampling conditions and analytical procedures on NAD(P)(H) measurements in mammalian

tissues; and 3) highlights of crucial steps in the pre-analytical and analytical procedures that need to be optimized.

2.2. Methods

2.2.1. Literature Search

"Epub Ahead of Print", "In-Process & Other Non-Indexed Citations", "Versions", "PubMed-Not-MEDLINE", "Daily update", "Front segment weekly update", "Back files from 1946 to start of front segment" citations between 1946 and June 20, 2021, in the MEDLINE ALL (Ovid) database were searched and reviewed for articles containing quantitative data of NAD(P)(H) metabolite levels in mammalian tissues as outlined in supplementary table 1. The search query strategy yielded 3377 articles. An additional blood focused search was performed using the same database and yielded 1513 articles (Supp. table 2).

2.2.2. Screening methodology

The 4890 records obtained from the systematic searches underwent abstracts screening to identify all articles reporting NAD(P)(H) metabolite quantification in mammalian tissues. All abstract reviews were verified with a second review by a different reviewer and any conflicts resolved. Following abstracts screening 643 publications were selected for full-text review for the tissue-focused search and 272 for the blood-focused search (Supp. Fig. 3). Studies that only presented relative NAD(P)(H) metabolite data were excluded during the full-text screening, with the exception of studies reporting NAD^+/NADH ratios. Results derived strictly from tissues, cells, isolated organelles maintained in media, or from blood effluent from perfusion were excluded. This full-text review led to the exclusion of 667 (457+210) articles due primarily to the lack of quantitative NAD(P)(H) data (50.5%), data derived from non-suitable specimens (36.3%), or data

presented as relative/arbitrary units (13.2%). Finally, 241 articles were included in the qualitative meta-analysis and 205 in the quantitative meta-analysis (Supp. Fig. 3). Although our initial search included studies published from 1946 to June 20, 2021. As mentioned above, the oldest study with quantitative NAD(P)(H) data that met our acceptance criteria was published in 1961.

2.2.3. Data extraction

Numerical data for NAD(P)(H) metabolites were either obtained directly from the articles or extracted from article figures using a semi-automatic data extraction software (WebPlotDigitizer (161)). Additionally, where applicable, the tissue sampling timepoints relative to sacrifice and/or tissue/blood sampling methods (i.e., method of anesthesia and/or euthanasia, tissue handling, and storage temperature) were recorded. For animal models, the species, characteristics (e.g., strain, genotype, age, and weight), and environmental conditions (e.g., sleep cycle, type of diet, feeding frequency, and feeding state relative to tissue sampling) were recorded. Additionally, for all studies, treatments (e.g., pharmacological treatments, surgeries, irradiation, tumor induction and other procedures applied to the study subjects) and all study group information (e.g., treatment or disease groups and corresponding controls) were extracted. Finally, the method of NAD(P)(H) quantification method (e.g., enzymatic assays, mass spectrometry based, HPLC, NMR, bioluminescence) and publication specifics (i.e., publication title, reference code [DOI, Medline UI, PMID] or hyperlink and year of publication) were noted (Appendix 3-Database).

2.2.4. Data analysis

Prior to analysis, all concentrations were converted to nmol/g of tissue or nmol/g of proteins for tissue samples or nmol/ml for blood fractions. Due to the low number of results normalized to protein content, we only show results normalized to tissue weight and blood volume.

Statistical analysis was performed with GraphPad Prism version 9 (GraphPad Software Inc., San Diego CA, USA).

2.3. Results

2.3.1. Meta-analysis of common quantification methods, along with species, sex and tissues studied

Historically, early methods used for NAD(P)(H) quantification relied on the spectrophotometric or fluorometric properties of these metabolites (121, 124). More recently, enzyme cycling methods coupled to spectrophotometric or fluorometric detection are more commonly used to distinguish NAD(P)(H) co-enzyme levels (122, 127, 162). The growing need for high sensitivity and resolution in the quantification of these co-enzymes, along with the necessity to measure other NAD^+-related metabolites, led to the use of high-performance liquid chromatography (HPLC) and LC-MS techniques. Of these approaches, LC-MS has become the preferred method, as mass spectrometry combined with liquid chromatography allows for the specific identification of eluted compounds along with the added benefit for including NAD(P)(H) isotope metabolites as internal spike-in quality controls. Despite their advantages over classic spectrophotometric or fluorometric assays, HPLC and LC-MS both remain expensive and time consuming, which explains why enzyme cycling assays persist in recent studies.

Using a systematic approach, of the 241 eligible studies (Appendix 3-Database), 205 studies that included quantitative meta-analysis of NAD(P)(H) concentrations in mouse, rat, and human tissues were selected for further analysis. Of these studies, 46.7% used enzyme cycling assays, of which included colorimetric (40.9%) or fluorometric (5.8%) detection, while 17.8% used HPLC methods (coupled with UV or fluorescence detectors) and 13.2% used LC-MS assays (Fig. 2a). Most studies did not include a detailed description of the metabolite extraction

procedures. However, commonly used extraction procedures consisted of either extraction buffers with or without surfactants (Triton®, Tris, Dodecyltrimethylammonium bromide), or polar organic solvents such as acetonitrile, methanol, ethanol, or chloroform. Previous studies have shown that enzyme inactivation and optimal pH and temperature conditions were efficient at preserving the stability of the different NAD(P)(H) forms (158, 163, 164). When disclosed, samples were processed under low-temperature conditions and no redox additives were mentioned in the included studies. Redox reactions were limited by the inactivation of the enzymes in the samples prior to NAD(P)(H) metabolites measurements, usually by precipitation with solvents such as ethanol, methanol, acetonitrile, or perchloric acid (PCA). However, the use of PCA was rare due to the acid-labile nature of the reduced forms (i.e. NADH and NADPH), as well as the necessity of an additional neutralization step. Thus among the studies reporting the use of PCA during the metabolite extraction (5.4%), 3.7% reported $NAD(P)^+$ results only or used a second non-acidic extraction method for proper NAD(P)H quantification. Only 1.7% of the studies reported NADH, total NAD(H), and/or NAD^+/NADH results using only the PCA extraction. The potential bias from these studies could not be analyzed due to the limited data.

Additionally, within the included studies 36.65% did not disclose the time of tissue harvest relative to sacrifice, and when disclosed, the majority used post-mortem samples (29.48%) while only 7.57% used pre-mortem samples (Fig. 2b). Most of these studies were performed on rat (31.7%), mouse (30.0%) or human (30.0%) subjects and only 21.46% included females, with 33.2% of the studies not disclosing the sex of their subjects (Fig. 2c-d). Finally, 27.5% of the studies examined liver tissue, with the rest being predominantly focused on blood (15.3%), brain (14.3%), muscle (12.5%) and kidney (8.0%) (Fig 2e).

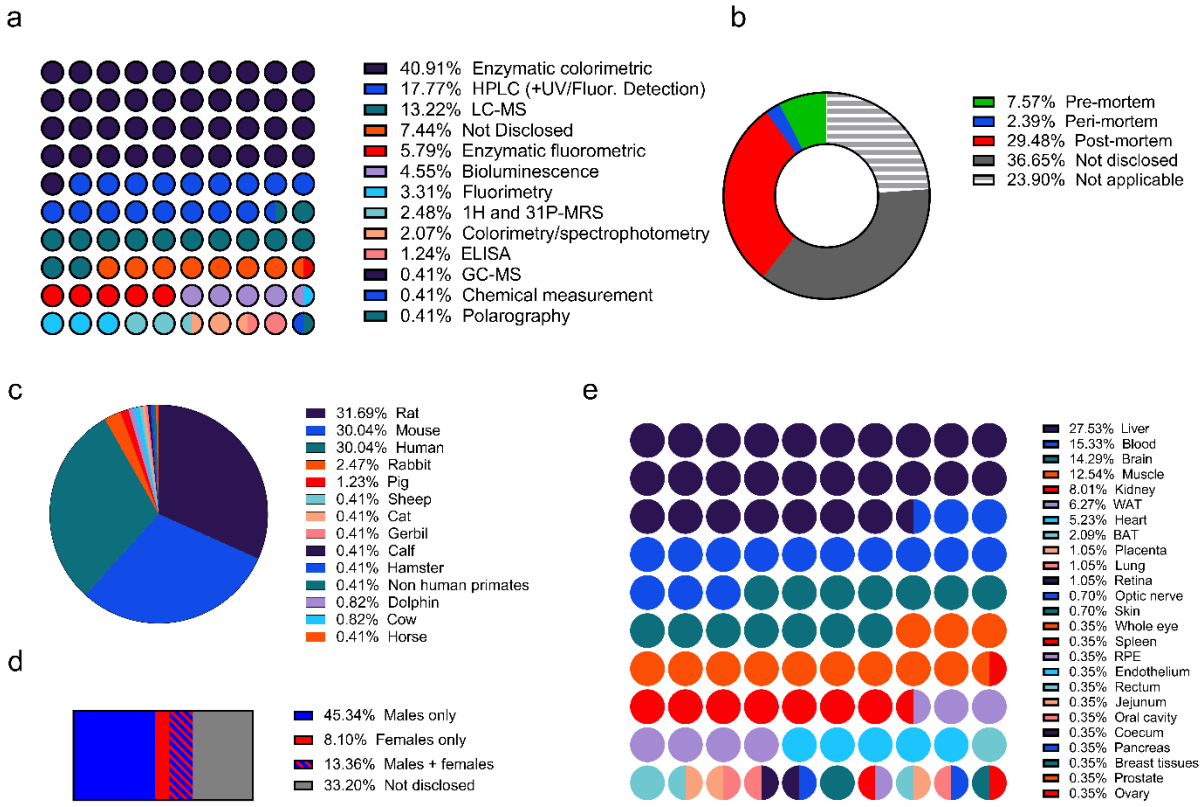

Figure 2: Methodological characteristics of included studies. Distribution of (a) NAD(P) quantification methods, (b) sampling timepoint relative to sacrifice, (c) mammalian species, (d) sex, and (e) tissues used among eligible studies. WAT: white adipose tissue, BAT: brown adipose tissue, RPE: Retinal pigment epithelium.

2.3.2. Comparison of mean physiological NAD(P)H levels across tissues for rodents and humans

To help identify the expected mean physiological NAD(P)(H) levels for the most commonly studied mouse, rat and human tissues, we compiled data from all control and wild-type cohorts from each of the included studies (Appendix 3-Database). Specifically, we recorded the mean NAD(P)(H) levels normalized to tissue weight or, in the case of blood, volume. Data from studies that normalized metabolite levels to protein content were included in our compiled dataset (Appendix 3-Database) but were not used for further analysis given the low number of reported results. Additionally, when possible, we calculated $NAD(P)^+$/NAD(P)H ratios, as a reflection of

the redox state, as well as the total NAD(P)(H) levels ($NAD(P)^+$ + NAD(P)(H)) which are common reporting outputs for NAD(P)(H) fluxes. The extracted data also included the species, strains, age, sex, quantification method, diet and feeding schedule, sample type, and sample collection method and time of harvest (pre- or post-mortem).

The meta-analysis of NAD(H) data identified the mean physiological concentrations for NAD^+ and NADH in mouse (Fig. 3a-b, Supp. Fig. 4 a-b) and rat (Supp. Fig. 5a-b) tissues, from animals younger than 14 months for mice and 18 months for rats. The extracted range of physiological NAD^+/NADH ratio values and total NAD(H) levels (NAD^+ + NADH) were plotted for mice (Fig. 3c-d) and rats (Supp. Fig. 5c-d). Unlike the mouse studies, most of the reported rat data did not include the age of the animals, however we chose to include these data provided that the study did not classify their cohorts as aged. Of the most prominently studied tissues, this meta-analysis shows that the median NAD^+ level for liver (596 nmol/g, n=26) is higher than all other tissues in mice, while surprisingly skeletal muscle (162.8 nmol/g, n=9) exhibits one of the lowest median values per gram of tissue (Fig. 3a). These results may either imply a reduced efficiency in NAD^+ metabolite extraction, due to the highly fibrous nature of muscle, or that there are important differences in muscle NAD^+ metabolism when compared to other highly metabolic tissues, such as liver and kidney.

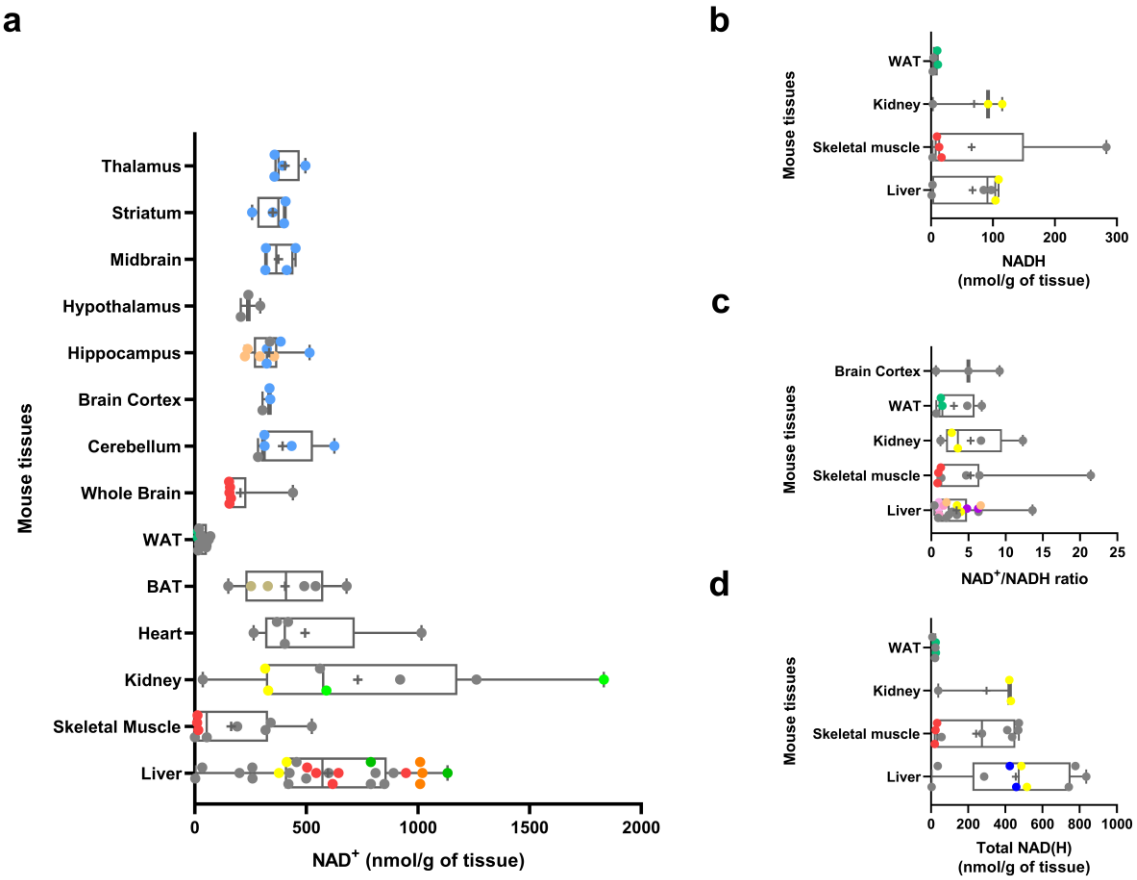

Figure 3: Reported physiological NAD$^+$, NADH, total NAD(H), and NAD$^+$/NADH ratio in mouse tissues with n≥3. a-d: Reported mean (a) NAD$^+$, (b) NADH, (c) NAD/NADH levels and (d) total NAD(H) in various mouse tissues (nmol/g of weight of tissue) collected from young (<14 months old) control mice. The boxes represent the 25th to 75th percentiles with the median represented by the line inside the box. The means are shown as "+" symbol. The whiskers cover the minimum to maximum values. For each study that included more than one measurement per tissue, similar colors were assigned to the corresponding datapoints. Datapoints colored in grey represent studies with just one reported measurement for a given tissue. WAT: white adipose tissue, BAT: brown adipose tissue.

Despite few quantitative aging studies, NAD$^+$ levels from aged mice were on average reduced in liver, muscle and retinal pigmented epithelium (RPE), when compared to their young cohorts, and in comparison to the mean of all studies performed with mice younger than 14 months of age (Supp. Fig. 6). A meta-analysis of NADH and the NAD$^+$/NADH ratio in aged animals was

not possible given that only one of these quantitative studies performed these measurements. These data demonstrate the lack of quantitative NAD(H) data in aging animals.

For the data retrieved from studies using healthy humans, the age ranges varied greatly across studies (from 15 to 92.3 years) and in most cases the data was not stratified across these ages. The most commonly measured human tissues included skeletal muscle and components of blood, due to their less invasive nature of collection (Fig. 4a-d). Results from other human tissues (n=1-2) are displayed in supplementary figure 7. This analysis exhibited a median NAD^+ concentration of 44.62 nmol/ml (n=23) in whole blood, with similar NAD^+ concentrations reported for red blood cells at 46.96 nmol/ml (n=7) (Fig. 4a; Supp. Table 3). However, blood plasma NAD^+ levels were substantially lower with a median of 0.37 nmol/ml (n=8) (Fig. 4a). The median NAD^+ levels found in skeletal muscle of humans was 191.9 (n=4) nmol/g in wet muscle preparations versus 1713 (n=3) nmol/g in freeze-dried preparations, a low temperature dehydration process that likely concentrates metabolites (Fig. 4a). In the more commonly investigated tissues for NADH measurements, the median levels in human red blood cells, plasma and freeze-dried skeletal muscle were 1.75 nmol/ml (n=7), 0.39 nmol/ml (n=8) and 136.8 nmol/g (n=6), respectively (Fig. 4b). The corresponding median NAD^+/NADH ratios were 23.65 (n=8), 1.57 (n=7) and 12.7 (n=3) (Fig. 4c). Interestingly, the median NAD^+/NADH ratio for red blood cells (23.65) and freeze-dried skeletal muscle (12.7) (Fig. 4c) were several fold higher than most mouse and rat tissues (Fig. 3c and Supp. Fig. 5c), indicating a highly oxidative redox state with an abundance of available NAD^+ in these human tissues. In the case of muscle tissue, this could have implications when considering the translational potential of rodent studies that have identified the benefits of boosting NAD^+ levels in muscle. However, an elevated NAD^+/NADH ratio in muscle may also be the result of

delayed sample freezing procedures in a clinical environment, which may lead to non-physiological changes in sample redox status.

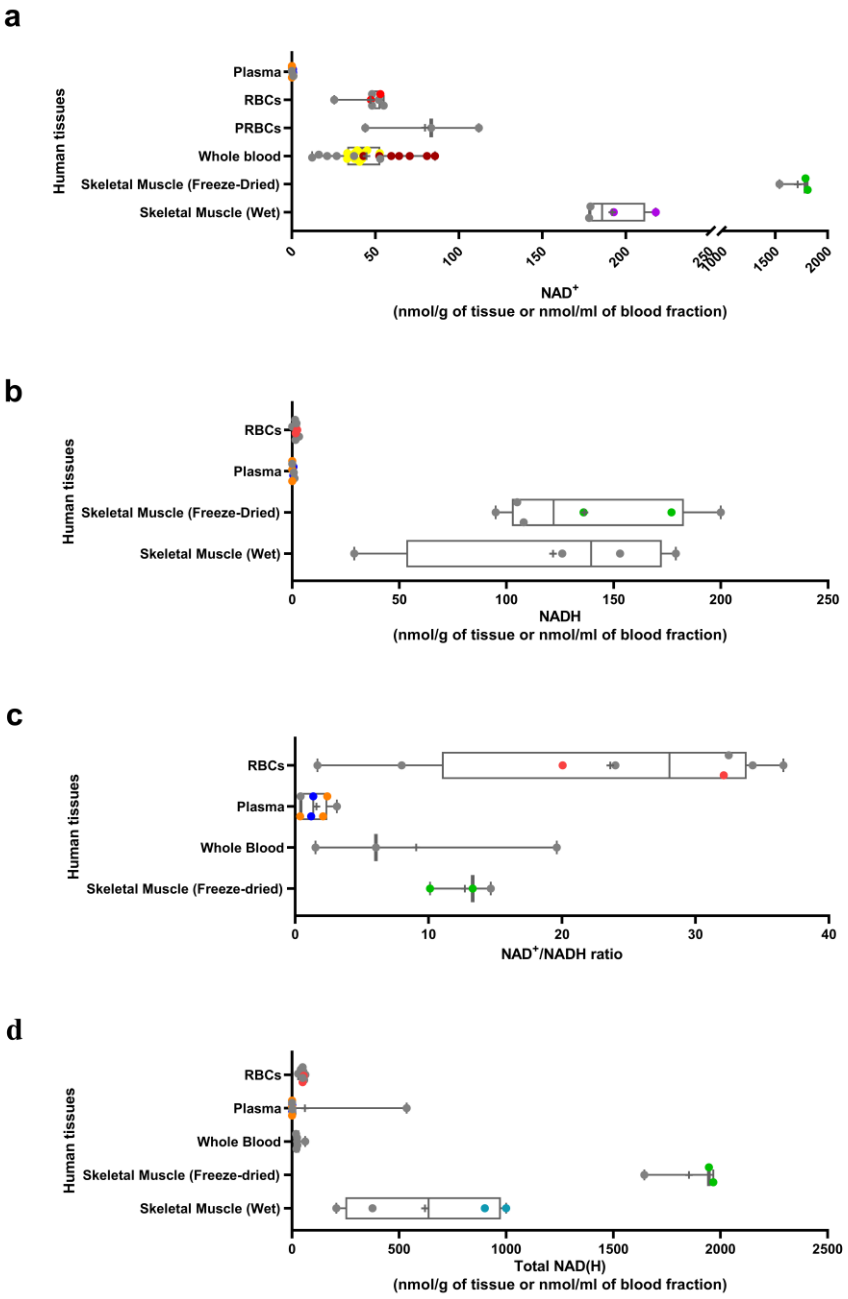

Figure 4: Reported physiological NAD$^+$, NADH, total NAD(H), and NAD$^+$/NADH ratio in human tissues with n≥3. a-d: Reported mean (a) NAD$^+$, (b) NADH, (c) NAD/NADH levels and (d) total NAD(H) in various human tissues (nmol/g of tissue weight or nmol/ml of blood fraction). The boxes represent the 25th to 75th percentiles with the median represented by the line inside the box. The means are shown as "+" symbol. The whiskers cover the minimum to maximum values. For each study that included more than one measurement per tissue, similar colors were assigned to the corresponding datapoints. Datapoints colored in grey represent studies with just one reported measurement for a given tissue. PRBCs: packed red blood cells, RBCs: red blood cells.

The physiological NADP(H) levels in rodent tissues were compiled, with the most common measurement being in liver. Mouse liver exhibited a median value of 124.2 nmol/g of $NADP^+$ (n=13) and 140.2 nmol/g of NADPH (n=4) (Fig. 5a,b), while rat liver showed a median of 95.11 nmol/g of $NADP^+$ (n=10) and 240.7 nmol/g of NADPH (n=9) (Supp. Fig. 8a,b). The median $NADP^+$/NADPH ratio, derived from studies that measured both metabolites, was lower than 1 in most mouse and rat tissues (Fig. 5c, Supp. Fig. 8c). The median total NADP(H) levels in mouse and rat liver were 244.4 (n=3) (Fig. 5d) and 342.1 (n=9) (Supp. Fig. 8d), respectively. In humans, the most common measures of NADP(H) were performed in red blood cells showing a median of 33.2 nmol/ml for $NADP^+$ (n=14) and 22.4 nmol/ml for NADPH (n=12) from non-matching studies, with a median $NADP^+$/NADPH ratio of 1.27 and a median total NADP(H) of 52.0 nmol/ml from studies that measured both metabolites (n=11) (Fig. 5e-h). Overall, the amount of data available for NADP(H) is sparce in all species leading to lower confidence in the median values for each tissue.

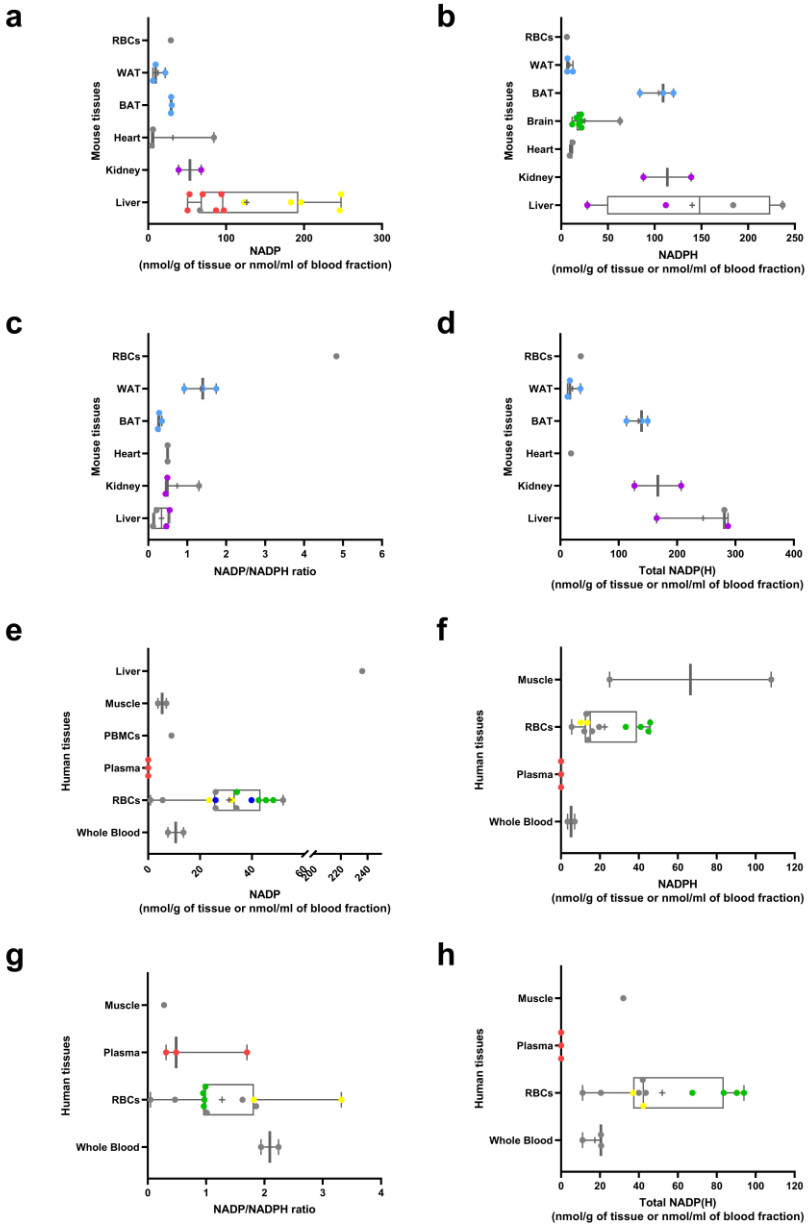

Figure 5: Reported mean physiological $NADP^+$, NADPH, total NADP(H), and $NADP^+$/NADPH ratio in mouse and human tissues. a-d: Reported mean physiological (a) $NADP^+$, (b) NADPH, (c) $NADP^+$/NADPH levels and (d) total NADP(H) in mouse tissues (nmol/g of tissue weight or nmol/ml of blood component) collected from young (<14 months old) control mice. e-h: Reported mean physiological (e) $NADP^+$, (f) NADPH, (g) $NADP^+$/NADPH levels and (h) total NADP(H) in human tissues. The boxes represent the 25^{th} to 75^{th} percentiles with the median represented by the line inside the box. The means are shown as "+" symbol. The whiskers cover the minimum to maximum values. For each study that included more than one measurement per tissue, similar colors were assigned to the corresponding datapoints. Datapoints colored in grey represent studies with just one reported measurement for a given tissue. PBMCs: peripheral blood mononuclear cells, RBCs: red blood cells, WAT: white adipose tissue, BAT: brown adipose tissue.

2.3.3. Analysis of bias and variability in NAD(P)(H) quantification methods

Given that a majority of the studies included in this meta-analysis examined NAD^+ levels in rodent liver samples (Fig. 2c and 2e), we used both mouse and rat liver physiological NAD^+ levels to identify any potential bias in the results that corresponds to the quantification method (Fig. 6a, b). The mean age of mice included in this analysis was 17.9 weeks (Range: 2 – 55 weeks), with 6 studies not disclosing the age of the animals. For rats, most studies did not disclose the age of the animals except three that ranged from 2 days to 8 months. None of the studies reported the use of old animals. In mouse liver, the large range of the reported concentrations for NAD^+ spanned from 1.8 to 1132 nmol/g of liver with a mean value of 596.0 (n=26) (Fig. 6a), while NADH concentrations ranged from 0.9 to 109 nmol/g of tissue with a mean value of 66.43 (n=6) (Supp. Fig. 9a). Importantly, a coefficient of variation of 52.5% and 76.5% was calculated for the mean physiological NAD^+ and NADH results in mouse liver, respectively, as measured by multiple quantification methods, showing the extent of the variability across studies. As predicted from these results, the mean NAD^+/NADH ratio in mouse liver (3.41 +/- 3.16 S.D., n=19) demonstrated an equally large range of variability with a C.V. of 92.7% (Supp. Fig. 9c). Similar variability in NAD^+ and NADH measures were also observed in rat liver (CV=42.6% for NAD^+ and CV= 44.4% for NADH). The corresponding concentrations for NAD^+ and NADH in rat liver ranged from 159 to 796 (n=16) and 65 to 265 (n=12) nmol/g, respectively (Fig. 6b, supp. Fig. 9b), while the NAD^+/NADH ratios exhibited a C.V. of 50.1% (Mean: 3.219 +/- 1.612 S.D., n=23) (Supp. Fig. 9d). The mean values and standard deviations for NAD^+, NADH, total NAD(H) and the NAD^+/NADH ratio data in mouse and rat liver, grouped by quantification method, are shown in supplementary table 4. Concerning NADP(H) levels and the NADP/NADPH ratio, similar variability was observed in liver tissues. NADP levels ranged from 50.4 to 247.4 nmol/g of tissue

for mice (Supp. Fig. 10a) and from 45.7 to 171 nmol/g of tissue for rats (Supp. Fig. 10b), while NADPH levels ranged from 28 to 236.9 nmol/g of tissue for mice (Supp. Fig. 10c) and from 90 to 409 nmol/g of tissue for rats (Supp. Fig. 10d). Lastly, the NADP/NADPH ratio ranged from 0.12 to 0.55 in mouse liver (Supp. Fig. 10e) and from 0.12 to 1.44 in rat liver (Supp. Fig. 10f).

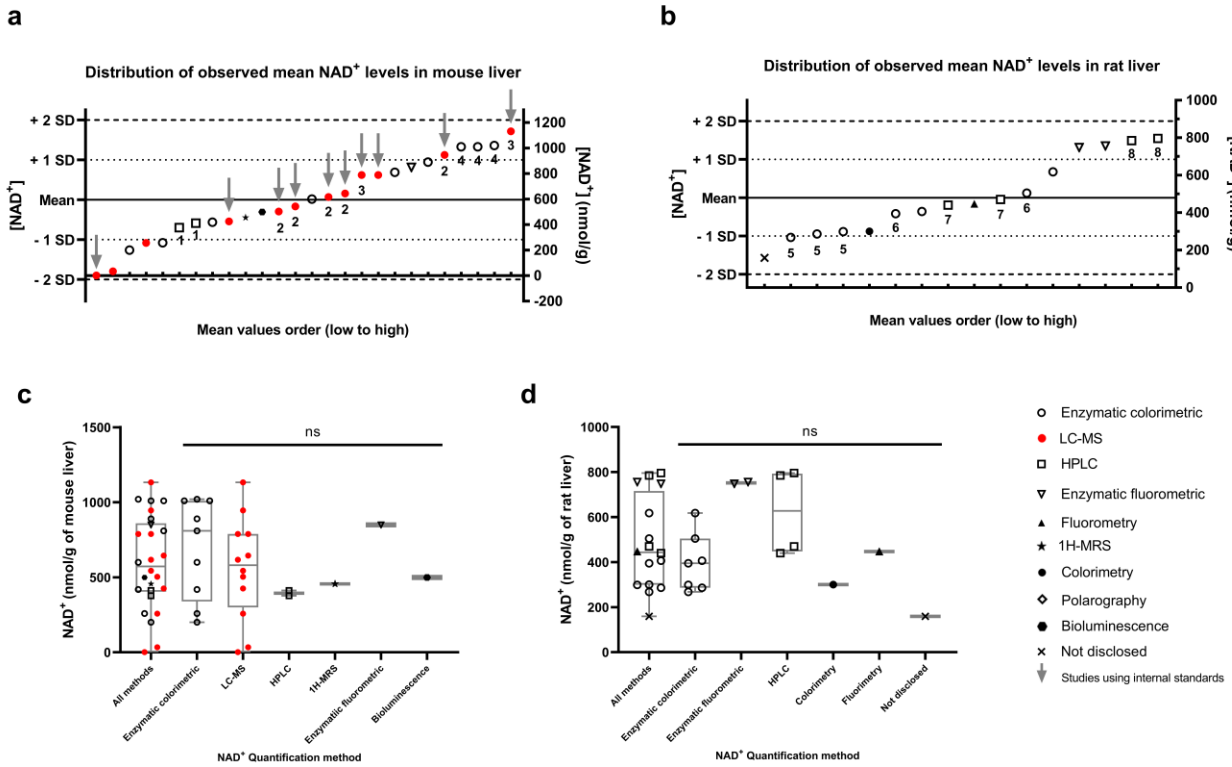

Figure 6: Distribution histogram of reported physiological NAD$^+$ levels in mouse and rat liver. Mean NAD$^+$ values measured using different quantification methods in (a) mice and (b) rat liver sorted from lowest to highest value (nmol/g of tissue weight). The represented data was collected from young control mice (<14 months old) and rats (<18 months old). For each study that included more than one measurement per tissue, the datapoints are labeled using a number that represent the study, respectively: 1: Gaikwad *et al.* (2001), 2: Dall *et al.* (2019), 3: Trammell *et al.* (2016), 4: Dietrich *et al.* (1968), 5: Ballard (1971), 6: Slater, Sawyer & Sträuli (1964), 7: Wendt *et al.* (2019), 8: Kiehlbauch *et al.* (1993). Arrows indicate LC-MS measurements that included the use of internal controls. NAD$^+$ levels in (c) mouse and (d) rat liver segregated by quantification method. A One-way ANOVA with Sidak *post hoc* test was conducted to compare the effect of the quantification methods on NAD$^+$ levels and did not show any significant differences between methods.

When specifically examining the variability of NAD^+ measures there was no significant differences between any particular quantification method in mice or rats (Fig. 6c-d). Even when considering the variability of the mouse liver NAD^+ data from LC-MS measurements, the method with the best array of potential controls, culminated in the largest range of results (1.8 to 1132.3 nmol/g). Even the most recent LC-MS studies examined exemplified the range of these NAD^+ values, including values of 1.8 nmol/g (165) and 33.8 nmol/g (166) and much higher values of 946.3 nmol/g (167) and 1132.3 nmol/g (28). In addition, the large range of LC-MS NAD^+ values did not appear to correlate to studies that excluded isotope-labeled internal standards (Fig. 6a), a method used to improve the identification of the metabolite and accuracy of the quantified value. However, the two identified LC-MS studies that relied solely on an external standard curve for NAD^+ quantification, rather than including an internal control, were on average lower than the mean for all measures (Fig. 6a). Further, the studies using internal standard normalization used different types of internal standards, such as the inclusion of a single labeled reference metabolite (168, 169) or labeled metabolite extracts from yeast (28, 167) or cell cultures (165). Interestingly, these studies that used yeast or cell culture extract-derived standards provided either the highest or lowest LC/MS-derived measures for liver NAD^+ levels. This potentially emphasizes how cellular extracts of isotope-rich standards can contribute to the variability in NAD^+ measurements as the matrix effect of the added standard yeast or cellular extract could interfere with the ionization efficiency and consequently the measured concentrations of the target metabolites.

The limitations of this analysis of quantification bias and variability include potential differences in environment, genetic background, sacrifice, sex, and age. All data for this analysis came from animals on chow diet but may differ in type. Upon sacrifice there are reported differences in fed or fasted state of the animal and time of day for sacrifice. Additionally, most

mouse studies were performed on a C57BL/6 background. Although the C57BL/6J substrain carries a mutation in the nicotinamide nucleotide transhydrogenase (Nnt) gene, coding for the mitochondrial $NADP^+$ transhydrogenase NNT(170), no significant difference in the liver NAD^+ levels was observed between C57BL/6J and C57BL/6N substrains with an average NAD^+ concentration of 587+/-319 S.D. (n=6) and 537+/-388 S.D. (n=5) nmol/g of liver, respectively. There was also no significant difference between these two substrains and the rest of the data including other substrains and unknown genetic background (Mean: 753 +/- 305 S.D., n=15). Unfortunately, there were no liver NADP(H) results from C57BL/6N mice among the analyzed studies for comparison. For rats, there was a larger range of backgrounds used for rats across studies (Wistar: 38%, Albino Wistar: 25%, and 6% for Hooded Wistar, Sprague-Dawley, Holtzman, ACI, Long-Evans and Zucker rats). Concerning the sex dimorphism, there were no statistical differences between male or female values for NAD^+, NADH, or total NAD(H) levels or for the NAD^+/NADH ratio across mouse liver studies (Supp. Fig. 11). Similar results were obtained by studies comparing NAD(H) levels between male and female (171, 172) mice although multiple studies have shown the important role of sex in the prevalence/occurrence/frequency of obesity, diabetes, and metabolic syndrome (173–175). A similar conclusion was obtained by our meta-analysis but we cannot draw definitive conclusions due to the limited number of female cohorts. Thus, it is unlikely that the variability in the measured NAD^+ results could be solely attributed to a specific genotype, sex, or quantification method but rather to a combination of various pre-analytical and analytical factors.

2.3.4. The effect of pre-mortem versus post-mortem tissue collection on NAD(P)(H) levels

We predicted that there may be some observable difference in NAD(P)(H) redox state that is dependent on tissue harvesting procedures. To answer this question, we examined the effect of pre- versus post-mortem tissue collection procedures on NAD(P)(H) redox status. For this analysis, we compared values from rat liver tissues given the larger number of studies defining their sacrifice protocol. When disclosed, all the reviewed studies stated that the tissue samples were kept cold and immediately extracted on ice or frozen at - 80°C prior to NAD(P)(H) measurements. This analysis determined that there was no significant difference in NAD^+ concentrations in rat liver (Fig. 7a) between tissues extracted before or after euthanasia. However, the reported NADH levels in rat liver are significantly higher in post-mortem samples (Fig. 7b). No differences in total NAD(H) levels (Fig. 7c) were observed but the NAD^+/NADH ratio was lower in tissues collected following euthanasia (Fig. 7d), which is consistent with the variation observed in NADH levels. NADP, NADPH, and the NADP/NADPH ratio results in rat liver grouped by tissue harvest timepoint are shown in supplementary figure 12; however, the insufficient number of pre-mortem samples does not allow us to interpret the effect of tissue harvest timepoint on NADP(H) levels. In mouse liver, there was no difference between pre- and post-mortem NAD^+ levels; however, the number of reporting studies was limiting (Fig 7e). No NADH, NADP, or NADPH pre-mortem data in mouse liver was available for comparison.

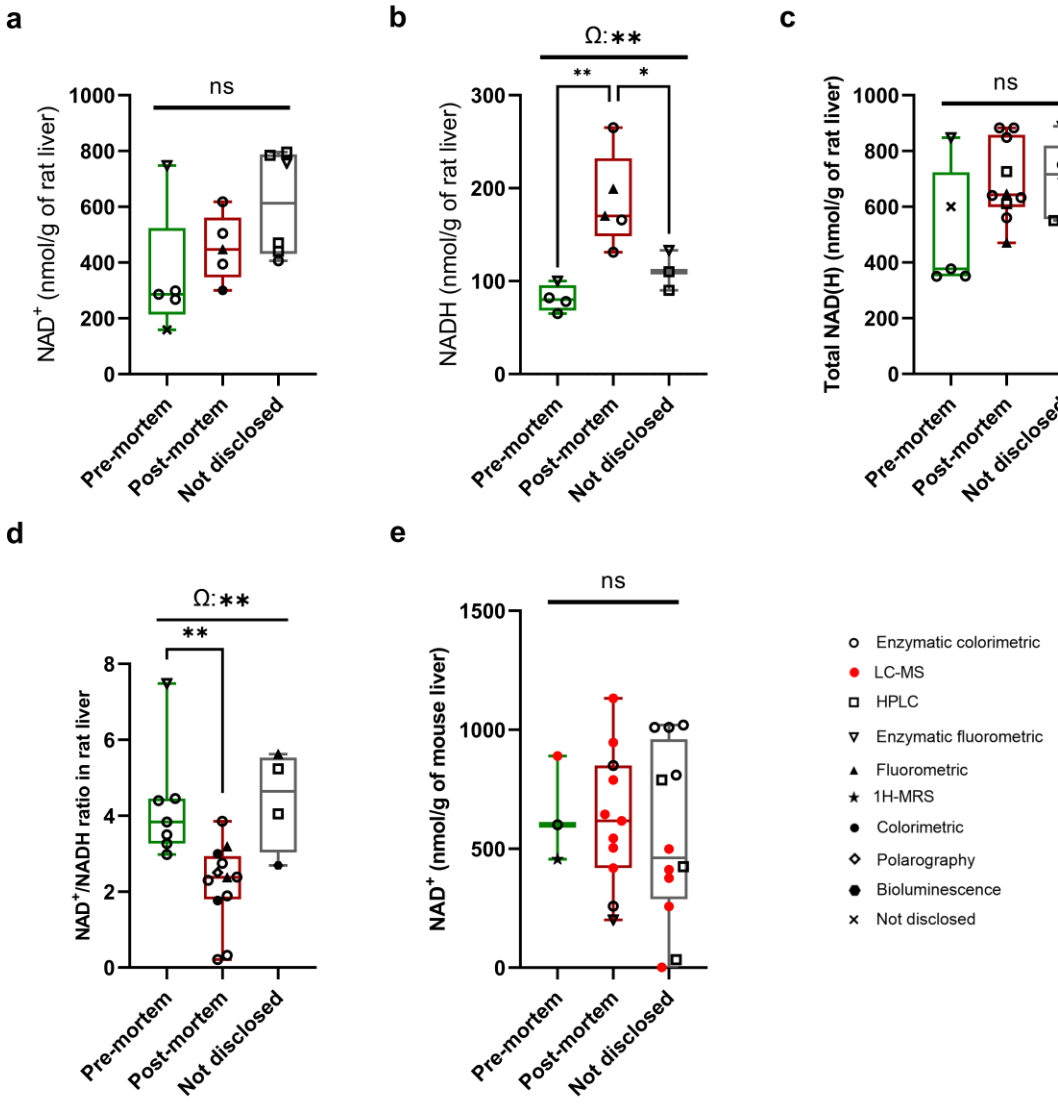

Figure 7: Effect of pre- versus post-mortem tissue collection on NAD(H) levels. a-d: Reported (a) NAD^+, (b) NADH, (c) total NAD(H) levels, and (d) NAD^+/NADH ratio in young (<18 months old) control rat liver samples harvested at different timepoints relative to sacrifice. e: NAD^+ levels in young (<14 months old) control mouse liver samples harvested at different timepoints relative to sacrifice. Boxes represent 25th and 75th percentile with median line. Whiskers show min. to max. values. Statistical significance was determined by one-way ANOVA with multiple comparisons using Tukey's test as *post hoc* test, setting $P < 0.05$ (*) and $P < 0.005$ (**) as significant. Ω: Overall effect of harvest timepoint relative to sacrifice.

2.4. Discussion

Many recent studies have demonstrated that NAD(P)(H) regulation is essential for cellular homeostasis and redox status. Data obtained from rodents have led to studies examining human blood NAD^+ levels, as a less invasive indicator of whole-body NAD^+ levels. Recent clinical studies demonstrated that NAD^+ levels were reduced in disease states (81, 176) and elevated following NAD^+ boosting strategies (28, 81, 177, 178). We performed a meta-analysis of all studies published between 1946 and June 20, 2021 that contained quantitative data for NAD(P)(H) levels in mammalian species with a special focus on mice, rats, and humans as they represent the most studied species in the biomedical field. This analysis was done in part to determine the mean standard level of NAD(P)(H) concentrations in normal mammalian tissues given the well-known variance in these measures across studies. We hope that these data can be used to stimulate standardized protocols in the field of NAD^+ research and to promote the use of NAD(P)(H) levels and redox ratios as reliable biomarkers for disease and treatment regimens.

Despite considerable variability in measures across rodent tissues, this meta-analysis displayed similar mean NAD^+ levels across tissues with some exceptions. Interestingly, mouse skeletal muscle exhibited lower median NAD^+ levels (Fig. 3a) than other highly metabolic tissues (i.e., liver, kidney, heart, and brain). This may indicate different NAD(H) redox status in skeletal muscle or may point to greater issues with metabolite extraction in fibrous tissues. However, these observations could not be verified in humans due to a lack of sampled tissues beyond blood and muscle.

Many potential factors could affect the accuracy of physiological NAD(P)(H) measurements in tissue samples, including pre-analytical parameters related to the research

subjects (i.e., sex, genetic background, age, diet, and feeding schedule) or to the sample storage and processing. When reported, all studies described tissues as being harvested and directly submerged into liquid nitrogen, or kept on ice before freezing or processing in order to preserve the heat-sensitive fractions (NAD^+ and $NADP^+$). The effect of pH on the various NAD(P)(H) fractions, such as the acid-labile nature of the reduced NAD(P)H forms, has lead to the use of pH-neutral extraction solvents by the majority of the studies. However, given the rapid interconversion of the reduced and oxidized metabolites and the effect of anoxia on NAD(H) (179–182), it is also important to ensure rapid extraction of tissue metabolites and the appropriate procedures for quenching cellular NAD(P)(H)-redox/consumption enzymes, such as through deproteinization. Along these lines, our analysis of pre- versus post-mortem tissue collection indicates that post-mortem analysis favors the reduction of NAD^+. The reduction of tissue NAD^+ has been previously described *in vivo* in the brain, heart and liver of rats exposed to an extended 2.5-hour hypoxic atmosphere (183), an environment that may be partially recapitulated by extended periods of post-sacrifice tissue collection before snap-freezing. This may indicate that extracting tissues while under anesthetic, or prioritizing the immediate harvest of tissues intended to be used for metabolite analysis post-sacrifice, should occur to obtain representative NAD(P)(H) measurements.

There is also the potential for various quantification methods, each having different limitations, to contribute to the overall intra-study variability of NAD(P)(H) measurements. In the last two decades, the most frequently used methods were enzyme cycling assays, LC-MS, and HPLC. Each of these methods is affected by metabolite extraction techniques, quantification parameters, and the implementation of proper quality controls. Using LC-MS, Lu *et al*. (2018) have shown that the interconversion between reduced and oxidized forms of NAD(P)(H) metabolites occurs at different rates in various extraction buffers or solvents with the

acetonitrile:methanol:water with 0.1 M formic acid mixture yielding the highest recovery with the least interconversions (159). However, when using LC-MS this interconversion can be monitored between individual samples of a study by spiking with internal controls such as NAD(P)(H) isotopes, which is an advantage of the LC-MS technique over that of HPLC and enzyme cycling assays (142, 159, 184). Nonetheless, even with well-controlled LC-MS techniques, various factors can interfere with the measured signal, including matrix effects and variations in ionization efficiency. For example, some studies use ^{13}C-labeled yeast extracts as internal standards in LC-MS-based metabolomics. However, spiking the extracted sample metabolite matrix with a ^{13}C-labeled yeast extract metabolite matrix can have various consequences, such as ion suppression, which reduces the signal of labeled and/or unlabeled metabolites, and can lead to errors in the absolute quantification if not detected by a thorough quality assessment (185). Also, although LC-MS techniques theoretically allow for the measurement of multiple NAD(P)(H) metabolites in one experiment, there are still limitations since optimal dilutions must be run if the metabolites of interest have large differences in concentrations. Thus, despite their advantages over the simpler enzyme cycling assays, the complexity of LC-MS methods imposes the necessity for thorough optimization. Recently, new analytical methods, such as NAD^+ biosensors and imaging-based mass spectrometry, have been developed but there is still insufficient quantitative data generated from these techniques to include in a meta-analysis. Although, one study included in our meta-analysis used a paper-based bioluminescent biosensor to measure NAD^+ levels in mouse liver and other sample types (186). This study was included in the bioluminescent assays group due to the similar method of detection (Fig. 2a).

For the purpose of this analysis, data from 677 studies were excluded. This included studies that provided relative NAD(P)(H) results (51%) rather than quantitative, as well as studies

in which NAD(P)(H) concentrations were not normalized to tissue weight, protein content, or blood volume (13%). 36% of the excluded studies were performed on non-suitable specimens (e.g., non-mammalian subjects, cell or tissue cultures). Beyond the excluded studies, major limitations in this meta-analysis include the variation of, or lack of reported information related to, pre-analytical procedures (pre- or post-mortem extraction or extraction buffer information) and/or the analytical methods, along with the age, sex, genetic background, diet and feeding status at sacrifice for rodents.

Although our meta-analysis highlights the inter-study variability and the necessity to standardize NAD(P)(H) quantitative measurements, our analysis does not assess or debate the validity of the comparative results within an individual study. Given the implications of multiple NAD(P)(H) metabolites serving as biomarkers of health in humans, the standardization or thorough study optimization of pre-analytical and analytical procedures will allow for better comparisons of results across studies. This becomes even more crucial with an increasing number of clinical studies testing the effect of drugs or supplements used to alter tissue NAD(P)(H) levels to improve health in humans.

Chapter 3: Quantitative targeted LC-MS-based NAD metabolomics method using stable isotopic internal standards

3.1. Introduction

The temperature and pH sensitivity, as well as the inherent redox properties of NAD(H) and NADP(H), make their accurate quantification in tissue and blood samples challenging. Even though LC-MS techniques are the most sensitive methods for the simultaneous quantification of NAD and its metabolites, they are still not widely used because of the tedious method development, the numerous execution steps (tissue processing, metabolite extraction, preparation of tissue extracts for analysis, incorporation of external and internal quality, as well as the cost of equipment and consumables. Additionally, the data analysis phase is crucial to assess the quality of the raw data and translate it into meaningful results.

As seen in the previous chapters, multiple methods have been used to measure NAD^+ and its metabolites, such as enzyme cycling methods, HPLC coupled to UV or fluorometric detection, NMR, bioluminescence, and polarography. However, these methods are not as sensitive or specific as LC-MS. In some cases, when the focus is on the quantification of NAD^+, $NADP^+$, and their reduced forms, enzyme cycling methods can be more practical as they are relatively inexpensive, fast, and easy to implement, especially when commercial kits are available. Additionally, they only require spectrophotometers, which are available in most research and medical laboratories. The interpretation of the results is also easier than LC-MS even though they are less specific and can lead to erroneous results in the case of contamination or interferences from other substances in the samples. Further, these methods don't offer the advantage of the simultaneous screening of the entire metabolome, which is possible with LC-MS. Thus, using LC-MS can provide quantitative

metabolomics measurements and give a clear picture of the entire NAD^+ metabolome, including metabolites involved in the biosynthesis, regeneration, or degradation of NAD(P)(H).

At the moment, there is no standard LC-MS methodology for the study of the NAD^+ metabolome. The few studies that have published quantitative LC-MS NAD metabolomics results have used various protocols. For example, focusing on the metabolite extraction and enzyme inactivation/quenching, Trammell and Brenner (2013) (141) developed an optimized NAD metabolite extraction using boiling ethanol on mammalian cells, inspired by previous NAD metabolite extraction methods applied to yeast cells (187–189). Other studies have used cold 80% methanol for metabolite extraction from mammalian cells (190) and plasma (191). Later on, Lu *et al.* (2018) (159) compared 7 different extraction solvents: a cold aqueous buffer with and without detergent, a hot aqueous buffer, and cold organic solvents (80% methanol, buffered 75% acetonitrile, and acidic 40:40:20 acetonitrile:methanol:water with either 0.02 M or 0.1 M formic acid). They showed that the organic solvents yielded the best extraction efficiency with the least interconversions between the oxidized and reduced NAD(P)(H) metabolites. The generally recognized pre-analytical conditions, such as low temperatures, minimal handling (time), avoiding extreme pH, and enzyme inactivation early in metabolite extraction process, ensures the stability of the various forms of NAD(P)(H) (159, 190, 192, 193). Even though the metabolite extraction step is critical, other factors can also influence the quantification, such as the type of chromatographic column and mobile phases, the mass spectrometry equipment and parameters, and the choice of quality controls. Another challenge faced when studying the NAD^+ metabolome is the large range of concentrations of the metabolites of interest. The dilution of samples is often required prior to LC-MS measurements; however, when examining multiple NAD^+-related metabolites, the ideal dilution may be difficult to obtain. This can then be compounded when

comparing tissues with and without NAD^+-altering treatments. Therefore, the main aim of this chapter is to thoroughly describe the steps of our LC-MS method development and optimization for NAD metabolomics, including the preparation of a ^{13}C-labeled internal standard from a yeast culture.

3.2. Materials and Methods

3.2.1. Materials and reagents

High-purity LC-MS grade metabolite standards were obtained from various suppliers. ADPR was purchased from Santa Cruz Biotechnology, Inc. (Dallas, Texas, U.S.A.). Me2PY and Me4PY were purchased from Toronto Research Chemicals (Toronto, Ontario, Canada). The rest of the metabolite standards were purchased from Sigma-Aldrich Canada Co. (Oakville, Ontario, Canada). Nicotinamide riboside chloride (Niagen®) was obtained from ChromaDex inc.

^{13}C-labeled metabolite standards were prepared by growing yeast in minimal media containing U-^{13}C-glucose followed by metabolite extraction. All the yeast minimal media constituents including the D-Glucose-13C6 (≥99 atom % 13C) were obtained from Sigma-Aldrich Canada Co. (Oakville, Ontario, Canada) except potassium chloride KCl (J.T.Baker) and calcium chloride dihydrate CaCL2*2H2O (ThermoFisher Scientific). The commercial ^{13}C-labeled metabolite yeast extract (U-13C, 98%) from the Cambridge Isotope Laboratories inc. was purchased from the local distributor ACP Chemicals Inc. (Montreal, Quebec, Canada).

LC-MS grade solvents were provided by the uOttawa metabolomics core. Methanol, acetonitrile, ammonium formate, ammonium acetate, and formic acid (Optima™ LC-MS) were purchased from Fisher chemicals, dichloromethane, (HPLC plus, ≥99.9%) from Sigma, and the Infinity Lab deactivator additive was purchase from Agilent technologies.

To minimize contamination and variations between batches, similar high-quality microcentrifuge tubes were used for all standards and samples: Qiagen sample tubes RB 2 ml and Eppendorf tubes 5 ml.

3.2.2. Animal protocols

3 months old C57BL/6J female mice were fed a chow diet and kept under a 12:12-h light-dark cycle. 7 control mice were anesthetized by intra-peritoneal (I.P.) injection of 100 µl of Euthanyl (Pentobarbital sodium: 65mg/ml) until non-responsive. Pre-mortem tissue samples were extracted and snap-frozen in liquid nitrogen: Liver, one kidney, one skeletal muscle of each type (Gastrocnemius, tibialis anterior, soleus). For euthanasia, mice received a second I.P. injection of 150 µl of Euthanyl and a cervical dislocation was performed. In the same mouse post-mortem samples of a different lobe of liver, kidney, and skeletal muscle were harvested 8 minutes after euthanasia and snap-frozen. For each mouse, tissues were obtained in the same order and for the liver, we extracted the same location on the same lobe of liver for pre- and post-mortem sacrifices. After snap freezing, samples were kept at -80°C. The animal use protocol (MEe-1772-R5 A1) was approved by the Animal Care Committee (ACC) of the University of Ottawa.

Previously frozen tissue samples were placed inside aluminum foil pockets and powdered in an enclosed pouch on an aluminum block using a hammer, both cooled with liquid nitrogen. Samples were processed quickly while enclosed in aluminum pouches to avoid condensation around each tissue. The hammer and block were cooled between samples. Powdered tissues were immediately stored at - 80 °C until analysis.

3.2.3. Liver sample processing for LC-MS metabolomics analysis

Approximately 40 mg (+/- 10%) of each powdered liver sample was immersed in 1800 µl of 80% methanol pre-cooled to -80°C then homogenized with four 2.8 mm ceramic beads using

the MagNa Lyser bead homogenizer at 2000 rpm for 45 seconds. Bead beating is repeated until the tissue was completely disrupted (Generally 2 to 3 cycles). Between beatings, tubes were kept on dry ice.

For lipid removal, 1800 µl of dichloromethane at - 20°C and 900 µl of ice-cold water were added to the methanolic extract (194). The samples were vigorously vortexed and left to partition on ice for 10 minutes. After centrifugation, the upper aqueous phase containing the water-soluble metabolites was aliquoted and dried overnight. While various drying methods have been tested at various temperatures (141, 159), we took advantage of the availability of an exclusive refrigerated centrifugal concentrator (Labconco Refrigerated CentriVap Benchtop Vacuum Concentrator) that allows drying at low temperatures (-4°C). This allowed us to maintain the samples at low temperatures during all the pre-analytical steps. The dried extracts were then frozen at - 80°C until analysis.

3.2.4. Preparation of ^{13}C-labeled yeast internal standards

To produce a ^{13}C-labeled internal standard mix, we cultured the yeast *Pichia pastoris*, also known as *Komagataella phaffii*, in minimal media containing ^{13}C-labeled glucose (10 g/L). Media composition is detailed in supplementary table 5 and was adapted from Neubauer *et al.* 2012 (195). The media was sterilized by membrane filtration (Pore size: 0.2µm). The lyophilized yeast sample (Strain: ATCC 76273) was reconstituted according to enclosed instructions and grown in minimal media with unlabeled glucose. From this culture, a 15% glycerol yeast stock using 30% glycerol v/v with minimal media was produced and frozen in a cryovial at -80°C. For the yeast revival, the glycerol stock was maintained on dry ice and a small piece of the frozen stock was scraped with a sterile stainless-steel spatula and used to inoculate solid YPD (yeast extract peptone dextrose) agar media in a 100 mm Petri dish (Media composition: yeast extract 10g/L,

peptone 20g/L, D-glucose 20g/L, and agar 15 g/L). Using the streaking technique, the inoculum was spread over the agar plate and incubated at 28°C for 24 to 48 hours. When white round smooth colonies appeared, one colony was picked with a sterile spatula to inoculate 10 ml of fresh sterile ^{13}C-labeled minimal media (pre-culture). The pre-culture was incubated at 28°C in a shaking incubator (250 rpm). To follow the yeast growth, 10 ml of unlabeled media (control media) was also inoculated and sampled at various timepoints to check the OD600. When the OD600 of the control media reached 1, the OD600 of the ^{13}C-labeled media was measured. When the OD600 of the ^{13}C-labeled media was approximately 1 (after 48 to 72 hours of incubation), 90 ml of the ^{13}C-labeled minimal media was inoculated with the pre-culture (10 ml) and incubated in a sterile 1000 ml flask connected by autoclaved tubing to 2 flasks of potassium hydroxide (KOH) solution (4 mol/L) and 1 flask of sterile water (250 ml of KOH or water in 500 ml flasks). Air was directed through the first flask of water via tubing capped with a 0.2 µm syringe filter (Fisherbrand™ Basix™), then through the flasks of potassium hydroxide before supplying the flask of yeast with air. The potassium hydroxide solutions allow the absorption of carbon dioxide (CO_2) from the air to minimize the incorporation of ^{12}C atoms into the yeast metabolites (195). A vacuum pump (Millipore Pump XX5500000) connected to the yeast culture flask was used to maintain negative pressure and sufficient airflow into the culture media (Supp. Fig. 13a). The entire system was maintained inside a shaking incubator set to 28°C / 250 rpm. To determine the exponential growth phase and the optimal time of harvest, a culture with unlabeled glucose was performed under identical conditions that allowed the construction of a growth curve (Supp. Fig. 13b). To obtain a sufficient amount of yeast cells and a balanced metabolome with no excess degradation metabolites, yeast growth in the ^{13}C-labeled media was stopped at 18 hours. The OD600 was measured to calculate the yield of the culture knowing that an OD600 of 1 corresponds to ~3x 10^7

cells/ml. The media was split into 2 sterile centrifuge tubes and centrifuged at 4000g for 10 minutes at +4°C. The media was removed, and the yeast pellet was washed with sterile water then either frozen at -80°C or extracted immediately.

Two methods were used to produce the ^{13}C-labeled internal standards from the yeast pellets: the standard 75% boiling ethanol extraction, as performed by Neubauer *et al.* (2012) (195), and the cold 80% methanol extraction, which is similar to our metabolite extraction procedure for tissues. The boiling ethanol method used 75% ethanol tempered at 85°C to resuspend the yeast pellet. The volume of ethanol was calculated according to the desired final cell count number (Target cell count: 8-16 x 10^7 cells in each 80 µl aliquot). The yeast pellet was vigorously vortexed for 10s and incubated at 85°C for 3 minutes, 1.5 minutes, and 3 minutes with vigorous vortexing in between. The extract was rapidly cooled on ice and centrifuged at 4000g at -4°C for 5 minutes. The ethanolic extract was decanted and centrifuged a second time at 4000g at -4°C for 5 minutes to remove all cell debris. Finally, ethanolic extracts were pooled and split into an appropriate number of aliquots to obtain the desired cell count and to avoid freeze-thaw damage to the sample.

3.2.5. Preparation of calibration standards for NAD metabolomics analysis

NAD^+-related metabolites were resuspended to obtain 10 mg/ml stock solutions, except for cADPR which was reconstituted at 0.6 mg/ml. Stock solutions of all metabolites were mixed and diluted to produce an NAD standard mix (NSM) containing all the cited metabolites. After drying and reconstituting in 200 µl of solvent (75% acetonitrile or ^{13}C-labeled yeast extract reconstituted in 75% acetonitrile), all the metabolites will be at a concentration of 50 µM, except for NR, nicotinuric acid (NUA) (final concentration of 5 µM), and cADPR (final concentration of 3 µM)). The NSM was further diluted in series (1:2:2:2:2:2:5:2:2:2:2) to obtain 11 points calibration curves to quantify NAD^+-related metabolites (NSM1-NSM11). The concentrations of

the NAD^+-related metabolites in each NSM are shown in supplementary table 6. 2µl of each dilution (with and without internal standard) was injected into the LC-MS system starting with the lowest dilution first to avoid carryover from the more highly concentrated calibration points.

3.2.6. Targeted LC-MS-based NAD metabolomics analysis

The analysis was carried out on an Agilent 6545B Quadrupole-Time of Flight (Q-TOF) Mass Spectrometer (in positive electrospray ionization mode) coupled to an Agilent 1290 InfintyII ultra-high performance liquid chromatography. Continuous internal mass calibration was executed using signal from purine [12,000 full width at half maximum (FWHM) resolution] and hexakis (1H, 1H, 3H-tetrafluropropoxy) phosphazine (24,000 FWHM resolution). Metabolite separation was obtained using the InfinityLab Poroshell 120 HILIC-Z chromatographic column (Hydrophilic interaction liquid chromatography-zwitterionic column, 2.1 x 100 mm, 2.7 µm, PEEK lined) for separating polar analytes (Agilent technologies inc. Santa Clara, CA, USA). The chromatographic solvent composition and gradient as well as the Q-TOF parameters are detailed in supplementary table 7.

The dried tissue extracts were reconstituted on ice using cold LC-MS-grade 75% acetonitrile and spiked with ^{13}C-labeled internal standards (ISTD) from yeast extract to obtain a final volume of 50 µL. 2 µL of each spiked sample was injected into the LC-MS system. Because of the instability of some NAD metabolites, each sample was reconstituted shortly before injection into the LC-MS system. Within each batch, tissue samples were randomized, and quality control (QC) samples, made from pooling equal volumes (10 µl) of each tissue sample extract, were included in the analysis sequence as the first samples to be injected in order to condition the column. The QC samples were then injected after every 6-8 samples to monitor the stability of the LC-MS signal. Multiple blanks (solvent only) were run at the beginning and end of each batch,

and specifically, after the NSM to determine the instrument noise and avoid contamination of the tissue extracts by carry-over metabolites from the high-concentration NSM standard (NSM11).

The data acquisition and processing were performed on the Agilent Q-TOF Quantitative Analysis software (Agilent technologies inc. Santa Clara, CA, USA). Retention times and blank signals were adjusted according to the batch data. The calibration curves were generated using 1/x weighted linear regressions. The calibration range was optimized for each metabolite. The peaks were automatically detected, and the peak areas were integrated using the Agile2 integrator. Additionally, the peaks were visually inspected for accurate identification and peak limits were adjusted manually if necessary. Peaks with a signal-to-noise ratio of 10 or lower were not used for quantification, thus keeping calibration points with a signal-to-noise ratio of at least 10 as the lower limit of quantification (LLOQ). The acceptable accuracy range was set between 80 and 120%. The lower limit of quantification was defined by the lowest concentration with an acceptable accuracy and signal-to-noise ratio. The limit of detection (LOD) was estimated as LLOQ/3. Unlabeled metabolites were linked to the corresponding labeled metabolites. When all acceptance criteria were met, the calculated metabolite concentrations from the tissue samples were automatically normalized by the internal standard signal (ISTD) and dilution factors were applied. The adjusted metabolite concentrations were further manually normalized by the initial weight of each tissue sample.

3.2.7. Statistical analysis:

Statistical analyses for the yeast extracts comparisons, including t-tests, Principal Component Analysis (PCA), Partial least squares-discriminant analysis (PLS-DA), and hierarchical clustering analysis were carried out using the free online software MetaboAnalyst version 5.0 (https://www.metaboanalyst.ca). For the yeast extract comparison, the data was

normalized by a sample-specific factor, which was the yeast cell count for each extract. A log10 normalization was also applied for data transformation.

3.3. Results

3.3.1. Construction and optimization of NAD^+-related metabolites calibration curves

The first step of our metabolomics method development consisted of the identification of NAD^+-related metabolites in the external standards which consist of 11 dilutions of the NAD standards mix (NSM1-11), as well as the construction of calibration curves for each metabolite. This step was performed using negative and positive ionization modes in order to examine the quality and intensity of each metabolite signal and determine their experimental retention times (RT). All the external NAD-related standards were successfully detected in positive ionization mode except quinolinic acid (QUIN), which was only detected in negative ionization mode (Table 1) and NADPH, which displayed abnormal peak shapes in positive ionization mode. NADPH peak shape was improved in negative ionization mode with the incorporation of medronic acid (deactivator additive) in the mobile phase (Supp. Fig. 14b). In some cases, the extracted ion chromatograms contained more than one peak like the NAD^+ [M+1] peak that is observed in the NAAD transition (Supp. Fig. 14d), which was also observed in other studies using HILIC columns (189). However, the peaks were completely resolved, the retention times (RTs) were reproducible, and the molecular ion $[M+H]^+$ peaks mass-over-charge ratio (m/z) allowed us to clearly identify each metabolite (m/z=664.1169-664.1175 for NAD^+ and m/z=665.1004-665.1018 for NAAD). Overall, positive ionization mode improved the signal for the majority of the NAD^+-related metabolites (Supp. Fig. 14) and allowed us to obtain calibration curves with a better linear dynamic range (Table 2).

Table 1: NAD^+-related metabolites were measured in the NAD standards mix (NSM) using positive and negative ESI modes to determine precursor ion (m/z) and retention times (min) in positive (RT+) and negative (RT-) modes. A qualitative assessment of the chromatograms and mass spectra was performed to identify the optimal conditions for each metabolite analysis: ✓: Detectable and quantifiable, ✓✓: Better signal quality and/or linearity, ×: Not detected, low signal-to-noise ratio, poor peak shape. $[M+H]^+$: Protonated molecular ion mass, $[M-H]^-$: Deprotonated molecular ion mass, $[M+Cl]^-$: Chloride adduct mass, $[M+Hac-H]^-$: Acetic acid adduct mass.

Acronym	Full Name	Chemical Formula	Molecular Weight (MW)	Compound Monoisotopic MW	[M+H]+	RT+	MS+ signal	[M-H]-	[M+Cl]-	[M+Hac-H]-	RT-	MS- signal
3-HAA	3-Hydroxyanthranilic acid	C7H7NO3	153.14	153.0426	154.0499	1.2	✓	152.0353			2.31	✓
Melatonin	Melatonin	C13H16N2O2	232.28	232.1212	233.1285	1.2	✓	231.1139			0.97	✓
NAM	Nicotinamide	C6H6N2O	122.12	122.048	123.0553	1.39	✓	121.0407			1.22	×
Me2PY	N1-Methyl-2-pyridone-5-carboxamide	C7H8N2O2	152.15	152.0586	153.0659	1.63	✓✓	151.0513			1.336	✓
NA	Nicotinic acid	C6H5NO2	123.11	123.032	124.0393	2.72	✓✓	122.0247			2.435	✓
Serotonin	Serotonin	C10H12N2O	176.22	176.095	177.1023	3.39	✓	175.0877			2.602	×
L-Kyn	L-Kynurenine	C10H12N2O3	208.21	208.0848	209.0921	3.77	✓	207.0775			2.469	✓
L-Tryp	Tryptophan	C11H12N2O2	204.23	204.0899	205.0972	3.87	✓✓	203.0826			2.635	✓
NUA	Nicotinuric Acid	C8H8N2O3	180.16	180.0535	181.0608	3.95	✓	179.0462			3.135	✓✓
3-HK	3-Hydroxy-L-kynurenine	C10H12N2O4	224.21	224.0797	225.087	4.09	✓	223.0724			3.06	✓
MeNAM	1-Methylnicotinamide	C7H9N2O+	172.61	136.0642	137.0715	4.1	✓	135.0569		195.078	4.1	×
5-HTP	5-Hydroxy-L-tryptophan	C11H12N2O3	220.22	220.0848	221.0921	4.48	✓	219.0775			3.476	✓
NR	Nicotinamide Riboside	C11H15N2O5+	255.25	254.0908	255.098	4.78	✓	253.0835	289.0596	313.1041	/	✓
NADH	Nicotinamide adenine dinucleotide (Reduced)	C21H29N7O14P2	709.4	665.1248	666.1321	7.59	✓✓	664.1175			5.749	✓
ADPR	ADP-Ribose	C15H23N5O14P2	582.32	559.0717	560.079	7.68	✓	558.0644			5.891	✓
NMN	Nicotinamide mononucleotide	C11H15N2O8P	334.22	334.0566	335.0639	7.75	✓✓	333.0493				×
NAD	Nicotinamide adenine dinucleotide	C21H27N7O14P2	663.43	663.1091	664.1164	7.78	✓✓	662.1018			6.299	✓
NAMN	Nicotinic acid mononucleotide, Nicotinate D-ribonucleotide	C11H14NO9P	335.2	335.0406	336.0479	7.8	✓	334.0333			7.248	×
cADPR	Cyclic ADP-Ribose	C15H21N5O13P2	541.3	541.0611	542.0684	8	✓	540.0538			6.449	×
NAAD	Nicotinic acid adenine dinucleotide	C21H27N6O15P2+	664.41	664.0937	665.101	8.4	✓	663.0864			6.457	×
NADP	Nicotinamide adenine dinucleotide phosphate	C21H28N7O17P3	743.41	743.0754	744.0827	9.25	✓	742.0681			7.598	✓✓
NADPH	Nicotinamide adenine dinucleotide phosphate (reduced)	C21H30N7O17P3	1142.12	745.0911	746.0984	9.31	×	744.0838			7.182	✓
QUIN	Quinolinic acid	C7H5NO4	167.12	167.0219	168.0292	/	×	166.0146			5.991	✓

Table 2: Calibration curve equations, correlation coefficient, and linear dynamic range of NAD^+-related metabolites in the NAD standards mix (NSM) measured by LC-MS in positive ionization mode.

Acronym	Calibration curve equation	Correlation coefficient (R^2)	Linear range (µM)
NAD^+	y = 116120.01x + 22428.42	0.9982	0.0195-50
NADH	y = 64980.50x + 16409.53	0.9983	0.0195-25
Melatonin	y = 34472772.25x + 394726.63	0.9899	0.0195-0.3125
3-HAA	y = 725692.04x + 7499.07	0.9976	0.0195-6.25
NAM	y = 5143243.34x + 31691.33	0.9965	0.0195-3.125
Me2PY	y = 13869531.81x + 115789.10	0.9967	0.0195-1.5625
NA	y = 1437393.36x + 15154.93	0.9939	0.0195-1.5625
Serotonin	y = 797089.46x + 982.74	0.9968	0.0195-12.5
L-Kyn	y = 1020831.10x + 3248.84	0.9985	0.0195-25
NUA	y = 763229.01x + 491.48	0.9959	0.0016-0.3125
L-Tryp	y = 764055.43x + 14888.25	0.9939	0.0195-12.5
MeNAM	y = 19640568.07x + 95754.70	0.9955	0.0195-1.5625
3-HK	y = 208823.27x + 3054.59	0.9935	0.0195-12.5
5-HTP	y = 81071.25x + 1181.01	0.9981	0.0195-25
NR	y = 1251936.05x + 18634.40	0.9998	0.0016-5
NMN	y = 128573.96x + 10413.07	0.9690	0.0195-25
NAMN	y = 83287.47x + 2525.15	0.9994	0.0195-26
cADPR	y = 83374.12x + 1166.98	0.9985	0.0012-3
ADPR	y = 89211.60x + 1737.87	0.9943	0.0195-12.5
NAAD	y = 167535.38x + 17519.31	0.9976	0.0195-25
NADP	y = 65937.69x + 3460.11	0.9613	0.0195-25

3.3.2. Application of the quantitative method to trial liver samples

As a second step of the method development, tissue samples were run in positive and negative ionization modes with no ISTD to determine the expected concentration ranges for the target metabolites and whether the detection of the NAD metabolites in the liver samples would be similar to the external standards. This would also allow us to identify any matrix effects from the liver extracts that could interfere with the identification and quantification of the metabolites. The tissue processing and metabolite extraction protocols, described in the Methods section and the NAD metabolomics workflow (Fig. 8), were selected to preserve the heat-sensitive metabolites and inactive enzymes in the samples. 80% Methanol at -80°C was assayed in previous studies (159, 163, 191) and shown to be an effective extraction solvent. The addition of dichloromethane at - 20°C allowed us to separate the lipophilic phase from the hydrophilic phase (194) to reduce interferences and improve the signal of our metabolites of interest. Finally, the aqueous layer was dried in a refrigerated vacuum concentrator at -4°C, which further helped in preserving heat-sensitive metabolites and allowed more flexibility to adjust the final metabolite concentrations.

To avoid temperature variations and the potential effect of residual enzymatic activities or non-enzymatic redox reactions, we thawed and reconstituted each sample (liver extract) shortly before injecting it into the LC-MS system. The liver extracts were analyzed in a batch including blanks, an external calibration curve (NSM1-11), and using QC samples (liver extracts mix) as described in the methods section. The QC samples were assessed for intra-day precision on two consecutive days and showed repeatable retention times (Supp. Table 8) and concentrations (Supp. Table 9) for the detected metabolites. The trial liver samples were randomized to avoid false discoveries due to sample order. This analysis allowed us to determine the expected range of concentrations for each metabolite in control liver samples. The quantification results of the

metabolites normalized to tissue weight obtained in both ionization modes are summarized in table 3.

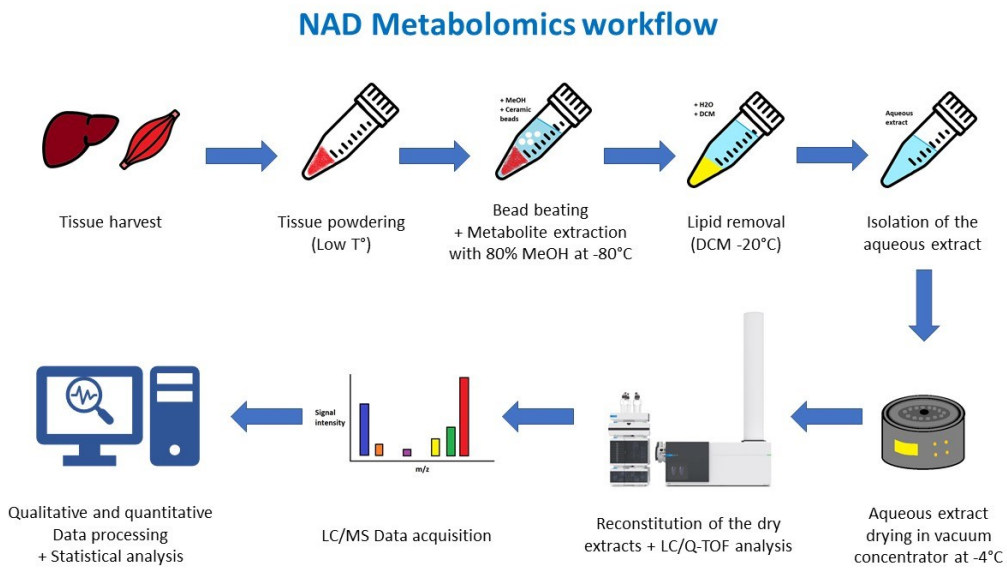

Figure 8: NAD metabolomics workflow for targeted and untargeted analysis of tissue samples. Prior to metabolomics analysis, tissue samples are homogenized, and metabolites are extracted under optimal conditions. The dry extracts are then reconstituted with 75% acetonitrile and injected into the Agilent 6545 LC/Q-TOF system. Finally, the acquired raw data undergoes qualitative and quantitative data processing and statistical analysis. Image usage permission was obtained from Agilent Technologies, Inc.

Table 3: NAD^+-related metabolite concentrations normalized to tissue weight (nmol/g of tissue) in mouse liver samples. Trial liver samples were analyzed in positive and negative ion modes with no internal standard normalization.

Positive ionization mode

	Samples					
Compounds	T1	T2	T3	T4	T5	T6
NAD^+	217.43	305.76	533.43	295.33	449.11	501.89
NADH	65.9	113.06	244.06	109.23	195.53	241.34
NAM	251.13	379.7	230.42	204.22	294.4	257.73
MeNAM	3.67	6.68	6.35	5.53	6.73	6.33
Me2PY	2.77	3.01	2.99	3.19	2.55	2.99
ADPR	80.55	461.43	227.98	46.95	253.11	294.86
L-Trp	113.29	177.8	96.36	132.84	130.37	80.89
5-HTP	4.56	2.77	3.26	4.07	3	4.39
L-Kyn	0.24	0.13	0.11	0.47	0.31	0.22

Negative ionization mode

	Samples					
Compounds	T1	T2	T3	T4	T5	T6
NADP	160.43	679.38	617.21	560.96	373.22	639.1
NADPH	644.28	1167.85	2279.24	2413.42	596.46	1489.22

3.3.3. Preparation of a ^{13}C-labeled internal standard mix

One of the limitations of LC-MS is the matrix effect, which occurs when the ionization of target molecules is affected by other components of the biological sample eluting at the same time. Generally, the result is suppressed ionization, which leads to a lower signal. One way to circumvent this problem is to use stable isotope labeled standards (ISTD) to help correct for the unlabeled metabolite signal variations as the labeled metabolites elute at the same time as the unlabeled metabolites from the samples and should suffer from similar matrix effects. The ideal internal standard mix would contain the individual labeled metabolites matching our metabolites of interest. However, stable isotope labeled standards for all of our NAD^+-related metabolites of interest were not commercially available, thus the ideal alternative was to use ^{13}C-labeled yeast extracts produced by feeding yeast cells with ^{13}C-glucose to obtain labeled internal standard mix

(ISTD), as has been done previously (28, 141, 167, 189). Beyond their use for accurate quantification, the ISTD helps to confirm the identity of a given metabolite and detect shifts in retention time during chromatography (Table 4). Concerning the efficiency of isotopic enrichment for the ISTD, the majority of the ^{13}C-labeled metabolites were fully labeled (on all carbons) but some metabolites with a high number of carbons (NAD^+ and NADH) had a small fraction of isotopologues with one unlabeled carbon atom (Supp. Fig. 15), similar to that found in commercial yeast extracts.

Table 4: Mass to charge (m/z) values and retention time (RT) for the unlabeled metabolites from the NSM and the corresponding ^{13}C-labeled metabolites from the ISTD measured in positive ionization mode.

(^{12}C) Unlabeled metabolites (NSM)	m/z	^{13}C-labeled metabolites (ISTD)	m/z	RT+
Melatonin	233.1285	Melatonin + 13	246.1721	1.149
3-HAA	154.0499	3-HAA + 7	161.0734	1.242
NAM	123.0553	NAM + 6	129.0754	1.427
Me2PY	153.0659	Me2PY + 7	160.0894	1.63
NA	124.0393	NA + 6	130.0595	2.84
Serotonin	177.1023	Serotonin + 10	187.1358	3.453
L-Kyn	209.0921	L-Kyn + 10	219.1256	3.807
NUA	181.0608	NUA + 8	189.0876	3.927
L-Tryp	205.0972	L-Tryp + 11	216.1341	3.94
MeNAM	137.0715	MeNAM + 7	144.0945	4.024
3-HK	225.087	3-HK + 10	235.1206	4.169
5-HTP	221.0921	5-HTP + 11	232.129	4.505
NR	255.098	NR +11	266.1345	4.793
NMN	335.0639	NMN + 11	346.1008	7.127
NADH	666.1321	NADH + 21	687.2025	7.846
NAD	664.1164	NAD + 21	685.1869	7.886
NAMN	336.0479	NAMN + 11	347.0848	7.918
cADPR	542.0684	cADPR + 15	557.1187	7.97
ADPR	560.079	ADPR + 15	575.1293	8.014
NAAD	665.101	NAAD + 21	686.1709	8.689
NADP	744.0827	NADP + 21	765.1532	9.414
NADPH	746.0984	NADPH + 21	767.1689	9.501

At first, we assayed a commercially available ^{13}C-labeled yeast extract (U-13C, 98%, Cambridge Isotope Laboratories, Inc.) (195), which contained at least 2×10^9 Pichia pastoris cells per vial and was previously tested as an internal standard for NAD^+-related metabolite quantification in human cells and primate skeletal muscle (189). Despite the commercial ISTD being suitable for blood, in order to maintain an optimal internal standard-to-sample ratio (i.e., labeled-to-unlabeled metabolite ratio) in liver tissue, we determined that the amount of ^{13}C-labeled yeast extract needed would have been cost-prohibitive for large numbers of samples. Additionally, following the hot ethanol extraction method, used by the manufacturer to produce the ISTD, there was a significant amount of contaminants and lipophilic compounds (Supp. Fig. 16b). Therefore, we aimed to produce an in-house ^{13}C-labeled yeast extract that would be more concentrated, cost-effective and contains minimal contaminants. We compared two different extraction methods for our in-house ^{13}C-labeled yeast extract: the recommended boiling ethanol method (195) versus our cold extraction with 80% methanol and dichloromethane. We were able to efficiently extract metabolites from a yeast pellet using the cold extraction procedure, which allowed us to separate the water-soluble and lipophilic metabolites, thus improving the resolution of our chromatographic separation. The metabolite yields were similar between both extraction methods, as shown by the total ion chromatogram in supp. Fig. 16a. As expected, these extracts were also more concentrated than the commercial yeast extract (Supp. Fig. 16, supp. Fig. 17). However, as in the commercial extract, the boiling ethanol method generated more contaminants (Supp. Fig. 16c) when compared to the cold methanol/dichloromethane extraction (Supp. Fig. 16d).

To confirm the efficient extraction of NAD^+-related metabolites following the cold methanol/dichloromethane extraction procedure, we measured the NAD^+-related metabolite levels within the in-house generated yeast extracts. The heatmap in figure 9a below shows the relative

labeled metabolites signal, which is defined by the peak area of labeled metabolites divided by the peak area of unlabeled metabolites from NSM (NSM 7) normalized to each yeast extract cell count. The NAD metabolite levels were comparable between the two extraction methods. However, compared to the methanol/dichloromethane extraction, the hot ethanol extracts displayed significantly higher concentrations of the ^{13}C-labeled metabolites NAM (NAM+6) (p-value = 5.0115e-09) and ADPR (ADPR+15) (p-value = 3.4553e-07), which are likely products of ^{13}C-NAD^+ (NAD+21) degradation by heat (196, 197) (Fig. 9b). Moreover, the cold extracts clustered together even though the batches were not all obtained from the same yeast culture, adding confidence to the results (Fig. 9c). Concerning the efficiency of isotopic enrichment, the majority of the ^{13}C-labeled metabolites were fully labeled (on all carbons) but some metabolites with a high number of carbons (NAD^+ and NADH) had a small fraction of isotopologues with one unlabeled carbon atom (Supp. Fig. 15), similar to that found in the ^{13}C-labeled commercial yeast extract.

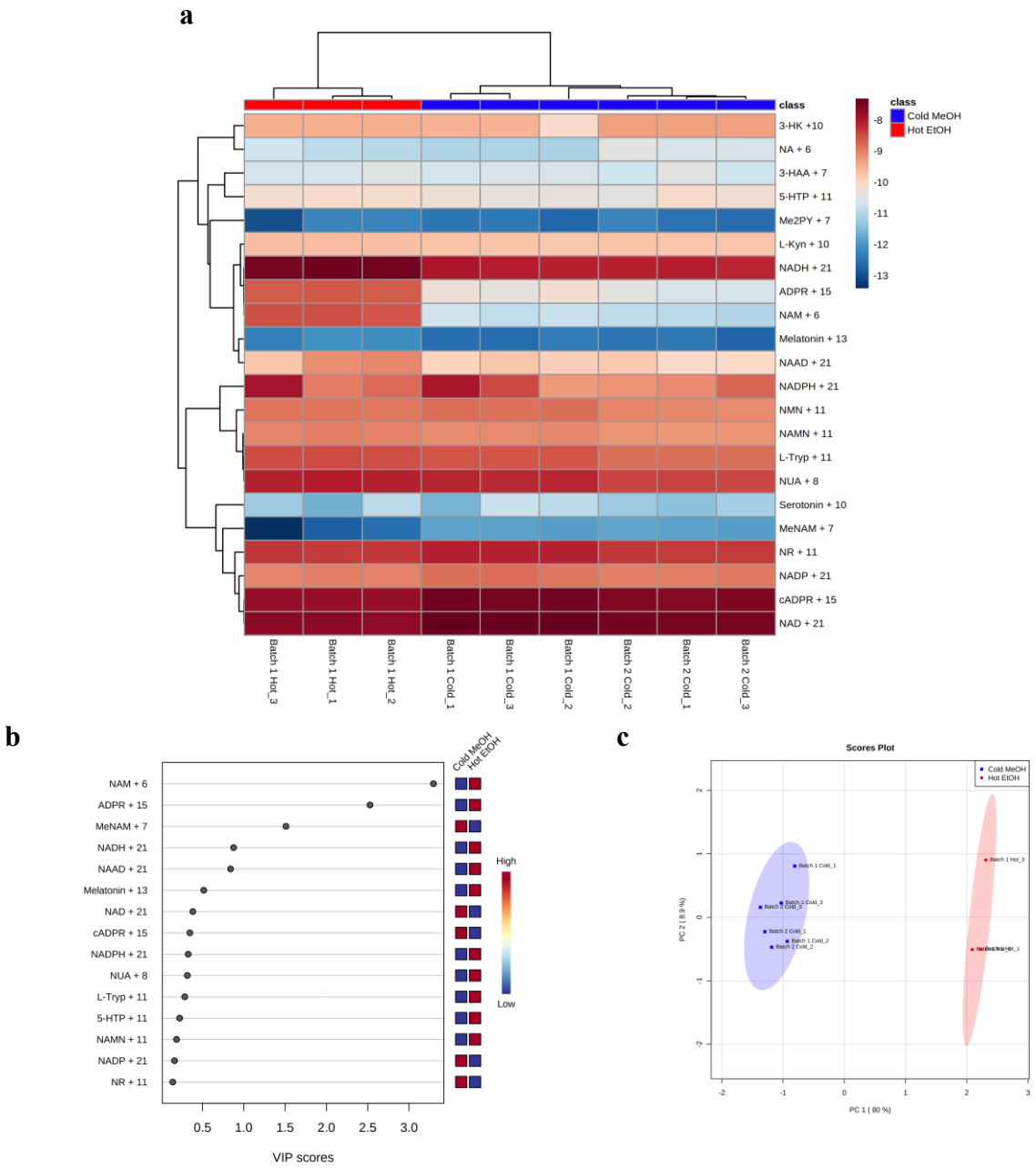

Figure 9: Statistical analysis of the metabolomics data obtained from the in-house yeast extracts comparison. a: Heatmap generated using the ratio of unlabeled to labeled metabolites signal (peak area labeled metabolite/peak area unlabeled standard) normalized to yeast cell count. One yeast culture batch of the hot ethanol (EtOH) extraction was compared with two batches of the cold methanol/dichloromethane (MeOH) extraction in 3 replicates. Each replicate was spiked with the calibrator NSM7. Distance was measured using correlation, and complete-linkage clustering was used for the hierarchical clustering. b: Important features identified by Partial Least Squares Discriminant Analysis (PLS-DA). The colored boxes on the right indicate the relative concentrations of the corresponding metabolite in each type of yeast extract, blue and red being the lowest and highest, respectively. c: Principal component analysis score plot (principal component 1, x-axis and principal component 2, y-axis).

Finally, four different amounts (100%, 40%, 20% and 5%) of internal standard were tested to determine the optimal sample to labeled yeast ISTD spiking ratio that would provide a sufficient signal for the labeled metabolites without causing ion suppression or other matrix effects. The optimal liver tissue/yeast labeled ISTD ratio was 2.125 (34 µl tissue extract/16 µl yeast labeled ISTD) (Table 5, supp. Table 10). 16 µl representing 20% ($1/5^{th}$) of the reconstituted ISTD aliquot (Cell count: $17.81x10^9$ cells) from the in-house generated ^{13}C-labeled yeast extract. This ratio should be optimized for different tissue types and for treatments that may alter tissue NAD metabolite concentrations, as well as different yeast cell counts. For this particular ratio, spiking the highest concentrations of NSM (NSM9 to NSM11) resulted in saturation and ion suppression, which led to a loss of linearity and a decrease in the labeled metabolites signal. Therefore, to calculate the average concentrations, only quantitative results obtained from 8 calibration points (NSM1 to NSM8) spiked with ISTD were considered (Table 5). All NSM calibrators and samples spiked with ITSD were assessed for quality and the extracted ion chromatograms (EICs) for all labeled and unlabeled metabolites were inspected (Supp. Fig. 18 and 19). Only metabolites that passed the qualitative quality assessment (as explained in the method section) were considered for quantitative data analysis. To test the effect of spiking the ISTD before and after the extraction, we spiked a pool of liver extracts with 100% and 20% of the ISTD before and after the extraction. The 100% spiked yeast extracts suffered from ionization suppression due to the high concentration of the labeled metabolites. The 20% spiking showed metabolite recovery of 82 to 122% (Mean: 98%) for the measured metabolites (Supp. Table 11). These variations were considered acceptable, and the following measurements were performed with ISTD spiking after the metabolite extraction to allow a better repeatability of the ISTD signal and more flexibility in the choice of dilution used for the tissue extracts.

Table 5: ^{13}C-Labeled metabolite concentrations measured in the calibration standards (NSM1-11) spiked with 20% of in-house generated yeast internal standards (ISTD). 20% of ^{13}C-Labeled yeast ISTD corresponds to 17.81x10^{9} cells. NSM: NAD standard mix. S.D.: Standard deviation. R.S.D.: Relative standard deviation.

	^{13}C-Labeled metabolite conc. (µM)											**Average conc. NSM1-8 (n=9)**	**SD**	**RSD**
Compound	NSM1	NSM2	NSM3	NSM4	NSM5	NSM6	NSM7	NSM8	*NSM9*	*NSM10*	*NSM11*			
^{13}C-3HK	0.23	0.21	0.18	0.22	0.25	0.19	0.23	0.17	*0.17*	*0.11*	*0.07*	***0.21***	***0.03***	***12.48***
^{13}C-cADPR	1.67	1.41	1.49	1.63	1.78	1.72	1.89	1.46	*1.52*	*1.18*	*0.93*	***1.63***	***0.17***	***10.22***
^{13}C-Tryp	1.15	1.23	1.11	1.27	1.28	1.02	1.25	0.91	*0.84*	*0.72*	*0.53*	***1.15***	***0.13***	***11.47***
^{13}C-NAD^{+}	36.74	31.86	32.22	34.06	37.69	34.61	39.67	31.50	*30.15*	*23.30*	*17.40*	**34.79**	***2.99***	***8.59***
^{13}C-NADH	7.34	6.31	6.08	6.58	7.38	6.82	7.88	6.20	*6.22*	*4.66*	*3.83*	**6.83**	***0.65***	***9.53***
^{13}C-NR	4.04	3.57	3.59	3.83	4.18	3.91	4.51	3.71	*3.81*	*3.35*	*2.71*	**3.92**	***0.32***	***8.19***

3.4. Discussion

During the preparatory phase of the NAD metabolomics method development, thorough planning has been performed to consider important factors such as the physicochemical and structural properties of the target metabolites (Water solubility, heat sensitivity, pH stability…), the type of sample and the adequate tissue disruption technique, metabolite extraction method and solvents, temperature, and the suitable chromatography columns. As well as the available information about previously developed methods on various LC-MS systems. When choosing an MS instrument, we preferred the Q-TOF system because of its higher mass resolution, better selectivity and larger mass range. Additionally, the Q-TOF offered the possibility to collect untargeted data and has previously been optimized to detect NAD-related metabolites (181, 182). Finally, we considered the recommended quality control requirements, such as external calibration curves, internal standards, and QC samples (198, 199).

Pure NAD^+-related metabolite standards were assayed in negative or positive ionization modes, which resulted in the detection of 22 different metabolites in both modes, except quinolinic acid that was detected only in negative ionization mode. The positive ionization mode yielded a better signal for the majority of metabolites, including better peak shape, lower signal-to-noise ratio and better accuracy. The calibration curves were built with 11 points in order to accurately quantify the various metabolites despite the wide range of their tissue concentrations. All the calibration curves were assessed for quality and any datapoints that did not meet the quality assessment criteria were removed from the curves. To obtain the best quantitative results for most of the metabolites, we therefore chose to use the positive ionization mode for all NAD metabolomics measurements.

When optimizing the pre-analytical conditions for our NAD metabolomics, we maintained liver tissue samples and extracts under cold conditions at all times, starting from the tissue extraction and processing to the final metabolite extraction. The extraction using cold 80% methanol and dichloromethane allowed us to inactivate the enzymes and isolate the polar metabolites while maintaining cold temperatures. These extraction solvents were evaporated in a refrigerated vacuum concentrator at -4°C and the liver extracts were reconstituted shortly before injection into the LC-MS system and run along with an external calibration curve (NSM1-11), blanks, and QC samples. The use of QC samples after every 6 to 8 samples, confirmed the stability and reproducibility of the signal during the run. This step allowed us to identify the NAD^+-related metabolites present in the liver extracts and determine their usual concentrations in mouse liver. As expected in tissue samples, metabolite concentrations ranges varied widely, some metabolites were undetectable or under the limit of quantification in control mouse liver samples, including NA, NAMN, cADPR, 3-HK and 3-HAA.

According to the United States Food & Drug Administration (U.S. FDA) (198) and the European Medicines Agency (EMA) (199), any quantitative analytical methods must incorporate multi-point (≥ 6) external calibration curves, internal quality controls, and matrix matching to be considered absolute quantification. In biomedical sciences, the measurement of metabolites within two groups or conditions (i.e.: disease group vs healthy control group, before vs after treatment, etc.) commonly relies on relative quantification (using an external standard curve with no internal standards), which does not allow for the comparison of results obtained from different studies. Quantification relying on external standards curves and internal standards is the most reliable method to obtain meaningful and reproducible quantitative results. As not all NAD-related metabolites are commercially available in their labeled form, the ^{13}C-labeled yeast extracts

represent a practical alternative to a mixture of commercial NAD metabolite internal standards (200). In-house production of ^{13}C-labeled yeast extracts is more cost-effective and can allow for the modulation of metabolite concentrations to suit the linear dynamic range and the sample type. Moreover, by increasing metabolite concentrations and removing lipids, we were able to improve the detection and quantification of NAD metabolites in liver samples. We also demonstrated that the cold methanol/dichloromethane extraction of yeast metabolites was comparable to the hot ethanol extraction in terms of metabolite concentrations, but the hot ethanol extracts displayed more contaminants and degradation metabolites. Moreover, the cold methanol/dichloromethane extraction proved to be efficient for lysing the *Pichia pastoris* yeast membrane and is the preferred method for tissue and blood metabolite extraction, thus making it the best choice for yeast-derived labeled ISTDs.

The use of external and internal standards during the LC-MS-based metabolomics analysis enabled the confirmation of the identity and accuracy of the measured signal for each NAD^+-related metabolite in mouse liver samples. We observed slight shifts in RTs between the labeled and unlabeled metabolites, but all the peaks were in the acceptable RT windows/ranges, as shown in supplementary figures 18 and 19. However, ^{13}C-labeled yeast extracts still require a thorough quality processing as they pose additional matrix effects, induced by mixing the yeast matrix with the mammalian tissue matrix, and due to the variability of the metabolite concentrations within different yeast extracts. In brief, the quality assessment of the labeled metabolites signal must be stringently conducted to ensure the accuracy of the final quantitative results.

3.5. Limitations

This study has some limitations, including the unpredictable nature of matrix effects and ionization suppression that occur due to the addition of yeast extracts to the mouse liver extracts. We used ^{13}C-labeled yeast extracts because they are still the most used and cost-effective alternative in comparison to single ^{13}C-labeled metabolites, which are not readily available. Additionally, the best strategy was to spike the ISTD prior to tissue extraction to normalize any pre-analytical variations during tissue metabolite extraction, which could impact the final quantitative results. However, we determined that the ISTD spiking with the 20% ratio before or after did not significantly affect the measured metabolites signal (Supp. Table 11), and we chose to add the ISTDs to the liver extracts as we expected the need to use multiple dilutions for the liver extracts to quantify most of the NAD^+-related metabolites.

Chapter 4: Effect of Nicotinamide Riboside on the NAD^+ Metabolome of Mouse Liver and Skeletal Muscle

4.1. Introduction

Given that the sirtuin family of deacetylases has been linked to mitochondrial homeostasis, metabolism, and cell cycle regulation (33), and has been found to be greatly dependent on cellular NAD^+ levels (19), the interest in NAD^+ metabolism has become increasingly important for human health. Beyond sirtuins, other signaling enzymes also rely on NAD^+ as a co-substrate for ADP-ribosylation reactions, catalyzed by mono- or poly-ADP-ribosyl polymerases (60, 201), or for the biosynthesis of second messengers by ADP-ribosyl cyclases (202–204).

As thoroughly explored in the introductory chapter, NAD^+ homeostasis has a significant impact on various pathological conditions, which has led to the development of different NAD^+-boosting strategies. Currently, the safest and most efficient way to boost NAD^+ levels *in vivo* is through supplementation with NAD^+ precursors, including nicotinic acid (NA; Niacin), nicotinamide (NAM), and nicotinamide riboside (NR) (26). Nicotinic acid (NA) has been used to reduce triglycerides and LDL-cholesterol and increase HDL-cholesterol levels (89, 205). On the other hand, despite NAM treatments showing benefits to metabolism following its conversion to NAD^+ and activation of Sirtuins (206–208), it has also been shown to inhibit Sirtuins in a dose- and time-dependent manner (90, 209, 210). In addition, hepatotoxicity and other side effects of NAM have been reported in animal (47, 211, 212) and human (47, 213) studies. The side effects associated with NA and NAM, have not been observed with NR (92, 94, 214), which makes NR a good alternative for NAD^+-boosting or maintenance. Since the discovery of NR and the NR Kinase genes in humans (27), multiple studies on the efficacy and safety of NR have been performed (28, 92–94, 214, 215) on animal models and humans. One of these studies compared the efficiency of

the 3 NAD^+ precursors (NA, NAM, and NR) and showed that orally administered NR significantly increased NAD^+ and its metabolites to higher levels than the other precursors in mouse liver and human blood (28). Another study, using isotope tracer analysis, showed that oral NR was more efficient at increasing circulating NAM levels than nicotinamide mononucleotide (NMN) in mouse tissues (52). However, the mechanisms of action and the pharmacokinetics of NR still need further evaluation. Additionally, various studies have shown varying results with NR in humans (93, 100, 216) despite encouraging animal results (168, 217–219). For example, NR (1g/day for 21 days) increased NAD^+ and its metabolites and decreased pro-inflammatory markers in aged human muscle (70-80 years old) (177), while the same dose for 6 weeks increased muscle NAD^+ metabolites, body lean mass, sleeping metabolic rate, and acetylcarnitine concentrations in muscle with no effect on insulin sensitivity, mitochondrial function, or hepatic lipid accumulation (100). Other studies did not show any effect of NR on muscle function, body composition, or insulin sensitivity after 12 weeks of supplementation with a 2 g/day dose in obese men (93, 216) or after a 7-day supplementation with 1 g/day in young adult males (220). In contrast, NR was effective in improving insulin sensitivity, weight loss (217, 218), muscle function (218), and liver damage (168, 219) as well as reducing the development and progression of mitochondrial myopathy (221) in mice. Therefore, it seems necessary to reconsider comprehensive animal studies to further examine the effect of single or multiple doses of NR on the NAD^+ metabolome and explain the observed discrepancies between animal and human studies and between different clinical studies.

In this chapter, the two last research objectives will be addressed. Notably, the determination of changes in the NAD^+ metabolome in mouse tissues after acute and chronic supplementation with NR and the comparison of metabolite levels in tissue samples harvested before and after euthanasia.

4.2. Materials and Methods

4.2.1. NR supplementation protocols

3 months old C57BL/6J female mice were fed a chow diet and kept under a 12:12-h light-dark cycle. No significant difference in NAD(H) levels was identified between male and female mice or different C57BL/6 mice (See section 2.3.3) thus we chose the C57BL/6J strain as it is a widely used model for human disease and is the most represented strain in studies focusing on NAD^+ metabolism. To reduce the number of animals in each group, we chose female mice to cover any potential variability due to the estrous cycle. To examine the acute effects of different doses of oral NR supplementation, 4 groups of 3 mice each were fasted overnight before receiving different doses of NR chloride (NIAGEN®): 0.5, 1, 2 g/Kg, and water for the control group by oral gavage. Two hours after oral gavage, mice were anesthetized by intra-peritoneal injection of 100 µl of Euthanyl (Pentobarbital sodium: 65mg/ml) until non-responsive. Pre-mortem tissue samples were extracted and snap-frozen in liquid nitrogen: Liver, one kidney, and skeletal muscle from one leg (Gastrocnemius, tibialis anterior, soleus). For euthanasia, mice received a second I.P. injection of 150 µl of Euthanyl and a cervical dislocation was performed. The brains were extracted and snap-frozen immediately after death. In the same mouse post-mortem samples of liver, kidney, and skeletal muscle were harvested and snap-frozen over the course of one minute after waiting for 8 minutes following euthanasia. Tissues were stored at - 80 °C until analysis.

Treatment	Dosage (g/kg)	Frequency	Number of animals	Tissue harvest timepoint vs euthanasia	Tissue harvest timepoint vs NR administration
NR	0	Unique acute dose	3	Pre- and Post-mortem	2 hours
	0.5		3		
	1		3		
	2		3		

Similarly, we examined the effect of a single dose of the highest NR treatment (2g/Kg) after multiple acute timepoints (2-16 hours) and then also chronically with repeated daily

treatments for 5 days. Specifically, 4 groups of 3 mice each received a single acute dose of 2 g/Kg of NR via oral gavage and were euthanized 2, 4, 8, and 16 hours later. Control mice received water and were euthanized 2 hours after oral gavage. Another group of 3 mice received a 5-day daily treatment of 2 g/Kg of NR via oral gavage to study the cumulative effect of repeated doses. Pre- and post-mortem tissue samples were extracted for the control and 2-hour timepoint groups. For the other groups, only pre-mortem tissue samples were harvested. All tissues were stored at - 80°C until analysis.

<table>
<tr><th>Treatment</th><th>Dosage (g/kg)</th><th>Frequency</th><th>Number of animals</th><th>Tissue harvest timepoint vs euthanasia</th><th>Tissue harvest timepoint vs NR administration</th></tr>
<tr><td rowspan="7">NR</td><td>0</td><td rowspan="4">Unique acute dose</td><td>3</td><td rowspan="2">Pre- and Post-mortem</td><td>2 hours</td></tr>
<tr><td rowspan="6">2</td><td>3</td><td>2 hours</td></tr>
<tr><td>3</td><td rowspan="4">Pre-mortem only</td><td>4 hours</td></tr>
<tr><td>3</td><td>8 hours</td></tr>
<tr><td>3</td><td>16 hours</td></tr>
<tr><td>Repeated daily dose for 5 days</td><td>3</td><td>24 hours</td></tr>
</table>

The oral route of administration was used instead of a more bio-available route (such as intravenous administration) because oral supplementation is the preferred route of administration in humans, especially if daily doses are needed. The choice of dosage was motivated by the lowest observed adverse effect level (LOAEL) for NR in rats, which was 1000 mg/kg/day (222). The equivalent doses in humans and mice would be 161 and 1980 mg/Kg/day according to dose conversion recommendations (223, 224). The animal use protocol (MEe-1772-R5) was approved by the Animal Care Committee (ACC) of the University of Ottawa.

4.2.2. NAD^+ and NADH quantification using an enzyme cycling kit

Mouse tissues were powdered using a stainless-steel pestle and mortar system cooled with liquid nitrogen. Approximately 20 mg of each tissue sample was homogenized in 400 µl of Extraction Buffer (BioVision NAD/NADH quantitation kit) using a rotor-stator homogenizer (Fisher Scientific PowerGen 700) for 15-20 seconds followed by a resting period of 30-45 seconds

on ice. The procedure was repeated until complete tissue disruption (3 times for soft non-fibrous tissues such as liver, kidney, and brain and 5 times for skeletal muscle). Between samples, the probe was washed with 70% ethanol and wiped with a Kimwipe™. Total NAD and NADH levels were measured using the BioVision NAD/NADH quantitation kit. To measure the NADH fraction only, aliquots of the tissue samples were heated at 60°C for 30 minutes in a heating block to decompose the heat-sensitive fraction NAD^+.

4.2.3. Tissue processing prior to LC-MS-based metabolomics analysis

Liver samples were processed as described in the previous chapter. However, for fibrous tissues like muscle, which contain a significant amount of connective tissue, bead beating was insufficient, thus it was replaced by a 2-step disruption protocol combining 4-6 cycles of bead-beating and 1-2 cycles of 15-20 seconds of rotor-stator homogenization (Fisher Scientific PowerGen 700). The dried extracts were then frozen at - 80°C until analysis.

4.2.4. LC-MS-based metabolomics analysis

Liver and muscle samples were analyzed using LC-MS, as described in the last chapter. Preliminary experiments helped determine the appropriate sample dilutions and ISTD ratios for the liver samples, however, due to the large range of concentrations of multiple NAD^+-related metabolites in the liver samples following NR supplementation, all liver samples were assayed twice using two different dilutions (1/4 and 1/50). The 1/4 dilutions were obtained by reconstitution of the dry tissue extracts with 136 µl of 75% acetonitrile (ACN). For the 1/50 dilutions, 6 µl of the 1/4 dilutions were further diluted with 69 µl of solvent. For both dilutions, 34 µl of the dilution was mixed with 16 µl of ISTD to maintain the optimal sample-to-ISTD ratio. For the muscle samples, only the 1/4 dilutions were necessary. Similar ISTD ratios were maintained across all samples and external standards. All tissue samples were reconstituted on ice and spiked

with ISTD immediately before injection into the LC-MS system. QC samples consisting of previously run test liver or muscle samples were added to the batch at regular intervals to confirm the stability and precision of the signal. Blank samples were also run at the beginning and end of the sequence and between the external standards and samples. Internal standard normalization was performed for metabolites with appropriate internal standard signal. For metabolites that displayed inconsistencies in the internal standard signal, which was mainly due to ion suppression, the metabolite peak areas were used to calculate the concentrations by interpolation from the NAD standards mix (NSM) calibration curves in order to avoid errors by normalizing to the internal standard signal.

4.3. Results

4.3.1. Acute NR supplementation increases tissue NAD(H) in mouse liver only at the 2-hour timepoint

To examine the effect of oral acute NR supplementation on NAD(H) levels mouse tissues were harvested 2 hours after oral gavage to determine the dose-response. Additionally, these tissues were harvested pre- and post-mortem to identify potential differences due to the harvest time relative to sacrifice. The supplementation with various doses of oral NR (0.5, 1, and 2 g/Kg) revealed an overall dose-dependent increase in NAD^+, NADH and total NAD concentrations in mouse liver in both pre- and post-mortem samples (Fig. 10 a-c. Interestingly, the NAD^+/NADH ratio was lower in pre-mortem samples at higher NR doses in comparison to the vehicle control (Fig. 10 d). Overall, post-mortem liver samples showed overall lower values when compared with pre-mortem for NAD^+ levels (p=0.045) (Fig. 10a), yet did not reach significance for the NAD^+/NADH ratio (p=0.059), total NAD (p=0.07) and NADH values (p=0.517) (Fig. 10 b-d). The multiple comparisons analysis revealed a significant increase in NAD^+, NADH, and total

NAD levels with the 1 and 2 g/Kg doses compared to the control group in both pre- and post-mortem samples.

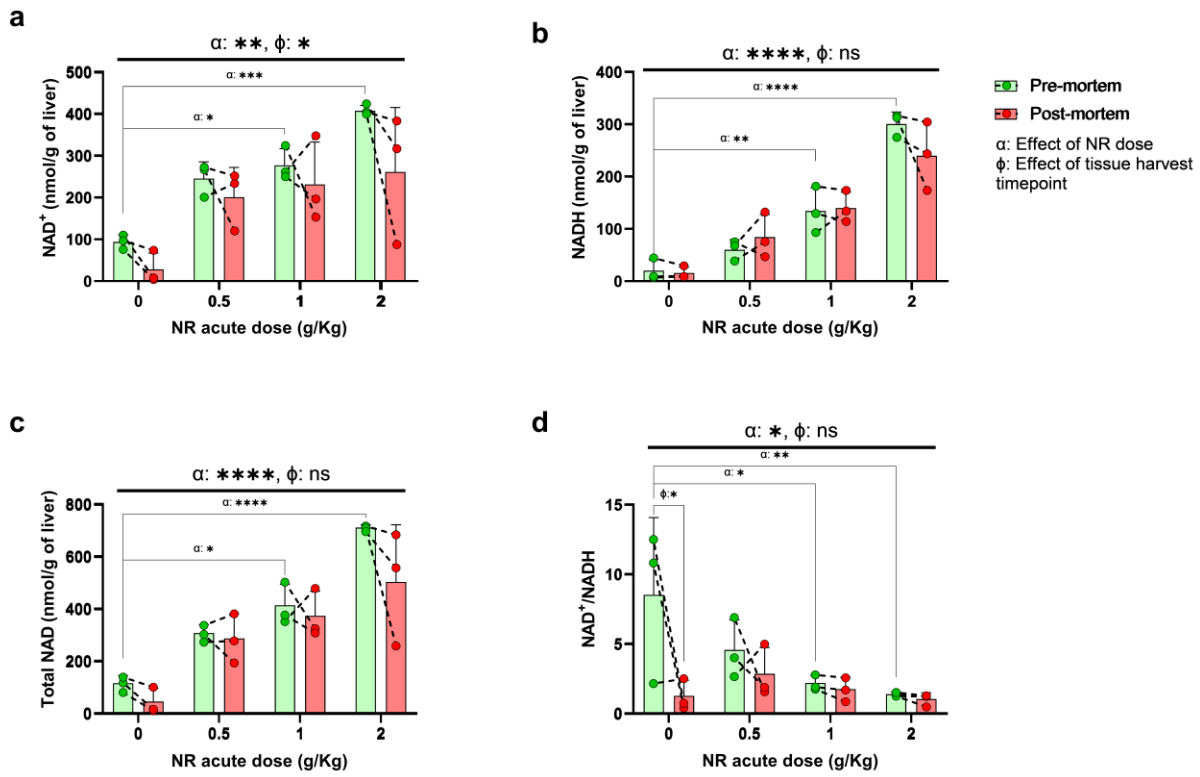

Figure 10: NAD$^+$, NADH, total NAD(H) levels (nmol/g of tissue), and NAD$^+$/NADH ratio in mouse liver tissues harvested 2 hours after supplementation with acute doses of NR (0.5, 1, or 2 g/Kg). (a-c): NAD$^+$(a), NADH(b), and total NAD(c) levels, along with the NAD$^+$/NADH ratio(d), measured in liver samples by enzymatic colorimetric method . Different liver lobes were harvested from the same mouse under anesthesia and before euthanasia (Pre-mortem) or 8 minutes after euthanasia (Post-mortem). Each group contained samples from 3 different animals. For statistical analysis, repeated measure two-way ANOVA with multiple comparisons were performed. Sidak *post hoc* test was used for the multiple comparisons and significant results for the effect of NR in pre-mortem treatment groups versus control group and for the effect of harvest time between pre- and post-mortem samples are graphed. Similar results were obtained for NR dose effect comparison between the post-mortem samples in each treatment group versus the control group. α: Effect of NR dose. Φ: Effect of tissue harvest timepoint. *: p<0.05, **: p<0.01, ***: p<0.001, ****: p<0.0001.

In contrast to liver samples, no significant changes in metabolite concentrations, or in the NAD$^+$/NADH ratio, were observed at 2 hours post-supplementation with any dose of NR in either tibialis anterior (Fig. 11a-d) or gastrocnemius muscle (Fig. 11e-h). Additionally, no significant

differences were observed between pre- and post-mortem samples in all groups. In mouse kidney (Fig. 12a-c) and brain (Fig. 12e-h), mice from this same cohort did not exhibit differences between the treatment groups and the control group at the 2hr timepoint except for a 2-fold increase in the NAD^+/NADH ratio in the pre-mortem kidney samples following a 2g/Kg dose (Fig. 12d). In brain samples, even though the NAD^+ levels (Fig. 12e) and NAD^+/NADH ratio (Fig. 12h) trended higher with the 2g/Kg dose, they did not reach overall significance (One-way ANOVA: p=0.054 for the NAD^+/NADH ratio and p=0.21 for NAD^+) (Fig. 12e, g). Concerning the effect of harvest time on the kidney samples, the overall NAD^+ (Fig. 12a) and total NAD levels (Fig. 12c), as well as the NAD^+/NADH ratios (Fig. 12d), were significantly lower in post-mortem versus pre-mortem kidney samples with no overall difference in NADH levels (Fig. 12b). Ultimately, at 2 hours post-supplementation, it is clear that oral NR was metabolized to NAD(H) in the liver but was not yet distributed to the other tissues.

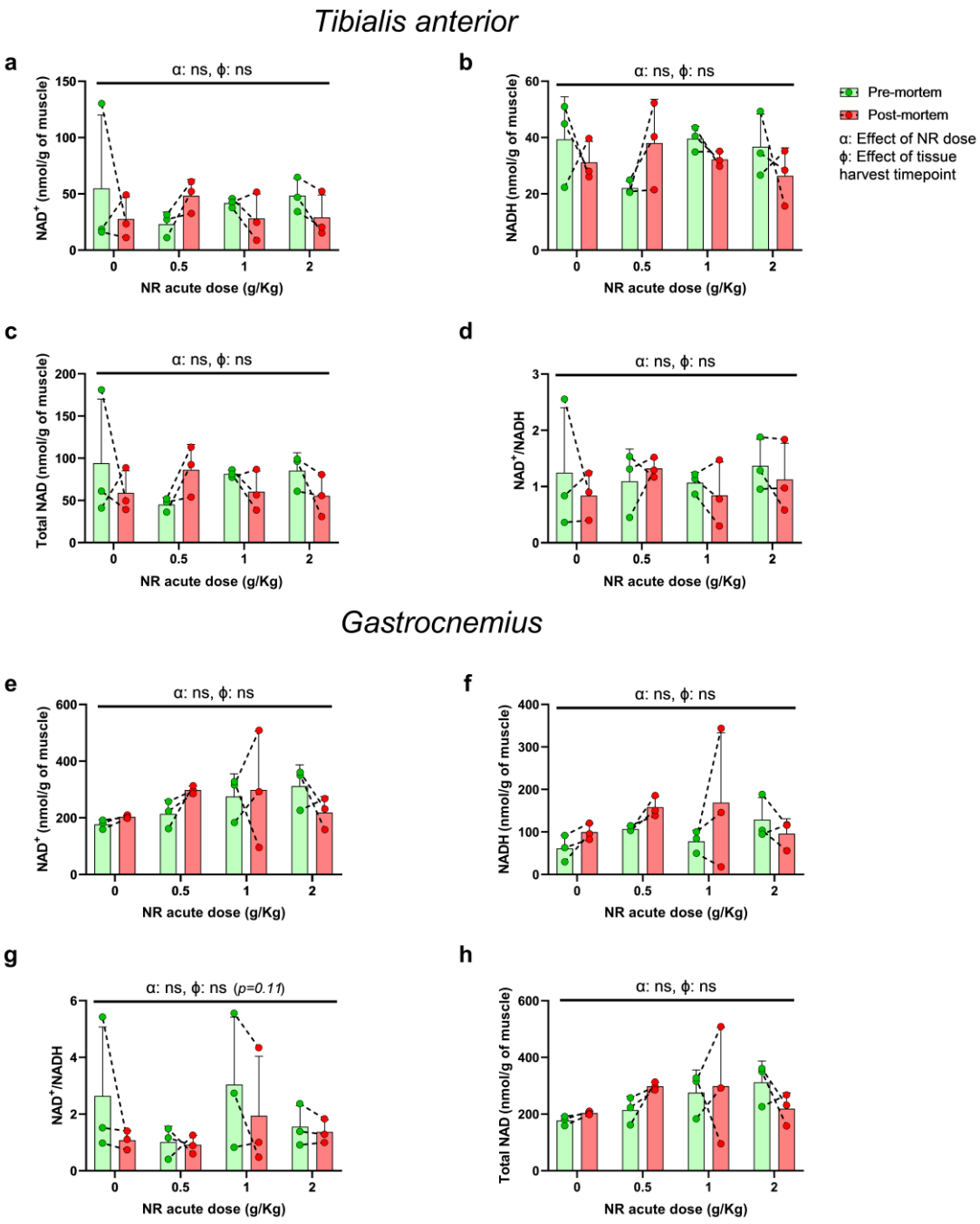

Figure 11: NAD$^+$, NADH, total NAD(H) levels (nmol/g of tissue), and NAD$^+$/NADH ratio in mouse skeletal muscles harvested 2 hours after supplementation with an acute dose of NR (0.5, 1, or 2 g/Kg). *Tibialis anterior* (a-d) and *gastrocnemius* (e-h) muscles from each mouse were harvested under anesthesia and before euthanasia (Pre-mortem) or after euthanasia (Post-mortem). Each group contained samples from 3 different mice. Metabolite levels were measured by enzymatic colorimetric method. For statistical analysis, repeated measure two-way ANOVAs with Sidak *post hoc* test for multiple comparisons were performed. α: Effect of NR dose. Φ: Effect of tissue harvest timepoint.

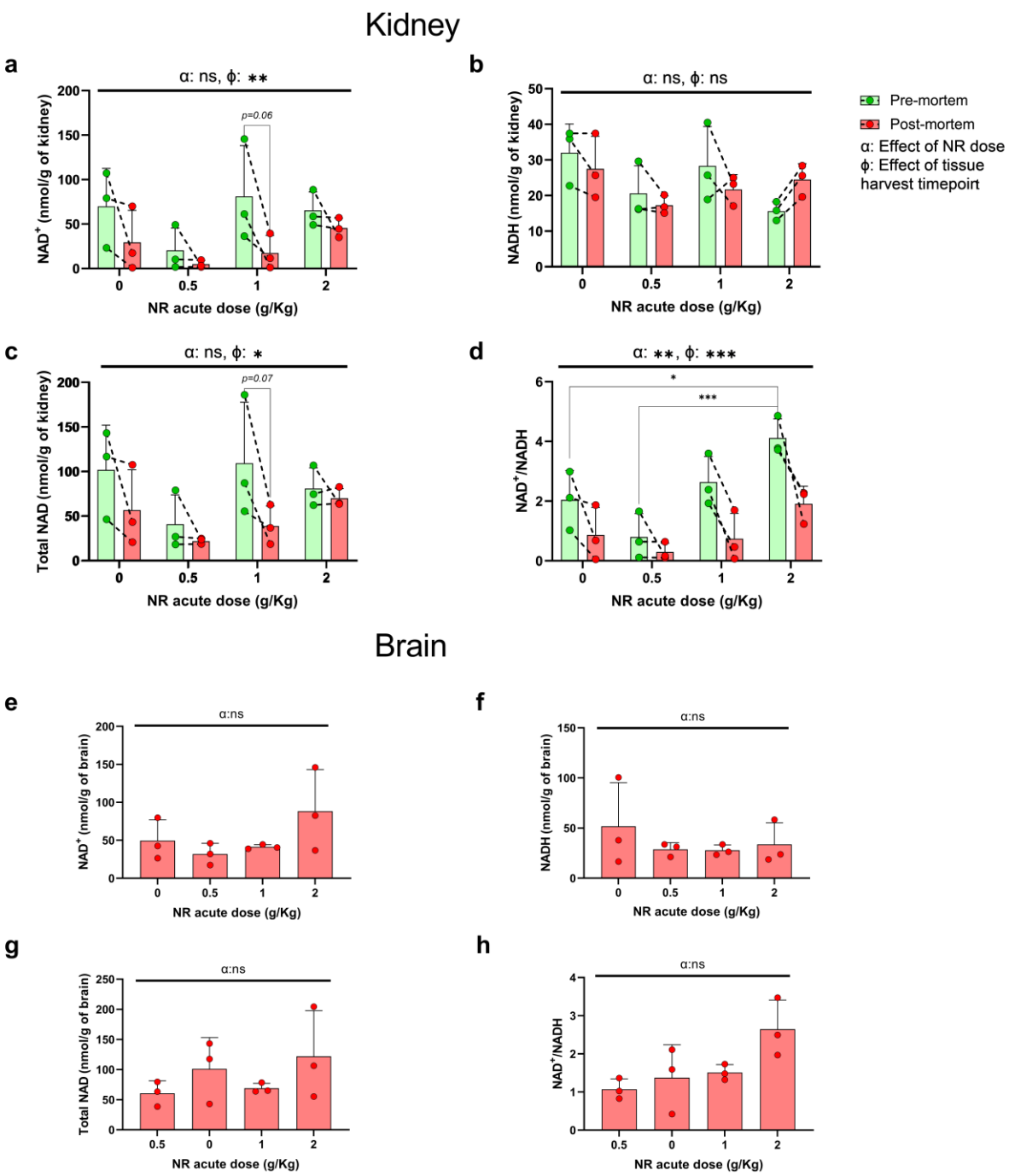

Figure 12: NAD$^+$, NADH, total NAD(H) levels (nmol/g of tissue), and NAD$^+$/NADH ratio in mouse kidney and brain samples harvested 2 hours after supplementation with acute doses of NR (0.5, 1, or 2 g/Kg). Kidney samples (a-d) from each mouse were harvested under anesthesia and before euthanasia (Pre-mortem) or after euthanasia (Post-mortem). Brain cortex samples (e-h) were harvested post-mortem. Each group contained samples from 3 different mice. Metabolite levels were measured by enzymatic colorimetric assay. For statistical analysis, repeated measure two-way ANOVAs with Sidak *post hoc* test for multiple comparisons were performed. α: Effect of NR dose. Φ: Effect of tissue harvest timepoint.

4.3.2. Acute and chronic NR supplementation reveals a significant increase in multiple NAD^+-related metabolites at multiple time points in mouse liver and muscle

To determine the effect of NR supplementation on the NAD^+ metabolome and its kinetics, we examined NAD^+-related metabolite levels at multiple timepoints following an acute dose. By examining the time course of whole-body NAD(H) changes following NR supplementation, we also studied changes in skeletal muscle, following liver metabolization and distribution. Additionally, we included a chronic daily treatment for 5 days to detect potential cumulative effects of the daily supplementation.

a. Liver

In liver samples, the majority of the metabolites displayed maximal concentrations between 4 and 8 hours after NR supplementation (Fig. 13 and 14). NAD^+ and NADH levels at 8 hours trended higher (12 and 7.5-fold higher than the control group, respectively) (Fig. 14a,b), but did not reach significance due to the between-subject variability within each group. Interestingly, the NAD^+/NADH ratio increased significantly with the acute doses and reached a plateau between 4 and 16 hours (Fig. 14c). NAM and its degradation metabolites: MeNAM and Me2PY were significantly increased, demonstrating the responsive activity of the NAD^+-consuming enzymes to a dose of NR (Fig. 13a-c). Among these metabolites, only MeNAM persisted after the last dose of the repeated 5-day supplementation. The metabolites of the NAM-salvage pathway, NR (Fig. 13d) and NMN (Fig. 14d), were significantly increased as a result of the acute dose but did not persist with the long-term 5-day treatment. Nonetheless, most of the measured metabolites reversed back to baseline 24 hours after the last dose of the 5-day treatment.

The increase in the Preiss-Handler pathway metabolites: NAAD, NAMN, NA, and the degradation metabolite of NA named nicotinuric acid (NUA) (Fig. 13e-h), has also been observed in a previous study following NR supplementation (28). Interestingly, this is despite the fact that only bacteria can transform NAM to NA, with no known similar enzymatic reaction in mammals. Thus, the increase in the Preiss-Handler metabolites after NR supplementation could be explained by three hypotheses: 1) the possible degradation of NAM by the intestinal flora into NA prior to its absorption or the existence of a similar enzyme in mammalian cells; 2) the potential accumulation of the Preiss-Handler metabolites due to the negative feedback on the NAD synthase enzyme; and 3) the existence of an enzyme responsible for NAD deamidation into NAAD, similar to NADP deamidation into NAADP as hypothesized by Trammell *et al.* (28).

Concerning the *de novo* pathway and other tryptophan metabolites, as expected, there was no significant increase in the quantifiable metabolites: tryptophan, serotonin (Fig. 14e,f), or L-Kynurenine (L-Kyn) (Fig. 13i) except a slight increase in 3-Hydroxykynurenine (3-HK) at 2 hours (Fig. 14g). 5-Hydroxytryptophan (5-HTP) and melatonin were undetectable in the liver samples.

ADPR levels (Fig.14h) displayed a ~2-fold increase at 16 hours after the acute dose and 24 hours after the repeated daily dose but did not reach overall significance (One-way ANOVA: p=0.37). cADPR levels (Fig.14i) peaked at 8 hours with a 13-fold increase but did not reach overall significance (One-way ANOVA: p=0.29). No changes were observed in NADP concentrations (Fig. 14j). Unfortunately, we were not able to quantify NADPH in positive ionization mode due to an abnormal peak shape.

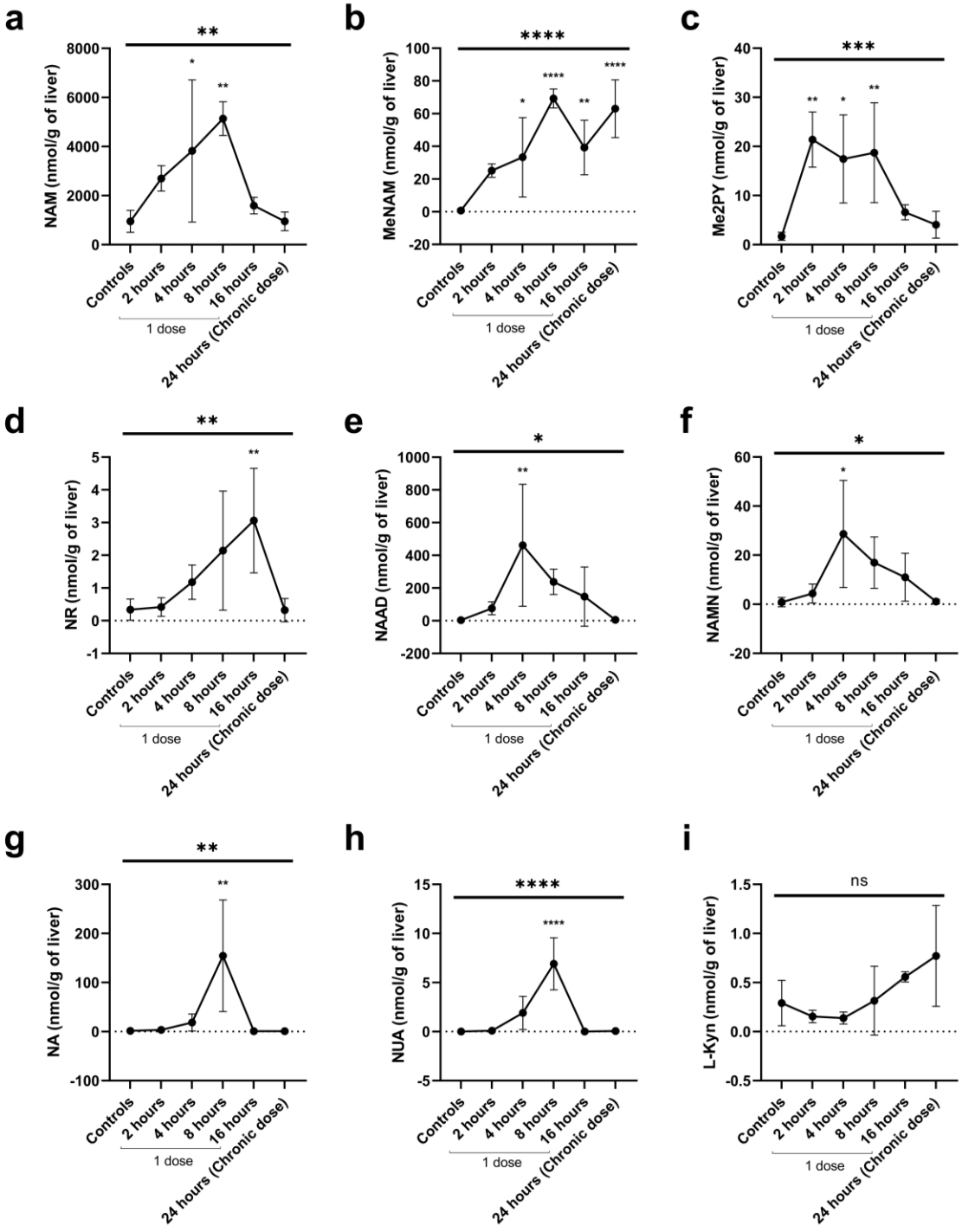

Figure 13: NAD$^+$-related metabolites concentrations in mouse liver samples after supplementation with an acute and chronic dose of NR (ISTD-normalized concentrations). Metabolites were quantified using a positive ionization mode LC-MS method with an external standard curve and internal standard spiking (^{13}C-labeled yeast extract). Statistical analysis: One-way ANOVA with Tukey's multiple comparisons tests.

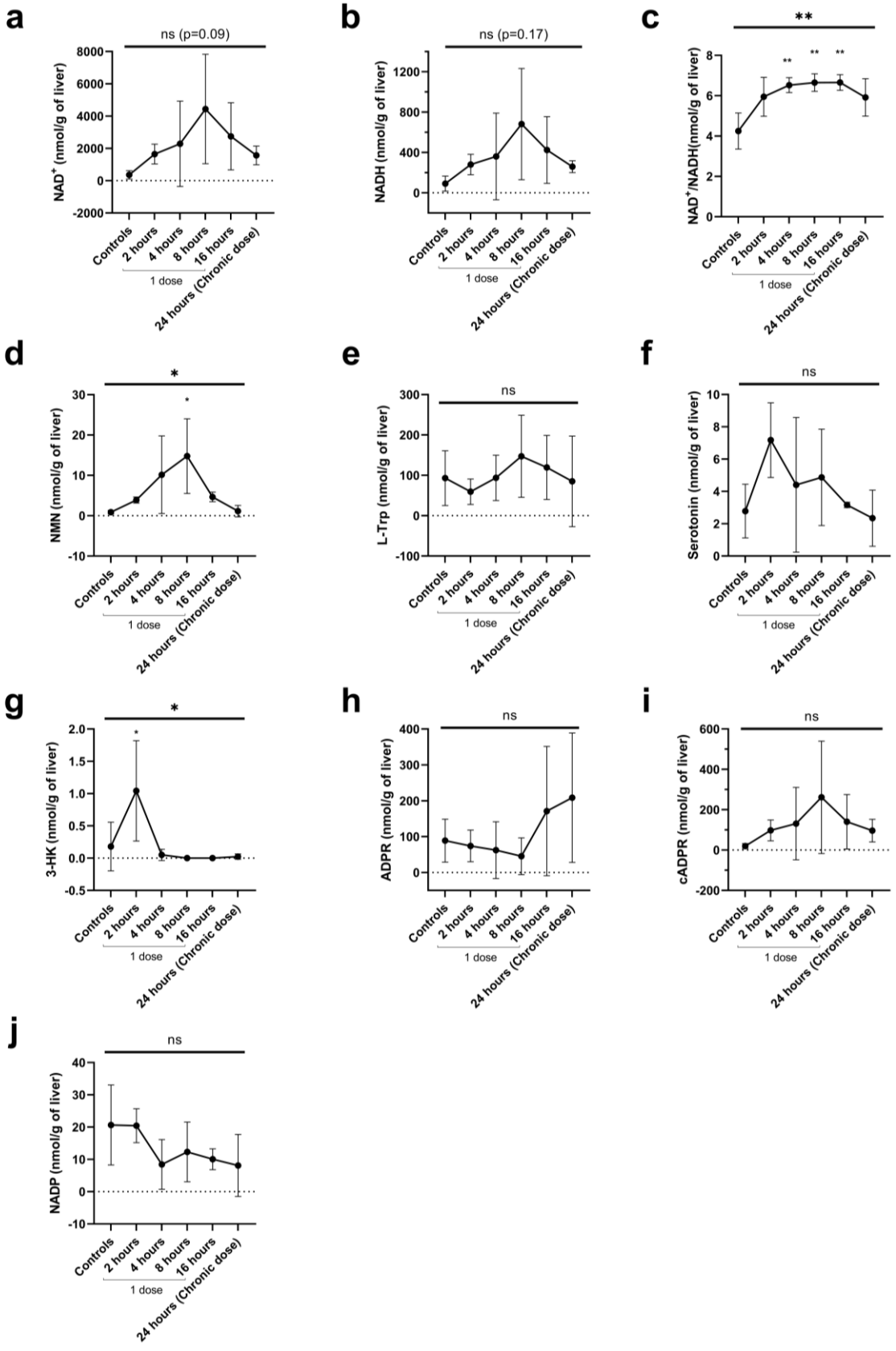
a
ns (p=0.09)
NAD+ (nmol/g of liver)
8000
6000
4000
2000
0
-2000
b
ns (p=0.17)
NADH (nmol/g of liver)
1200
800
400
0
c
**
NAD+/NADH(nmol/g of liver)
8
6
4
2
0
d
*
NMN (nmol/g of liver)
30
20
10
0
-10
e
ns
L-Trp (nmol/g of liver)
300
200
100
0
-100
f
ns
Serotonin (nmol/g of liver)
10
8
6
4
2
0
g
*
3-HK (nmol/g of liver)
2.0
1.5
1.0
0.5
0.0
-0.5
h
ns
ADPR (nmol/g of liver)
400
300
200
100
0
i
ns
cADPR (nmol/g of liver)
600
400
200
0
-200
j
ns
NADP (nmol/g of liver)
40
30
20
10
0
-10
Controls
2 hours
4 hours
8 hours
16 hours
24 hours (Chronic dose)
1 dose

Figure 14: NAD^+-related metabolites concentrations in mouse liver samples after supplementation with an acute and chronic dose of NR. Metabolites were quantified using a positive ionization mode LC-MS method with an external standard curve. Statistical analysis: One-way ANOVA with Tukey's multiple comparisons tests.

To better visualize the individual metabolite changes for each metabolic pathway involved in NAD^+ biosynthesis or degradation, the Log2 fold change of the mean concentrations of the 8-hour acute dose group versus the control group were mapped in figure 15. The *de novo* pathway did not display any changes except in the last reactions where it is merged with the Preiss-Handler pathway, which showed the most important increase in the metabolite concentrations at 8 hours (Fig. 15) but these changes did not persist in the long-term treatment group (Fig. 13e-h). As expected, the NAM-salvage pathway exhibited an increase in its metabolites and the corresponding downstream degradation products (MeNAM and Me2PY) (Fig. 15). Additionally, while most of these metabolites, including NR, NMN, and NAM, quickly decreased over time, MeNAM persisted in the 5-day treatment (Fig. 13b).

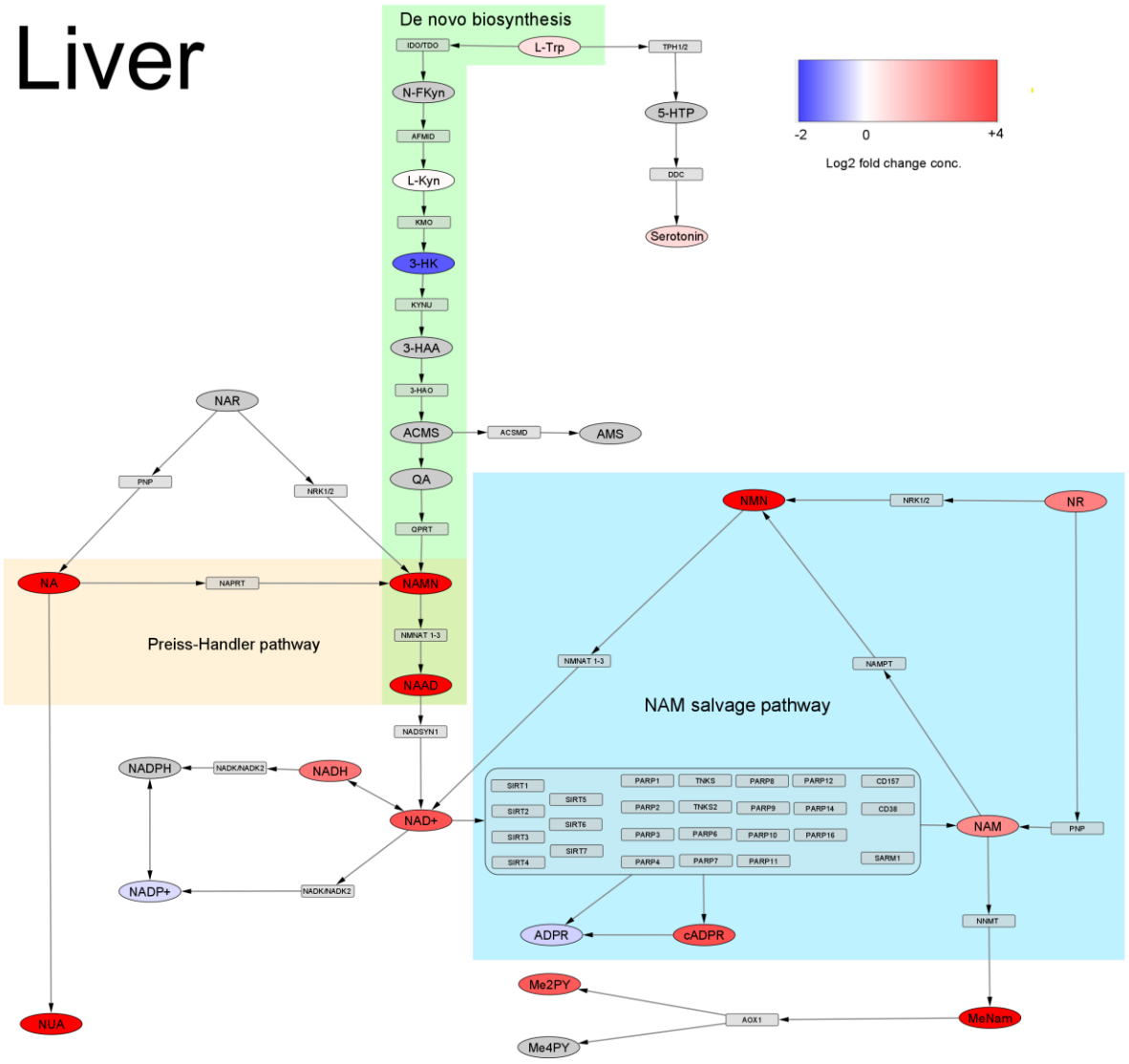

Figure 15: Overview of the liver NAD$^+$ metabolome with a heatmap of log2 fold change of average metabolite levels at 8 hours after oral NR supplementation versus non-treated controls. Metabolites are represented by oval shapes with the inner color representing the log2 fold change of the metabolite concentrations in the treated group 8 hours after supplementation versus the control group. Metabolites in grey were either below the limit of quantification or not measured due to the unavailability of the corresponding external standards. Enzymes are represented by rectangular shapes.

Finally, we also compared metabolite levels in pre- and post-mortem liver samples in the control and 2-hour timepoint groups. NMN and NADP levels were significantly lower in post-mortem samples from the 2-hour supplementation group with no changes in the control group. Serotonin levels were significantly lower in post-mortem samples for the control group ($p=0.04$) and above significance for the 2-hour group ($p=0.086$). Me2PY was higher in post-mortem control samples but not in the 2-hour NR supplementation group. However, in both control and treatment groups, no significant changes were observed for the rest of the metabolites: NAD, NADH, NAM, MeNAM, L-Trp, ADPR, cADPR, 3-HK, NR, NA, NAMN, L-Kyn, NUA (Supp. Table 12).

b. Skeletal muscle

In comparison to the liver, muscle metabolite concentrations were overall lower and only 13 metabolites were quantifiable in the gastrocnemius muscle. Despite lower concentrations, the quantified metabolites in muscle displayed similar kinetics to the liver, with most of the metabolites peaking at 8 hours after the acute NR dose (Fig. 16 and 17). Similar to the liver results, changes in the NAD^+ and NADH concentrations were not statistically significant despite a 4.5- and 4.7-fold trend for increase, respectively, at 8 hours versus controls (Fig. 16a,b). Although not reaching significance, the maximum fold change of 1.7 in the NAD^+/NADH ratio of muscle in NR-treated mice at 16 hours was similar to the maximal fold change in liver (1.6) at 8 hours (Fig. 16c). In fact, NR started increasing at 2 hours and peaked at 4 hours but then quickly returned to baseline (Fig. 16d). NAM (Fig. 17a), MeNAM (Fig. 17b), and Me2PY (Fig. 16e) displayed the most significant changes with a peak at 8 hours, similar to that seen in liver samples. A transient and non-significant increase was observed for ADPR (Fig. 16f) and cADPR levels (Fig. 17c). NA and NUA (Preiss-Handler pathway) increased significantly after treatment with peaks at 8 hours (Fig. 17d,e). There were no significant changes in tryptophan (Fig. 16g), serotonin (Fig. 16h), and

NADP (Fig. 17f) levels. For the long-term NR treatment, all metabolites returned to baseline 24 hours after the last dose of the 5-day treatment, including MeNAM, which was still high in the liver samples at the same timepoint (Fig. 16a-c). This would indicate that there is no lasting or cumulative effect of NR treatment on muscle.

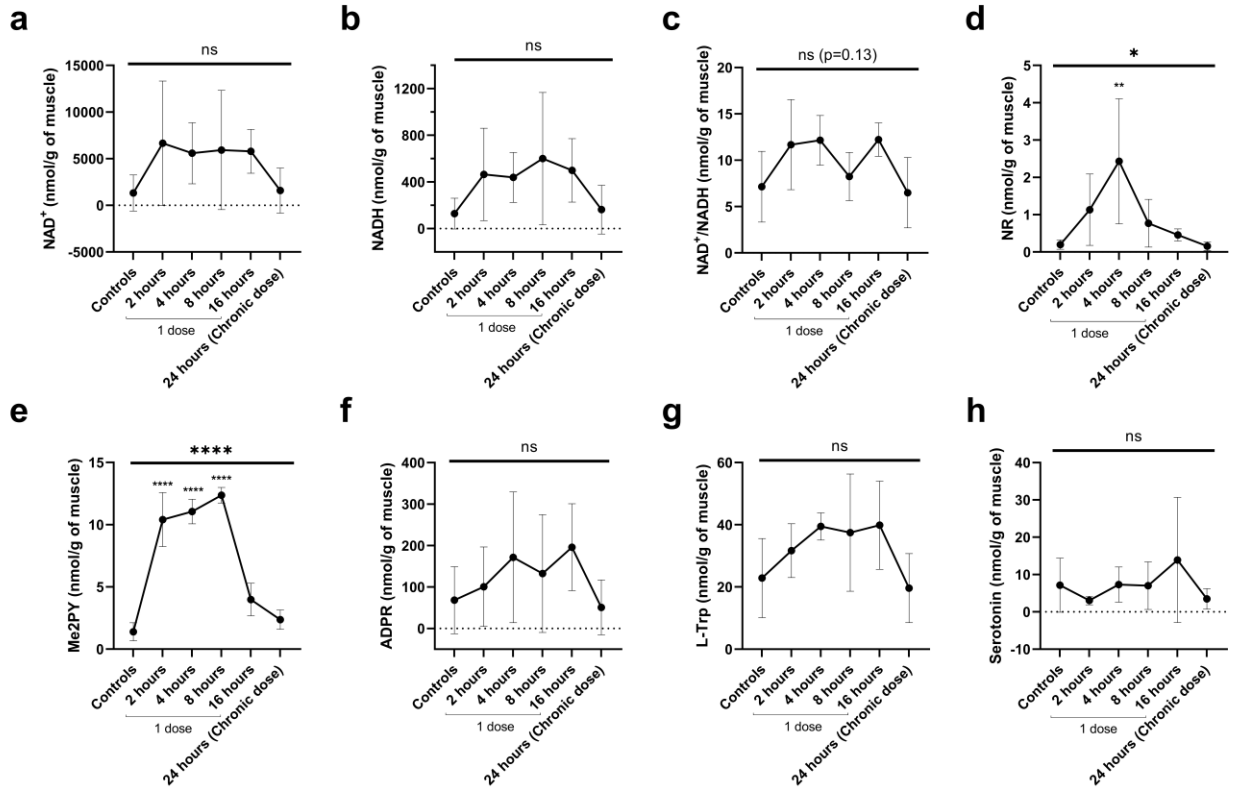

Figure 16: NAD$^+$-related metabolites concentrations in mouse skeletal muscle samples after supplementation with an acute and chronic dose of NR (ISTD-normalized concentrations). Metabolites were quantified using a positive ionization mode LC-MS method with an external standard curve and internal standard spiking (^{13}C-labeled yeast extract). Statistical analysis: One-way ANOVA with Tukey's multiple comparisons tests.

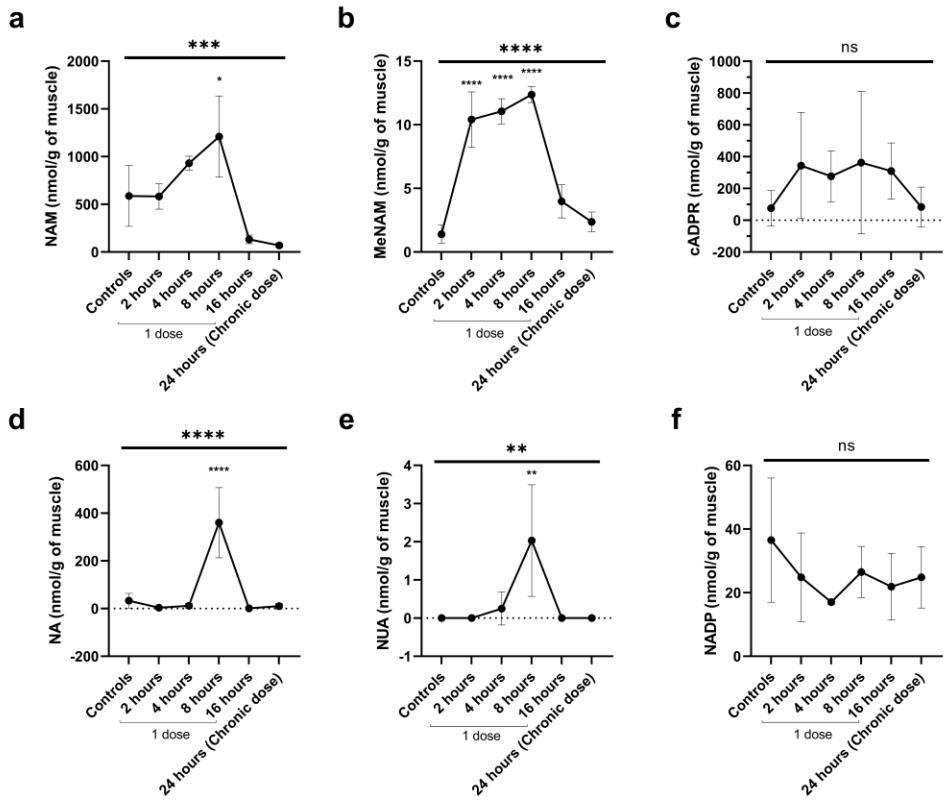

Figure 17: NAD$^+$-related metabolites concentrations in mouse skeletal muscle samples after supplementation with an acute and chronic dose of NR. Metabolites were quantified using a positive ionization mode LC-MS method with an external standard curve. Statistical analysis: One-way ANOVA with Tukey's multiple comparisons tests.

NMN, NAMN, NAAD, 3-HK, and L-Kyn were detected in muscle, but unlike liver, were not quantified in control samples, as they were close to or lower than the limit of detection (LOD). For these metabolites, null values (mainly from the control group) were replaced by the LOD/3 for the calculation of the log fold change of concentration at 8 hours, as shown in the heatmap of the muscle NAD$^+$ metabolome (Fig. 18). Similar to the liver results, 3-HK and L-Kyn (*De novo* pathway) did not show changes at 8 hours but the metabolites of the Preiss-Handler pathway, NAMN and NAAD, were significantly increased in the NR-treated while being undetectable in the control group, which is consistent with the liver results and the increase in NA and NUA in muscle (Fig. 18).

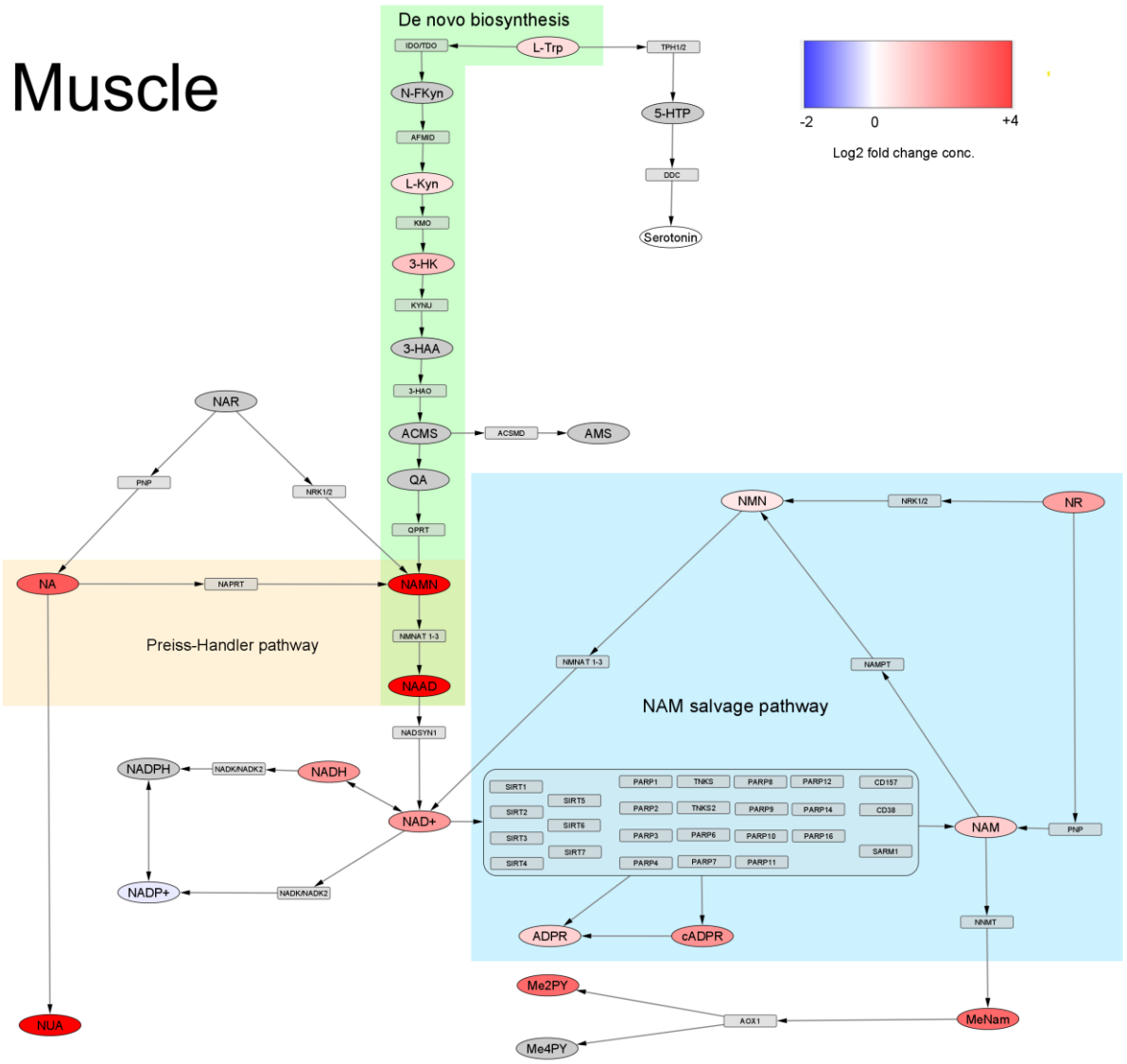

Figure 18: Overview of the skeletal muscle NAD$^+$ metabolome with a heatmap of log2 fold change of average metabolite levels at 8 hours after oral NR supplementation versus non-treated controls. Metabolites are represented by oval shapes with the inner color representing the log2 fold change of the metabolite concentrations in the treated group 8 hours after supplementation versus the control group. Metabolites in grey were either below the limit of quantification or not measured due to the unavailability of the corresponding external standards. Enzymes are represented by rectangle shapes.

Metabolite concentrations obtained from pre- and post-mortem harvest in the control and 2-hour post-supplementation groups were compared. The measured concentrations for the two harvest timepoints were not significantly different in both groups for the majority of the

metabolites considered for the analysis except for NAM (p=0.04) and NA (p=0.04) in the control group (Supp. Table 13).

4.4. Discussion

While most studies have focused on the short-term impact of acute supplementation with NAD^+ precursors on NAD^+ and NADH levels, there is still a lack of data on the dose- and time-dependent effects of NAD^+ precursor supplementation on the whole NAD^+ metabolome in various tissues. To complete the knowledge gaps, our study aimed to determine the quantitative variations in the NAD^+ metabolome in various tissues over time after acute and chronic oral supplementation with the NAD^+ precursor NR. Additionally, as NAD^+ metabolites have been mainly quantified in post-mortem samples, we also addressed the potential effect of the tissue harvest timepoint on the measured *in vivo* metabolite levels.

The preliminary analysis of NAD^+ and NADH variation after acute oral NR supplementation showed a significant dose-dependent increase in liver NAD^+ and NADH levels, validating the efficiency of NR supplementation. However, no significant changes were observed with any of the 3 doses (0.5, 1, and 2 g/Kg) at the same timepoint (2 hours) in the other tissues (skeletal muscle, brain, and kidney). Two potential explanations for the absence of changes in the other tissues are either: 1) Oral NR supplementation was inefficient in increasing NAD(H) levels in these tissues because of the hepatic first-pass effect and low bioavailability of the oral dose (52), or 2) The tissue harvest time was too early to detect changes in NAD(H) levels following NR supplementation in the target tissues. Thus, we decided to repeat the experiment and harvest tissue samples at different timepoints to monitor the changes in NAD^+ metabolome over time.

For the second NR supplementation experiment, mice received a single acute oral dose (2 g/Kg) of NR and tissues were harvested at 2, 4, 8, and 16 hours. A repeated daily dose (2g/Kg

per day for 5 days) was also used to detect any potential cumulative effect. Subsequently, we measured NAD^+-related metabolite levels in liver and skeletal muscle and showed that oral NR supplementation increased NAD^+-related metabolites in both liver and skeletal muscle with maximum metabolite concentrations occurring around 8 hours after the acute NR dose. The variability in metabolites levels observed between 4 and 16 hours can be explained by the low number of biological replicates and the differences in the bioavailability and/or asynchronous metabolism of NR by the different animal subjects in each group (Supp. Fig. 20). The maximum mean NAD^+ and NADH concentrations were 12 and 7.5-fold higher in the liver and trended to be 4.5- and 4.7-fold higher in the muscle, respectively. The maximal increase in the NAD^+/NADH ratio was similar between the liver (1.6-fold change at 8 hours) and the muscle (1.7-fold change at 16 hours) even though it did not reach significance in the muscle samples. Similar to our observations, NR has been shown to increase the NAD^+/NADH ratio in mouse tissues by previous studies (27, 218) but our 5-day daily supplementation results also show the transient nature of these changes, and the lack of cumulative effect, with a return to baseline at 24 hours after the last dose. Although increasing the NAD^+/NADH ratio has been shown to be beneficial against age-related metabolic disorders (86, 217, 225), it seems very likely that this increase in the ratio is capped in young healthy animals to maintain an optimal physiological level. Additionally, in both liver and skeletal muscle, the accumulation of NAM-salvage pathway metabolites (NAM, NR, NMN, cADPR) and the degradation metabolites: MeNAM and Me2PY, reveals the important activity of the NAD^+-consuming enzymes.

Our results are consistent with the metabolic fluxes quantified by Liu *et al.* following NR supplementation, which show that the liver uses NAM for NAD^+ production or releases it in the circulation (52). This explains the rapid decrease in liver NAM levels after the 8-hour timepoint.

In skeletal muscle, both NAM and its degradation metabolite MeNAM decrease after the 8-hour timepoint and do not accumulate with the repeated daily dose. In both tissues, we did not observe a cumulative effect with the 5-day daily dose as most of the metabolite levels were back to baseline 24 hours after the last dose except for MeNAM, which persisted in the liver at the 24-hour timepoint. The accumulation of MeNAM in the liver can be explained by the major detoxification role of the liver, including the methylation of metabolites as part of their excretion process (226, 227). The increase in NAM and liver methylation function raises questions about potential adverse effects that may arise from the depletion of the cellular methyl pool leading to altered DNA and protein methylation and the inhibition of PARPs, which can result in DNA repair defects (47, 228). Thus, the 2 g/Kg dose results may imply that long-term treatments at high doses are not safe, especially in cases where the hepatic detoxification function and/or the renal excretion efficiency are impaired (156, 229).

NR supplementation also raised metabolite levels from the Preiss-Handler pathway (NAAD, NAMN, NA, and NUA) in the liver and muscle samples, which is consistent with the observations made by Trammell *et al.* (28) and Martens *et al.* (94) in human PBMCs and/or mouse liver samples. Trammell *et al.* used labeled NR to show its incorporation in NAAD, which reinforces the hypothesis of the existence of a metabolic loop that allows the transformation of NR into the Preiss-Handler intermediates. This probably occurs via the deamidation of NAD^+ into NAAD at high NAD^+ concentrations. However, it is still unclear whether this activity would be due to an unknown mammalian enzyme or to the metabolization by the gut microbiome. As expected, no significant changes were observed in the *de novo* pathway in either tissue. Finally, concerning the effect of tissue harvest time, it seems that, overall, it does not drastically impact

the quantification results in these conditions where the tissue samples are extracted under low-temperature conditions and snap-frozen in liquid nitrogen immediately.

Overall, NR was efficient at increasing the NAD^+-related metabolites from the NAM-salvage and Preiss-Handler pathways. Our findings show that daily supplementation is necessary to maintain higher NAD^+ and NADH levels, as they are rapidly converted, utilized, and degraded. However, the important accumulation of degradation metabolites in healthy subjects, which can be exacerbated in pathological conditions, could have a major impact and potentially undesirable consequences on the activity of the enzymes involved in NAD^+ metabolism. Further studies will be necessary to determine the effect of NR supplementation on enzymatic activities, specifically on the NAD^+-consuming enzymes, which play a crucial role in metabolism and signalling pathways.

4.5. Limitations

In order to expand the study to multiple timepoints, only 3 biological replicates were used for the NR-supplemented groups, as the aim of this study was to determine the optimal doses and tissue-harvest timepoints for future evaluations.

Chapter 5: Conclusion

This research aimed to develop a targeted LC-MS-based method for the quantification of the NAD^+ metabolome and demonstrate the ability of the NAD^+ precursor nicotinamide riboside to increase *in vivo* tissue concentrations of NAD^+-related metabolites. Additionally, the meta-analysis of NAD(P)(H) quantification results outlined the various analytical methods used to quantify NAD^+ and its metabolites in tissue samples and addressed the important variability as well as the lack of standardization of the pre-analytical and analytical steps.

The main challenges when quantifying NAD^+ and its metabolites in tissue samples are the rapid enzymatic interconversion of the NAD^+-related metabolites in tissue samples (189), as well as the chemical instability of some metabolites under certain conditions (e.g., instability of the reduced metabolites NADH and NADPH in acidic solutions) (214). Therefore, it is crucial to maintain optimal conditions, such as pH and temperature, and to quickly inactivate the enzymes in the samples when studying the NAD^+ metabolome. The recent interest in LC-MS methods for the study of the NAD^+ metabolome has led to the development of various metabolite extraction and analysis protocols, which resulted in disparities between studies. Important factors that were considered as potential sources of errors were the sample collection and processing conditions, metabolite extraction procedures, and analytical parameters including the absence of appropriate quality controls. Most importantly, the inability to compare the quantitative results between studies stems from the lack of clear guidelines for quality assessment and the lack of compatibility in terminology, such as the use of the terms “absolute” and “relative” quantification.

By developing a quantitative LC-MS-based NAD metabolomics method including yeast-derived internal standards, this thesis brings to light the various challenges inherent to quantitative LC-MS analysis and the nature of NAD^+ metabolites in particular. The pre-analytical conditions

were selected to ensure the stability of NAD^+ and its metabolites and avoid any sources of contamination. The LC-Q/TOF method was optimized to detect and quantify the metabolites of interest in various tissue samples. As advised by the United States Food & Drug Administration (U.S. FDA) and the European Medicines (EMA) agencies, absolute quantification should include the use of internal controls. The stable labeled internal standards incorporated in this method were produced in-house from a yeast culture in ^{13}C-labeled minimal media. While we acknowledge that this type of internal standard can potentially add undesired interferences because of its origin, it is still the most practical internal quality control alternative available at the moment. Consequently, for every batch analysis, the yeast-derived internal standards must undergo a quality assessment for every measured metabolite to confirm whether they can be used for the internal normalization of the results.

After optimization, this method was used to study the NAD^+ metabolome *in vivo* after supplementing mice with the NAD^+ precursor NR. However, during the preliminary NR supplementation experiment, we preferred the use of an enzyme cycling method to first confirm the positive effect of NR on NAD^+ and NADH levels. Indeed, NR increased NAD^+ and NADH levels in liver samples 2 hours after supplementation. However, there were no effects of this in the other tissues (skeletal muscle, brain, and kidney). Based on these results, we designed a multiple-timepoint study with an acute dose, as well as a repeated daily dose, to examine the effect of NR on the NAD^+ metabolome over time. The quantitative LC-MS analysis results showed that NR was efficient at increasing the *in vivo* concentrations for most of the NAD^+-related metabolites, with the maximal increase occurring around the 8-hour timepoint. In particular, NR stimulated the activity of the NAM-salvage pathway in the liver and skeletal muscle, which increased NAD^+ consumption and the production of NAM and other degradation metabolites. While the

metabolomics results don't allow us to determine the type of enzymes involved in NAD^+ degradation into NAM, they raise concerns about potential adverse effects due to the accumulation of NAM and its methylated metabolites. Our results also confirm findings from other studies (28, 94) showing the increase in the Preiss-Handler pathway intermediates (NAAD, NAMN, NA) following NR supplementation even though there is no known enzymatic reaction converting NR to one of these intermediates. Further studies are needed to identify the link between NR supplementation and the unexpected changes in the Preiss-Handler pathway.

The main contributions of this research are the following 1) the collection and analysis of qualitative and quantitative data from published literature including quantitative NAD(P)(H) results; 2) the development of an LC-MS-based quantification protocol and the generation of yeast-derived stable isotope internal standards for the quantification of NAD^+-related metabolites; and 3) a thorough study of the impact of oral NR supplementation on the NAD^+ metabolome illustrating the dose- and time-dependent effects of NR on major target tissues.

Overall, our results confirm that NR is effective in increasing NAD^+ and stimulating the activity of the NAM-salvage pathway. Future studies should address the implications of long-term NR supplementation and particularly the potential effects of the accumulation of NAM, as well as other by-products, on cellular metabolism and signaling pathways. Furthermore, it is essential to optimize and standardize the quantification methods in order to guarantee the accuracy and reproducibility of NAD^+ metabolome measurements in pre-clinical and clinical studies. This will improve the assessment of therapeutic interventions on the NAD^+ metabolome, which is crucial for the development of safe and effective applications in human health.

Bibliography

1. Young AH and WJ. 1906. The alcoholic ferment of yeast-juice. Part II.—The coferment of yeast-juice. Proc Royal Soc Lond Ser B Contain Pap Biological Character 78:369–375.

2. Chelpin H von E. 1930. Fermentation of sugars and fermentative enzymes. Nobel lecture.

3. Warburg O, Christian W. 1936. Pyridin, der wasserstoffübertragende Bestandteil von Gärungsfermenten. Helv Chim Acta 19:E79–E88.

4. Goldberger J, Tanner WF. 1922. Amino-acid deficiency probably the primary etiological factor in pellagra. Public Health Reports (1896-1970) 35:462–486.

5. Elvehjem CA, Madden RJ, Strong FM, Woolley DW. 1937. The isolation and identification of the anti-black tongue factor. J Biol Chem 123:137-149.

6. Elvehjem CA, Madden RJ, Strong FM, Woolley DW. 1937. Relation of nicotinic acid and nicotinic acid amide to canine black tongue. J Am Chem Soc 59:1767–1768.

7. Kornberg A. 1948. The participation of inorganic pyrophosphate in the reversible enzymatic synthesis of diphosphopyridine nucleotide. J Biol Chem 176:1475.

8. Preiss J, Handler P. 1958. Biosynthesis of Diphosphopyridine Nucleotide: I. Identification of intermediates. J Biol Chem 233:488-492.

9. Preiss J, Handler P. 1958. Biosynthesis of diphosphopyridine nucleotide. II. Enzymatic aspects. J Biol Chem 233:493–500.

10. Goldsmith GA. 1958. Niacin-Tryptophan Relationships in Man and Niacin Requirement. Am J Clin Nutrition 6:479–486.

11. Goldsmith GA, Miller ON, Unglaub WG. 1961. Efficiency of Tryptophan as a Niacin Precursor in Man. J Nutrition 73:172–176.

12. Chambon P, Weill JD, Mandel P. 1963. Nicotinamide mononucleotide activation of a new DNA-dependent polyadenylic acid synthesizing nuclear enzyme. Biochem Bioph Res Co 11:39–43.

13. Chambon P, Weill JD, Doly J, Strosser MT, Mandel P. 1966. On the formation of a novel adenylic compound by enzymatic extracts of liver nuclei. Biochem Bioph Res Co 25:638–643.

14. Benjamin RC, Gill DM. 1980. ADP-ribosylation in mammalian cell ghosts. Dependence of poly(ADP-ribose) synthesis on strand breakage in DNA. J Biol Chem 255:10493–501.

15. Satoh M, Lindahl T. 1992. Role of poly(ADP-ribose) formation in DNA repair. Nature 356:356–358.

16. Berger NA. 1985. Poly(ADP-Ribose) in the Cellular Response to DNA Damage. Radiat Res 101:4.

17. Lazebnik YA, Kaufmann SH, Desnoyers S, Poirier GG, Earnshaw WC. 1994. Cleavage of poly(ADP-ribose) polymerase by a proteinase with properties like ICE. Nature 371:346–347.

18. Tewari M, Quan LT, O'Rourke K, Desnoyers S, Zeng Z, Beidler DR, Poirier GG, Salvesen GS, Dixit VM. 1995. Yama/CPP32β, a mammalian homolog of CED-3, is a CrmA-inhibitable protease that cleaves the death substrate poly(ADP-ribose) polymerase. Cell 81:801–809.

19. Imai S, Armstrong CM, Kaeberlein M, Guarente L. 2000. Transcriptional silencing and longevity protein Sir2 is an NAD-dependent histone deacetylase. Nature 403:795–800.

20. Luongo TS, Eller JM, Lu M-J, Niere M, Raith F, Perry C, Bornstein MR, Oliphint P, Wang L, McReynolds MR, Migaud ME, Rabinowitz JD, Johnson FB, Johnsson K, Ziegler M, Cambronne XA, Baur JA. 2020. SLC25A51 is a mammalian mitochondrial NAD+ transporter. Nature 588:174–179.

21. Bender DA. 1983. Effects of a dietary excess of leucine on the metabolism of tryptophan in the rat: a mechanism for the pellagragenic action of leucine. Brit J Nutr 50:25–32.

22. Bender DA, Olufunwa R. 1988. Utilization of tryptophan, nicotinamide and nicotinic acid as precursors for nicotinamide nucleotide synthesis in isolated rat liver cells. Brit J Nutr 59:279–287.

23. Ikeda M, Tsuji H, Nakamura S, Ichiyama A, Nishizuka Y, Hayaishi O. 1965. Studies on the biosynthesis of nicotinamide adenine dinucleotide. II. A role of picolinic carboxylase in the biosynthesis of nicotinamide adenine dinucleotide from tryptophan in mammals. J Biol Chem 240:1395–401.

24. Mouchiroud L, Houtkooper RH, Auwerx J. 2013. NAD+ metabolism: A therapeutic target for age-related metabolic disease. Crit Rev Biochem Mol 48:397–408.

25. Houtkooper RH, Cantó C, Wanders RJ, Auwerx J. 2010. The Secret Life of NAD+: An Old Metabolite Controlling New Metabolic Signaling Pathways. Endocr Rev 31:194–223.

26. Bogan KL, Brenner C. 2008. Nicotinic Acid, Nicotinamide, and Nicotinamide Riboside: A Molecular Evaluation of NAD+ Precursor Vitamins in Human Nutrition. Annu Rev Nutr 28:115–130.

27. Bieganowski P, Brenner C. 2004. Discoveries of Nicotinamide Riboside as a Nutrient and Conserved NRK Genes Establish a Preiss-Handler Independent Route to NAD+ in Fungi and Humans. Cell 117:495–502.

28. Trammell SAJ, Schmidt MS, Weidemann BJ, Redpath P, Jaksch F, Dellinger RW, Li Z, Abel ED, Migaud ME, Brenner C. 2016. Nicotinamide riboside is uniquely and orally bioavailable in mice and humans. Nat Commun 7:12948.

29. Belenky P, Bogan KL, Brenner C. 2007. NAD+ metabolism in health and disease. Trends Biochem Sci 32:12–19.

30. Osterloh JM, Yang J, Rooney TM, Fox AN, Adalbert R, Powell EH, Sheehan AE, Avery MA, Hackett R, Logan MA, MacDonald JM, Ziegenfuss JS, Milde S, Hou Y-J, Nathan C, Ding A, Brown RH, Conforti L, Coleman M, Tessier-Lavigne M, Züchner S, Freeman MR. 2012. dSarm/Sarm1 Is Required for Activation of an Injury-Induced Axon Death Pathway. Science 337:481–484.

31. Schreiber V, Dantzer F, Ame J-C, Murcia G de. 2006. Poly(ADP-ribose): novel functions for an old molecule. Nat Rev Mol Cell Bio 7:517–528.

32. Menzies KJ, Zhang H, Katsyuba E, Auwerx J. 2016. Protein acetylation in metabolism — metabolites and cofactors. Nat Rev Endocrinol 12:43.

33. Haigis MC, Sinclair DA. 2010. Mammalian Sirtuins: Biological Insights and Disease Relevance. Annu Rev Pathology 5:253–295.

34. Malavasi F, Deaglio S, Funaro A, Ferrero E, Horenstein AL, Ortolan E, Vaisitti T, Aydin S. 2008. Evolution and Function of the ADP Ribosyl Cyclase/CD38 Gene Family in Physiology and Pathology. Physiol Rev 88:841–886.

35. Fliegert R, Gasser A, Guse AH. 2007. Regulation of calcium signalling by adenine-based second messengers. Biochem Soc T 35:109–114.

36. Essuman K, Summers DW, Sasaki Y, Mao X, DiAntonio A, Milbrandt J. 2017. The SARM1 Toll/Interleukin-1 Receptor Domain Possesses Intrinsic NAD+ Cleavage Activity that Promotes Pathological Axonal Degeneration. Neuron 93:1334-1343.e5.

37. Hopkins EL, Gu W, Kobe B, Coleman MP. 2021. A Novel NAD Signaling Mechanism in Axon Degeneration and its Relationship to Innate Immunity. Frontiers Mol Biosci 8:703532.

38. O'Reilly T, Niven DF. 2003. Levels of nicotinamide adenine dinucleotide in extracellular body fluids of pigs may be growth-limiting for Actinobacillus pleuropneumoniae and Haemophilus parasuis. Can J Vet Res Revue Can De Recherche Vétérinaire 67:229–31.

39. Schwarzmann L, Pliquett RU, Simm A, Bartling B. 2021. Sex-related differences in human plasma NAD+/NADH levels depend on age. Bioscience Rep 41.

40. Bruzzone S, Guida L, Zocchi E, Franco L, Flora AD. 2001. Connexin 43 hemichannels mediate Ca2+-regulated transmembrane NAD+ fluxes in intact cells. Faseb J 15:10–12.

41. Bruzzone S, Franco L, Guida L, Zocchi E, Contini P, Bisso A, Usai C, Flora AD. 2001. A Self-restricted CD38-connexin 43 Cross-talk Affects NAD+ and Cyclic ADP-ribose Metabolism and Regulates Intracellular Calcium in 3T3 Fibroblasts*. J Biol Chem 276:48300–48308.

42. Billington RA, Travelli C, Ercolano E, Galli U, Roman CB, Grolla AA, Canonico PL, Condorelli F, Genazzani AA. 2008. Characterization of NAD Uptake in Mammalian Cells*. J Biol Chem 283:6367–6374.

43. Mutafova-Yambolieva VN, Hwang SJ, Hao X, Chen H, Zhu MX, Wood JD, Ward SM, Sanders KM. 2007. β-Nicotinamide adenine dinucleotide is an inhibitory neurotransmitter in visceral smooth muscle. Proc National Acad Sci 104:16359–16364.

44. Smyth LM, Bobalova J, Mendoza MG, Lew C, Mutafova-Yambolieva VN. 2004. Release of β-Nicotinamide Adenine Dinucleotide upon Stimulation of Postganglionic Nerve Terminals in Blood Vessels and Urinary Bladder*. J Biol Chem 279:48893–48903.

45. Kulikova V, Shabalin K, Nerinovski K, Yakimov A, Svetlova M, Solovjeva L, Kropotov A, Khodorkovskiy M, Migaud ME, Ziegler M, Nikiforov A. 2019. Degradation of Extracellular NAD+ Intermediates in Cultures of Human HEK293 Cells. Metabolites 9:293.

46. Synesiou E, Fairbanks LD, Simmonds HA, Slominska EM, Smolenski RT, Carrey EA. 2011. 4-Pyridone-3-carboxamide-1-β-D-ribonucleoside Triphosphate (4PyTP), a Novel NAD+ Metabolite Accumulating in Erythrocytes of Uremic Children: A Biomarker for a Toxic NAD+ Analogue in Other Tissues? Toxins 3:520–537.

47. Hwang ES, Song SB. 2020. Possible Adverse Effects of High-Dose Nicotinamide: Mechanisms and Safety Assessment. Biomol 10:687.

48. Love NR, Pollak N, Dölle C, Niere M, Chen Y, Oliveri P, Amaya E, Patel S, Ziegler M. 2015. NAD kinase controls animal NADP biosynthesis and is modulated via evolutionarily divergent calmodulin-dependent mechanisms. Proc National Acad Sci 112:1386–1391.

49. Chen L, Zhang Z, Hoshino A, Zheng H, Morley M, Arany Z, Rabinowitz JD. 2019. NADPH production by the oxidative pentose-phosphate pathway supports folate metabolism. Nat Metab 404–415.

50. Figueira TR, Francisco A, Ronchi JA, Santos GRRM dos, Santos W dos, Treberg JR, Castilho RF. 2021. NADPH supply and the contribution of NAD(P)+ transhydrogenase (NNT) to H2O2 balance in skeletal muscle mitochondria. Arch Biochem Biophys 707:108934.

51. Leopold JA, Zhang Y-Y, Scribner AW, Stanton RC, Loscalzo J. 2003. Glucose-6-Phosphate Dehydrogenase Overexpression Decreases Endothelial Cell Oxidant Stress and Increases Bioavailable Nitric Oxide. Arteriosclerosis Thrombosis Vasc Biology J Am Hear Assoc 23:411–417.

52. Liu L, Su X, Quinn WJ, Hui S, Krukenberg K, Frederick DW, Redpath P, Zhan L, Chellappa K, White E, Migaud M, Mitchison TJ, Baur JA, Rabinowitz JD. 2018. Quantitative Analysis of NAD Synthesis-Breakdown Fluxes. Cell Metab 27:1067-1080.e5.

53. Ratajczak J, Joffraud M, Trammell SAJ, Ras R, Canela N, Boutant M, Kulkarni SS, Rodrigues M, Redpath P, Migaud ME, Auwerx J, Yanes O, Brenner C, Cantó C. 2016. NRK1 controls nicotinamide mononucleotide and nicotinamide riboside metabolism in mammalian cells. Nat Commun 7:13103.

54. Xiao W, Wang R-S, Handy DE, Loscalzo J. 2018. NAD(H) and NADP(H) Redox Couples and Cellular Energy Metabolism. Antioxid Redox Sign 28:251–272.

55. Lunt SY, Heiden MGV. 2011. Aerobic Glycolysis: Meeting the Metabolic Requirements of Cell Proliferation. Annu Rev Cell Dev Bi 27:441–464.

56. Bai P, Cantó C, Oudart H, Brunyánszki A, Cen Y, Thomas C, Yamamoto H, Huber A, Kiss B, Houtkooper RH, Schoonjans K, Schreiber V, Sauve AA, Menissier-de Murcia J, Auwerx J. 2011. PARP-1 Inhibition Increases Mitochondrial Metabolism through SIRT1 Activation. Cell Metab 13:461–468.

57. Yang H, Yang T, Baur JA, Perez E, Matsui T, Carmona JJ, Lamming DW, Souza-Pinto NC, Bohr VA, Rosenzweig A, Cabo R de, Sauve AA, Sinclair DA. 2007. Nutrient-Sensitive Mitochondrial NAD+ Levels Dictate Cell Survival. Cell 130:1095–1107.

58. Hall JA, Dominy JE, Lee Y, Puigserver P. 2013. The sirtuin family's role in aging and age-associated pathologies. J Clin Invest 123:973–979.

59. Ryall JG, Dell'Orso S, Derfoul A, Juan A, Zare H, Feng X, Clermont D, Koulnis M, Gutierrez-Cruz G, Fulco M, Sartorelli V. 2015. The NAD+-Dependent SIRT1 Deacetylase Translates a Metabolic Switch into Regulatory Epigenetics in Skeletal Muscle Stem Cells. Cell Stem Cell 16:171–183.

60. D'Amours D, Desnoyers S, D'Silva I, Poirier GG. 1999. Poly(ADP-ribosyl)ation reactions in the regulation of nuclear functions. Biochem J 342:249–268.

61. Chang P, Jacobson MK, Mitchison TJ. 2004. Poly(ADP-ribose) is required for spindle assembly and structure. Nature 432:645–649.

62. Shall S, Sugimura T. 2006. What is new about ADP-ribosylation? Bioessays 28:97–99.

63. Cook BD, Dynek JN, Chang W, Shostak G, Smith S. 2002. Role for the Related Poly(ADP-Ribose) Polymerases Tankyrase 1 and 2 at Human Telomeres. Mol Cell Biol 22:332–342.

64. Yu S-W, Wang H, Poitras MF, Coombs C, Bowers WJ, Federoff HJ, Poirier GG, Dawson TM, Dawson VL. 2002. Mediation of Poly(ADP-Ribose) Polymerase-1-Dependent Cell Death by Apoptosis-Inducing Factor. Science 297:259–263.

65. Edinger AL, Thompson CB. 2004. Death by design: apoptosis, necrosis and autophagy. Curr Opin Cell Biol 16:663–669.

66. Bouchard VJ, Rouleau M, Poirier GG. 2003. PARP-1, a determinant of cell survival in response to DNA damage. Exp Hematol 31:446–454.

67. Bai P, Cantó C. 2012. The Role of PARP-1 and PARP-2 Enzymes in Metabolic Regulation and Disease. Cell Metab 16:290–295.

68. Bai P, Nagy L, Fodor T, Liaudet L, Pacher P. 2015. Poly(ADP-ribose) polymerases as modulators of mitochondrial activity. Trends Endocrinol Metabolism 26:75–83.

69. Gongol B, Marin T, Peng I-C, Woo B, Martin M, King S, Sun W, Johnson DA, Chien S, Shyy JY-J. 2013. AMPKα2 exerts its anti-inflammatory effects through PARP-1 and Bcl-6. Proc National Acad Sci 110:3161–3166.

70. Kim SH, Lu HF, Alano CC. 2011. Neuronal Sirt3 Protects against Excitotoxic Injury in Mouse Cortical Neuron Culture. Plos One 6:e14731.

71. Aksoy P, White TA, Thompson M, Chini EN. 2006. Regulation of intracellular levels of NAD: A novel role for CD38. Biochem Bioph Res Co 345:1386–1392.

72. Katsyuba E, Romani M, Hofer D, Auwerx J. 2020. NAD+ homeostasis in health and disease. Nat Metabolism 2:9–31.

73. Yaku K, Okabe K, Hikosaka K, Nakagawa T. 2018. NAD Metabolism in Cancer Therapeutics. Frontiers Oncol 8:622.

74. Donmez G, Wang D, Cohen DE, Guarente L. 2010. SIRT1 Suppresses β-Amyloid Production by Activating the α-Secretase Gene ADAM10. Cell 142:494–495.

75. Kaneko S, Wang J, Kaneko M, Yiu G, Hurrell JM, Chitnis T, Khoury SJ, He Z. 2006. Protecting Axonal Degeneration by Increasing Nicotinamide Adenine Dinucleotide Levels in Experimental Autoimmune Encephalomyelitis Models. J Neurosci 26:9794–9804.

76. Qin W, Yang T, Ho L, Zhao Z, Wang J, Chen L, Zhao W, Thiyagarajan M, MacGrogan D, Rodgers JT, Puigserver P, Sadoshima J, Deng H, Pedrini S, Gandy S, Sauve AA, Pasinetti GM. 2006. Neuronal SIRT1 Activation as a Novel Mechanism Underlying the Prevention of Alzheimer Disease Amyloid Neuropathology by Calorie Restriction. J Biol Chem 281:21745–21754.

77. Imai S, Yoshino J. 2013. The importance of NAMPT/NAD/SIRT1 in the systemic regulation of metabolism and ageing. Diabetes Obes Metabolism 15:26–33.

78. Hirschey MD, Shimazu T, Jing E, Grueter CA, Collins AM, Aouizerat B, Stančáková A, Goetzman E, Lam MM, Schwer B, Stevens RD, Muehlbauer MJ, Kakar S, Bass NM, Kuusisto J, Laakso M, Alt FW, Newgard CB, Farese RV, Kahn CR, Verdin E. 2011. SIRT3 Deficiency and Mitochondrial Protein Hyperacetylation Accelerate the Development of the Metabolic Syndrome. Mol Cell 44:177–190.

79. Borradaile N, Pickering J. 2009. NAD+, Sirtuins, and Cardiovascular Disease. Curr Pharm Design 15:110–117.

80. Ryu D, Zhang H, Ropelle ER, Sorrentino V, Mázala DAG, Mouchiroud L, Marshall PL, Campbell MD, Ali AS, Knowels GM, Bellemin S, Iyer SR, Wang X, Gariani K, Sauve AA, Cantó C, Conley KE, Walter L, Lovering RM, Chin ER, Jasmin BJ, Marcinek DJ, Menzies KJ, Auwerx J. 2016. NAD+ repletion improves muscle function in muscular dystrophy and counters global PARylation. Sci Transl Med 8:361ra139-361ra139.

81. Pirinen E, Auranen M, Khan NA, Brilhante V, Urho N, Pessia A, Hakkarainen A, Kuula J, Heinonen U, Schmidt MS, Haimilahti K, Piirilä P, Lundbom N, Taskinen M-R, Brenner C, Velagapudi V, Pietiläinen KH, Suomalainen A. 2020. Niacin Cures Systemic NAD+ Deficiency and Improves Muscle Performance in Adult-Onset Mitochondrial Myopathy. Cell Metab 31:1078-1090.e5.

82. Morigi M, Perico L, Rota C, Longaretti L, Conti S, Rottoli D, Novelli R, Remuzzi G, Benigni A. 2015. Sirtuin 3–dependent mitochondrial dynamic improvements protect against acute kidney injury. J Clin Invest 125:715–726.

83. Heer CD, Sanderson DJ, Voth LS, Alhammad YMO, Schmidt MS, Trammell SAJ, Perlman S, Cohen MS, Fehr AR, Brenner C. 2020. Coronavirus infection and PARP expression dysregulate the NAD metabolome: An actionable component of innate immunity. J Biol Chem 295:17986–17996.

84. Minhas PS, Liu L, Moon PK, Joshi AU, Dove C, Mhatre S, Contrepois K, Wang Q, Lee BA, Coronado M, Bernstein D, Snyder MP, Migaud M, Majeti R, Mochly-Rosen D, Rabinowitz JD, Andreasson KI. 2019. Macrophage de novo NAD+ synthesis specifies immune function in aging and inflammation. Nat Immunol 20:50–63.

85. Mouchiroud L, Houtkooper RH, Moullan N, Katsyuba E, Ryu D, Cantó C, Mottis A, Jo Y-S, Viswanathan M, Schoonjans K, Guarente L, Auwerx J. 2013. The NAD+/Sirtuin Pathway Modulates Longevity through Activation of Mitochondrial UPR and FOXO Signaling. Cell 154:430–441.

86. Zhang H, Ryu D, Wu Y, Gariani K, Wang X, Luan P, D'Amico D, Ropelle ER, Lutolf MP, Aebersold R, Schoonjans K, Menzies KJ, Auwerx J. 2016. NAD^+ repletion improves mitochondrial and stem cell function and enhances life span in mice. Science 352:1436–1443.

87. Lanska DJ. 2012. The Discovery of Niacin, Biotin, and Pantothenic Acid. Ann Nutr Metab 61:246–253.

88. Rajman L, Chwalek K, Sinclair DA. 2018. Therapeutic Potential of NAD-Boosting Molecules: The In Vivo Evidence. Cell Metab 27:529–547.

89. Benyó Z, Gille A, Kero J, Csiky M, Suchánková MC, Nüsing RM, Moers A, Pfeffer K, Offermanns S. 2005. GPR109A (PUMA-G/HM74A) mediates nicotinic acid–induced flushing. J Clin Invest 115:3634–3640.

90. Bitterman KJ, Anderson RM, Cohen HY, Latorre-Esteves M, Sinclair DA. 2002. Inhibition of Silencing and Accelerated Aging by Nicotinamide, a Putative Negative Regulator of Yeast Sir2 and Human SIRT1. J Biol Chem 277:45099–45107.

91. Rolfe HM. 2014. A review of nicotinamide: treatment of skin diseases and potential side effects. J Cosmet Dermatol-us 13:324–328.

92. Conze D, Brenner C, Kruger CL. 2019. Safety and Metabolism of Long-term Administration of NIAGEN (Nicotinamide Riboside Chloride) in a Randomized, Double-Blind, Placebo-controlled Clinical Trial of Healthy Overweight Adults. Sci Rep-uk 9:9772.

93. Dollerup OL, Christensen B, Svart M, Schmidt MS, Sulek K, Ringgaard S, Stødkilde-Jørgensen H, Møller N, Brenner C, Treebak JT, Jessen N. 2018. A randomized placebo-controlled clinical trial of nicotinamide riboside in obese men: safety, insulin-sensitivity, and lipid-mobilizing effects. Am J Clin Nutrition 108:343–353.

94. Martens CR, Denman BA, Mazzo MR, Armstrong ML, Reisdorph N, McQueen MB, Chonchol M, Seals DR. 2018. Chronic nicotinamide riboside supplementation is well-tolerated and elevates NAD+ in healthy middle-aged and older adults. Nat Commun 9:1286.

95. Simic P, Parada XFV, Parikh SM, Dellinger R, Guarente LP, Rhee EP. 2020. Nicotinamide riboside with pterostilbene (NRPT) increases NAD+ in patients with acute kidney injury (AKI): a randomized, double-blind, placebo-controlled, stepwise safety study of escalating doses of NRPT in patients with AKI. Bmc Nephrol 21:342.

96. Vannini N, Campos V, Girotra M, Trachsel V, Rojas-Sutterlin S, Tratwal J, Ragusa S, Stefanidis E, Ryu D, Rainer PY, Nikitin G, Giger S, Li TY, Semilietof A, Oggier A, Yersin Y, Tauzin L, Pirinen E, Cheng W-C, Ratajczak J, Canto C, Ehrbar M, Sizzano F, Petrova TV, Vanhecke D, Zhang L, Romero P, Nahimana A, Cherix S, Duchosal MA, Ho P-C, Deplancke B, Coukos G, Auwerx J, Lutolf MP, Naveiras O. 2019. The NAD-Booster Nicotinamide Riboside Potently Stimulates Hematopoiesis through Increased Mitochondrial Clearance. Cell Stem Cell 24:405-418.e7.

97. Yoshino M, Yoshino J, Kayser BD, Patti GJ, Franczyk MP, Mills KF, Sindelar M, Pietka T, Patterson BW, Imai S-I, Klein S. 2021. Nicotinamide mononucleotide increases muscle insulin sensitivity in prediabetic women. Science 372:1224–1229.

98. Huang H. 2022. A Multicentre, Randomised, Double Blind, Parallel Design, Placebo Controlled Study to Evaluate the Efficacy and Safety of Uthever (NMN Supplement), an Orally Administered Supplementation in Middle Aged and Older Adults. Frontiers Aging 3:851698.

99. 2015. ClinicalTrials.gov: ClinicalTrials.gov https://doi.org/10.18810/clinical-trials-gov.

100. Remie CME, Roumans KHM, Moonen MPB, Connell NJ, Havekes B, Mevenkamp J, Lindeboom L, de Wit VHW, van de Weijer T, Aarts SABM, Lutgens E, Schomakers BV, Elfrink HL, Zapata-Pérez R, Houtkooper RH, Auwerx J, Hoeks J, Schrauwen-Hinderling VB, Phielix E, Schrauwen P. 2020. Nicotinamide riboside supplementation alters body composition and skeletal muscle acetylcarnitine concentrations in healthy obese humans. Am J Clin Nutrition 112:413–426.

101. Nascimento EBM, Moonen MPB, Remie CME, Gariani K, Jörgensen JA, Schaart G, Hoeks J, Auwerx J, Lichtenbelt WD van M, Schrauwen P. 2021. Nicotinamide riboside enhances in vitro beta-adrenergic brown adipose tissue activity in humans. J Clin Endocrinol Metabolism https://doi.org/10.1210/clinem/dgaa960.

102. Giroud-Gerbetant J, Joffraud M, Giner MP, Cercillieux A, Bartova S, Makarov MV, Zapata-Pérez R, Sánchez-García JL, Houtkooper RH, Migaud ME, Moco S, Canto C. 2019. A Reduced Form of Nicotinamide Riboside Defines a New Path for NAD+ Biosynthesis and Acts as an Orally Bioavailable NAD+ Precursor. Mol Metab 30:192–202.

103. Gariani K, Ryu D, Menzies KJ, Yi H-S, Stein S, Zhang H, Perino A, Lemos V, Katsyuba E, Jha P, Vijgen S, Rubbia-Brandt L, Kim YK, Kim JT, Kim KS, Shong M, Schoonjans K, Auwerx J. 2017. Inhibiting poly ADP-ribosylation increases fatty acid oxidation and protects against fatty liver disease. J Hepatol 66:132–141.

104. Pirinen E, Cantó C, Jo YS, Morato L, Zhang H, Menzies KJ, Williams EG, Mouchiroud L, Moullan N, Hagberg C, Li W, Timmers S, Imhof R, Verbeek J, Pujol A, van Loon B, Viscomi C, Zeviani M, Schrauwen P, Sauve AA, Schoonjans K, Auwerx J. 2014. Pharmacological Inhibition of Poly(ADP-Ribose) Polymerases Improves Fitness and Mitochondrial Function in Skeletal Muscle. Cell Metab 19:1034–1041.

105. Kaye SB, Lubinski J, Matulonis U, Ang JE, Gourley C, Karlan BY, Amnon A, Bell-McGuinn KM, Chen L-M, Friedlander M, Safra T, Vergote I, Wickens M, Lowe ES, Carmichael J, Kaufman B. 2011. Phase II, Open-Label, Randomized, Multicenter Study Comparing the Efficacy and Safety of Olaparib, a Poly (ADP-Ribose) Polymerase Inhibitor, and Pegylated Liposomal Doxorubicin in Patients With BRCA1 or BRCA2 Mutations and Recurrent Ovarian Cancer. J Clin Oncol 30:372–379.

106. Kristeleit R, Swisher E, Oza A, Coleman RL, Scott C, Konecny G, Tinker A, O'Malley DM, Brenton J, Bell-McGuinn K, Oaknin A, Leary A, Lin KK, Raponi M, Giordano H, Maloney L, Goble S, Yelensky R, McNeish I. 2015. 2700 Final results of ARIEL2 (Part 1): A phase 2 trial to prospectively identify ovarian cancer (OC) responders to rucaparib using tumor genetic analysis. Eur J Cancer 51:S531–S533.

107. Sandhu SK, Schelman WR, Wilding G, Moreno V, Baird RD, Miranda S, Hylands L, Riisnaes R, Forster M, Omlin A, Kreischer N, Thway K, Gevensleben H, Sun L, Loughney J, Chatterjee M, Toniatti C, Carpenter CL, Iannone R, Kaye SB, Bono JS de, Wenham RM. 2013. The poly(ADP-ribose) polymerase inhibitor niraparib (MK4827) in BRCA mutation carriers and patients with sporadic cancer: a phase 1 dose-escalation trial. Lancet Oncol 14:882–892.

108. Puhalla S, Beumer JH, Pahuja S, Appleman LJ, Tawbi HA-H, Stoller RG, Lee JJ, Lin Y, Kiesel B, Yu J, Tan AR, Belani CP, Chew HK, Garcia AA, Morgan R, Giranda VL, Shepherd SP, Chen AP, Chu E. 2014. Final results of a phase 1 study of single-agent veliparib (V) in patients (pts) with either BRCA1/2-mutated cancer (BRCA+), platinum-refractory ovarian, or basal-like breast cancer (BRCA-wt). J Clin Oncol 32:2570–2570.

109. Almeida GS, Bawn CM, Galler M, Wilson I, Thomas HD, Kyle S, Curtin NJ, Newell DR, Maxwell RJ. 2017. PARP inhibitor rucaparib induces changes in NAD levels in cells and liver tissues as assessed by MRS. Nmr Biomed 30:e3736.

110. Fong PC, Yap TA, Boss DS, Carden CP, Mergui-Roelvink M, Gourley C, Greve JD, Lubinski J, Shanley S, Messiou C, A'Hern R, Tutt A, Ashworth A, Stone J, Carmichael J, Schellens JHM, Bono JS de, Kaye SB. 2010. Poly(ADP)-Ribose Polymerase Inhibition: Frequent Durable Responses in BRCA Carrier Ovarian Cancer Correlating With Platinum-Free Interval. J Clin Oncol 28:2512–2519.

111. Wainberg Z, Rafii S, Ramanathan R, Mina L, Byers LA, Chugh R, Goldman JW, Sachdev J, Matei D, Wheler J, Henshaw J, Zhang C, Gallant G, Bono JD. 2014. Safety and antitumor activity of the PARP inhibitor BMN673 in a phase 1 trial recruiting metastatic small-cell lung cancer (SCLC) and germline BRCA-mutation carrier cancer patients. https://meetinglibrary.asco.org/record/94898/abstract. Retrieved 1 December 2021.

112. Wang G, Han T, Nijhawan D, Theodoropoulos P, Naidoo J, Yadavalli S, Mirzaei H, Pieper AA, Ready JM, McKnight SL. 2014. P7C3 neuroprotective chemicals function by activating the rate-limiting enzyme in NAD salvage. Cell 158:1324–34.

113. Blaya MO, Wasserman JM, Pieper AA, Sick TJ, Bramlett HM, Dietrich WD. 2018. Neurotherapeutic Capacity of P7C3 Agents for the Treatment of Traumatic Brain Injury. Neuropharmacology 145:268–282.

114. Gardell SJ, Hopf M, Khan A, Dispagna M, Sessions EH, Falter R, Kapoor N, Brooks J, Culver J, Petucci C, Ma C-T, Cohen SE, Tanaka J, Burgos ES, Hirschi JS, Smith SR, Sergienko E, Pinkerton AB. 2019. Boosting NAD+ with a small molecule that activates NAMPT. Nat Commun 10:3241.

115. Camacho-Pereira J, Tarragó MG, Chini CCS, Nin V, Escande C, Warner GM, Puranik AS, Schoon RA, Reid JM, Galina A, Chini EN. 2016. CD38 Dictates Age-Related NAD Decline and Mitochondrial Dysfunction through an SIRT3-Dependent Mechanism. Cell Metab 23:1127–1139.

116. Barbosa MTP, Soares SM, Novak CM, Sinclair D, Levine JA, Aksoy P, Chini EN. 2007. The enzyme CD38 (a NAD glycohydrolase, EC 3.2.2.5) is necessary for the development of diet-induced obesity. Faseb J 21:3629–3639.

117. Kwong AKY, Chen Z, Zhang H, Leung FP, Lam CMC, Ting KY, Zhang L, Hao Q, Zhang L-H, Lee HC. 2012. Catalysis-Based Inhibitors of the Calcium Signaling Function of CD38. Biochemistry-us 51:555–564.

118. Boslett J, Hemann C, Zhao YJ, Lee H-C, Zweier JL. 2017. Luteolinidin protects the post-ischemic heart through CD38 inhibition with preservation of NAD(P)(H). J Pharmacol Exp Ther 361:jpet.116.239459.

119. Handler P. 1957. Methods in enzymology. Vol. III Edited by S. P. Colowick and N. O. Kaplan, McCollum-Pratt Institute, The Johns Hopkins University, Baltimore, Maryland. Academic Press Inc., New York, New York, 1957. 1154 pp. Price $26.00. Arch Biochem Biophys 70:632.

120. Rost FWD. 1995. Fluorescence Microscopy vol II. Cambridge University Press, New york, NY.

121. Colowick SP, Kaplan NO, Ciotti MO. 1951. The reaction of pyridine nucleotide with cyanide and its analytical use. J Biol Chem.

122. Jacobson KB, Astrachan L. 1957. Specific methods for the microdetermination of pyridine nucleotides and pyridine nucleotide enzymes. Arch Biochem Biophys 71:69–80.

123. Jacobson KB, Kaplan NO. 1957. Pyridine coenzymes of subcellular tissue fractions. J Biol Chem 226:603–613.

124. Kaplan NO, Colowick SP, Barnes CC. 1951. Effect of alkali on diphosphopyridine nucleotide. J Biol Chem 191:461–72.

125. Lowry OH, Roberts NR, Kapphahn JI. 1957. The fluorometric measurement of pyridine nucleotides. J Biol Chem 224:1047–1064.

126. Pande SV, Bhan AK, Venkitasubramanian TA. 1964. Fluorometric determination of tissue pyridine nucleotides. Anal Biochem 8:446–462.

127. Cartier PH. 1968. Dosage des pyridine nucléotides oxydés et réduits dans le sang et les tissus animaux. Eur J Biochem 4:247–255.

128. Minton AP. 2001. The Influence of Macromolecular Crowding and Macromolecular Confinement on Biochemical Reactions in Physiological Media. J Biol Chem 276:10577–10580.

129. Karp MT, Raunio RP, Lövgren TN-E. 1983. Simultaneous extraction and combined bioluminescent assay of NAD+ and NADH. Anal Biochem 128:175–180.

130. Sahlin K. 1983. NADH and NADPH in human skeletal muscle at rest and during ischaemia. Clin Physiol 3:477–485.

131. Bessho M, Tajima T, Hori S, Satoh T, Fukuda K, Kyotani S, Ohnishi Y, Nakamura Y. 1989. NAD and NADH values in rapidly sampled dog heart tissues by two different extraction methods. Anal Biochem 182:304–308.

132. Wallace KB. 1983. Hepatic redox homeostasis following acute adriamycin intoxication in rats. Biochem Pharmacol 32:2577–2582.

133. Wendt MMN, De Oliveira MC, Franco-Salla GB, Castro LS, Parizotto ÂV, Silva FMS, Natali MRM, Bersani-Amado CA, Bracht A, Comar JF. 2019. Fatty acids uptake and oxidation are increased in the liver of rats with adjuvant-induced arthritis. Biochimica Et Biophysica Acta Bba - Mol Basis Dis 1865:696–707.

134. Klaidman LK, Mukherjee SK, Adams JD. 2001. Oxidative changes in brain pyridine nucleotides and neuroprotection using nicotinamide. Biochimica Et Biophysica Acta Bba - Gen Subj 1525:136–148.

135. Breen LT, Smyth LM, Yamboliev IA, Mutafova-Yambolieva VN. 2006. β-NAD is a novel nucleotide released on stimulation of nerve terminals in human urinary bladder detrusor muscle. Am J Physiol-renal 290:F486–F495.

136. Yoon MJ, Yoshida M, Johnson S, Takikawa A, Usui I, Tobe K, Nakagawa T, Yoshino J, Imai S. 2015. SIRT1-Mediated eNAMPT Secretion from Adipose Tissue Regulates Hypothalamic NAD+ and Function in Mice. Cell Metab 21:706–717.

137. Shipkova P, Reily MD. 2013. Mass Spectrometry for Drug Discovery and Drug Development 387–401.

138. Wilkie DR, Dawson MJ, Edwards RHT, Gordon RE, Shaw D. 1984. Contractile Mechanisms in Muscle: 31P NMR Studies of Resting Muscle in Normal Human Subjects., p. 333–347. *In* . Springer, Boston, MA.

139. Verpoorte R, Choi YH, Mustafa NR, Kim HK. 2008. Metabolomics: back to basics. Phytochem Rev 7:525–537.

140. Lei Z, Huhman DV, Sumner LW. 2011. Mass Spectrometry Strategies in Metabolomics. J Biol Chem 286:25435–25442.

141. Trammell SA, Brenner C. 2013. Targeted, LCMS-based metabolomics for quantitative measurement of NAD+ metabolites. Comput Struct Biotechnology J 4:1–9.

142. Braidy N, Villalva MD, Grant R. 2021. NADomics: Measuring NAD+ and Related Metabolites Using Liquid Chromatography Mass Spectrometry. Life 11:512.

143. Hassa PO, Haenni SS, Elser M, Hottiger MO. 2006. Nuclear ADP-Ribosylation Reactions in Mammalian Cells: Where Are We Today and Where Are We Going? Microbiol Mol Biol R 70:789–829.

144. Takasawa S, Nata K, Yonekura H, Okamoto H. 1993. Cyclic ADP-ribose in insulin secretion from pancreatic beta cells. Science 259:370–373.

145. Wolf IMA, Diercks B-P, Gattkowski E, Czarniak F, Kempski J, Werner R, Schetelig D, Mittrücker H-W, Schumacher V, Osten M von, Lodygin D, Flügel A, Fliegert R, Guse AH. 2015. Frontrunners of T cell activation: Initial, localized Ca2+ signals mediated by NAADP and the type 1 ryanodine receptor. Sci Signal 8:ra102–ra102.

146. Gasser A, Bruhn S, Guse AH. 2006. Second Messenger Function of Nicotinic Acid Adenine Dinucleotide Phosphate Revealed by an Improved Enzymatic Cycling Assay*. J Biol Chem 281:16906–16913.

147. Kulkarni CA, Brookes PS. 2019. Cellular Compartmentation and the Redox/Nonredox Functions of NAD+. Antioxid Redox Sign 31:623–642.

148. McGuinness ET, Butler JR. 1985. NAD+ kinase—A review. Int J Biochem 17:1–11.

149. Cantó C, Menzies KJ, Auwerx J. 2015. NAD+ Metabolism and the Control of Energy Homeostasis: A Balancing Act between Mitochondria and the Nucleus. Cell Metab 22:31–53.

150. Kulikova VA, Gromyko DV, Nikiforov AA. 2018. The Regulatory Role of NAD in Human and Animal Cells. Biochem Mosc 83:800–812.

151. Oxenkrug G. 2013. Insulin Resistance and Dysregulation of Tryptophan–Kynurenine and Kynurenine–Nicotinamide Adenine Dinucleotide Metabolic Pathways. Mol Neurobiol 48:294–301.

152. Zhou C, Yang X, Hua X, Liu J, Fan M, Li G, Song J, Xu T, Li Z, Guan Y, Wang P, Miao C. 2016. Hepatic NAD+ deficiency as a therapeutic target for non-alcoholic fatty liver disease in ageing. Brit J Pharmacol 173:2352–2368.

153. Gregorio E de, Colell A, Morales A, Marí M. 2020. Relevance of SIRT1-NF-κB Axis as Therapeutic Target to Ameliorate Inflammation in Liver Disease. Int J Mol Sci 21:3858.

154. Verdin E. 2015. NAD+ in aging, metabolism, and neurodegeneration. Science 350:1208–1213.

155. Roggenkamp HG, Khansahib I, C. LCH, Zhang Y, Lodygin D, Krüger A, Gu F, Möckl F, Löhndorf A, Wolters V, Woike D, Rosche A, Bauche A, Schetelig D, Werner R, Schlüter H, Failla AV, Meier C, Fliegert R, Walseth TF, Flügel A, Diercks B-P, Guse AH. 2021. HN1L/JPT2: A signaling protein that connects NAADP generation to Ca2+ microdomain formation. Sci Signal 14:eabd5647.

156. Carrey EA, Smolenski RT, Edbury SM, Laurence A, Marinaki AM, Duley JA, Zhu L, Goldsmith DJA, Simmonds HA. 2003. Origin and characteristics of an unusual pyridine nucleotide accumulating in erythrocytes: positive correlation with degree of renal failure. Clin Chim Acta 335:117–129.

157. Rekharsky MV, Egorov AM, Gal'chenko GL, Berezin IV. 1981. Thermodynamics of redox reactions involving nicotinamide adenine dinucleotide. Thermochim Acta 46:89–101.

158. Rover L, Fernandes JCB, Neto G de O, Kubota LT, Katekawa E, Serrano SHP. 1998. Study of NADH Stability Using Ultraviolet–Visible Spectrophotometric Analysis and Factorial Design. Anal Biochem 260:50–55.

159. Lu W, Wang L, Chen L, Hui S, Rabinowitz JD. 2018. Extraction and Quantitation of Nicotinamide Adenine Dinucleotide Redox Cofactors. Antioxid Redox Sign 28:167–179.

160. Shabalin K, Nerinovski K, Yakimov A, Kulikova V, Svetlova M, Solovjeva L, Khodorkovskiy M, Gambaryan S, Cunningham R, Migaud ME, Ziegler M, Nikiforov A. 2018. NAD Metabolome Analysis in Human Cells Using 1H NMR Spectroscopy. Int J Mol Sci 19:3906.

161. Rohatgi. 2021. Webplotdigitizer: Version 4.5. https://automeris.io/WebPlotDigitizer. Retrieved 2021.

162. Lowry O, Passonneau J, Schulz D, Rock M. 1961. The Measurement of Pyridine Nucleotides by Enzymatic Cycling. J Biol Chem 236:2746–2755.

163. Wu JT, Wu LH, Knight JA. 2020. Stability of NADPH: effect of various factors on the kinetics of degradation. Clin Chem 32:314–319.

164. Lowry OH, Passonneau JV, Rock MK. 1961. The Stability of Pyridine Nucleotides. J Biol Chem 236:2756–2759.

165. Frederick DW, Trefely S, Buas A, Goodspeed J, Singh J, Mesaros C, Baur JA, Snyder NW. 2017. Stable isotope labeling by essential nutrients in cell culture (SILEC) for accurate measurement of nicotinamide adenine dinucleotide metabolism. Analyst 142:4431–4437.

166. Yaku K, Okabe K, Nakagawa T. 2018. Simultaneous measurement of NAD metabolome in aged mice tissue using liquid chromatography tandem-mass spectrometry. Biomed Chromatogr 32:e4205.

167. Dall M, Trammell SAJ, Asping M, Hassing AS, Agerholm M, Vienberg SG, Gillum MP, Larsen S, Treebak JT. 2019. Mitochondrial function in liver cells is resistant to perturbations in NAD+ salvage capacity. J Biol Chem 294:13304–13326.

168. Sambeat A, Ratajczak J, Joffraud M, Sanchez-Garcia JL, Giner MP, Valsesia A, Giroud-Gerbetant J, Valera-Alberni M, Cercillieux A, Boutant M, Kulkarni SS, Moco S, Canto C. 2019. Endogenous nicotinamide riboside metabolism protects against diet-induced liver damage. Nat Commun 10:4291.

169. Liang X, Yang L, Qin AR, Ly J, Liederer BM, Messick K, Ma S, Zak M, Dragovich PS, Dean BJ, Hop CECA, Deng Y. 2014. Measuring NAD(+) levels in mouse blood and tissue samples via a surrogate matrix approach using LC-MS/MS. Bioanalysis 6:1445–57.

170. Toye AA, Lippiat JD, Proks P, Shimomura K, Bentley L, Hugill A, Mijat V, Goldsworthy M, Moir L, Haynes A, Quarterman J, Freeman HC, Ashcroft FM, Cox RD. 2005. A genetic and physiological study of impaired glucose homeostasis control in C57BL/6J mice. Diabetologia 48:675–686.

171. Mitchell SJ, Madrigal-Matute J, Scheibye-Knudsen M, Fang E, Aon M, González-Reyes JA, Cortassa S, Kaushik S, Gonzalez-Freire M, Patel B, Wahl D, Ali A, Calvo-Rubio M, Burón MI, Guiterrez V, Ward TM, Palacios HH, Cai H, Frederick DW, Hine C, Broeskamp F, Habering L, Dawson J, Beasley TM, Wan

J, Ikeno Y, Hubbard G, Becker KG, Zhang Y, Bohr VA, Longo DL, Navas P, Ferrucci L, Sinclair DA, Cohen P, Egan JM, Mitchell JR, Baur JA, Allison DB, Anson RM, Villalba JM, Madeo F, Cuervo AM, Pearson KJ, Ingram DK, Bernier M, Cabo R de. 2016. Effects of Sex, Strain, and Energy Intake on Hallmarks of Aging in Mice. Cell Metab 23:1093–1112.

172. Velpen V, Rosenberg N, Maillard V, Teav T, Chatton J, Gallart-Ayala H, Ivanisevic J. 2021. Sex-specific alterations in NAD+ metabolism in 3xTg Alzheimer's disease mouse brain assessed by quantitative targeted LC-MS. J Neurochem https://doi.org/10.1111/jnc.15362.

173. Kim YM, Cha BS, Kim DJ, Choi SH, Kim SK, Ahn CW, Lim S-K, Kim KR, Huh KB, Lee HC. 2005. Predictive clinical parameters for therapeutic efficacy of rosiglitazone in Korean type 2 diabetes mellitus. Diabetes Res Clin Pr 67:43–52.

174. Donnelly LA, Doney ASF, Hattersley AT, Morris AD, Pearson ER. 2006. The effect of obesity on glycaemic response to metformin or sulphonylureas in Type 2 diabetes. Diabet Med 23:128–133.

175. Chen X, McClusky R, Itoh Y, Reue K, Arnold AP. 2013. X and Y Chromosome Complement Influence Adiposity and Metabolism in Mice. Endocrinology 154:1092–1104.

176. Breton M, Costemale-Lacoste J-F, Li Z, Lafuente-Lafuente C, Belmin J, Mericskay M. 2020. Blood NAD levels are reduced in very old patients hospitalized for heart failure. Exp Gerontol 139:111051.

177. Elhassan YS, Kluckova K, Fletcher RS, Schmidt MS, Garten A, Doig CL, Cartwright DM, Oakey L, Burley CV, Jenkinson N, Wilson M, Lucas SJE, Akerman I, Seabright A, Lai Y-C, Tennant DA, Nightingale P, Wallis GA, Manolopoulos KN, Brenner C, Philp A, Lavery GG. 2019. Nicotinamide Riboside Augments the Aged Human Skeletal Muscle NAD+ Metabolome and Induces Transcriptomic and Anti-inflammatory Signatures. Cell Reports 28:1717-1728.e6.

178. Zhou B, Wang DD, Qiu Y, Airhart S, Liu Y, Stempien-Otero A, O'Brien KD, Tian. R. 2020. Boosting NAD Level Suppresses Inflammatory Activation of PBMC in Heart Failure. J Clin Invest 130:6054–6063.

179. Dóra E. 1985. Effect of "flow anoxia" and "non flow anoxia" on the NAD/NADH redox state of the intact brain cortex of the cat. Pflügers Archiv 405:148–154.

180. Piavchenko G, Kozlov I, Dremin V, Stavtsev D, Seryogina E, Kandurova K, Shupletsov V, Lapin K, Alekseyev A, Kuznetsov S, Bykov A, Dunaev A, Meglinski I. 2021. Impairments of cerebral blood flow microcirculation in rats brought on by cardiac cessation and respiratory arrest. J Biophotonics 14:e202100216.

181. Park Y, Kehrer JP. 2009. Oxidative Changes in Hypoxic-Reoxygenated Rabbit Heart: A Consequence of Hypoxia Rather Than Reoxygenation. Free Radical Res Com 14:179–185.

182. Oldham WM, Clish CB, Yang Y, Loscalzo J. 2015. Hypoxia-Mediated Increases in l-2-hydroxyglutarate Coordinate the Metabolic Response to Reductive Stress. Cell Metab 22:291–303.

183. Yurkov YuA, Safonova TYa. 1976. Effect of hypoxia on nicotinamide coenzyme content in tissues of newborn rats. B Exp Biol Med+ 82:1656–1658.

184. Evans J, Wang T-C, Heyes MP, Markey SP. 2002. LC/MS Analysis of NAD Biosynthesis Using Stable Isotope Pyridine Precursors. Anal Biochem 306:197–203.

185. Aretz I, Meierhofer D. 2016. Advantages and Pitfalls of Mass Spectrometry Based Metabolome Profiling in Systems Biology. Int J Mol Sci 17:632.

186. Yu Q, Pourmandi N, Xue L, Gondrand C, Fabritz S, Bardy D, Patiny L, Katsyuba E, Auwerx J, Johnsson K. 2019. A biosensor for measuring NAD+ levels at the point of care. Nat Metabolism 1:1219–1225.

187. Evans C, Bogan KL, Song P, Burant CF, Kennedy RT, Brenner C. 2010. NAD+ metabolite levels as a function of vitamins and calorie restriction: evidence for different mechanisms of longevity. Bmc Chem Biology 10:2.

188. Bogan KL, Evans C, Belenky P, Song P, Burant CF, Kennedy R, Brenner C. 2009. Identification of Isn1 and Sdt1 as Glucose- and Vitamin-regulated Nicotinamide Mononucleotide and Nicotinic Acid Mononucleotide 5′-Nucleotidases Responsible for Production of Nicotinamide Riboside and Nicotinic Acid Riboside*. J Biol Chem 284:34861–34869.

189. Demarest TG, Truong GTD, Lovett J, Mohanty JG, Mattison JA, Mattson MP, Ferrucci L, Bohr VA, Moaddel R. 2019. Assessment of NAD+metabolism in human cell cultures, erythrocytes, cerebrospinal fluid and primate skeletal muscle. Anal Biochem 572:1–8.

190. Bustamante S, Jayasena T, Richani D, Gilchrist RB, Wu LE, Sinclair DA, Sachdev PS, Braidy N. 2017. Quantifying the cellular NAD+ metabolome using a tandem liquid chromatography mass spectrometry approach. Metabolomics 14:15.

191. Clement J, Wong M, Poljak A, Sachdev P, Braidy N. 2019. The Plasma NAD+ Metabolome Is Dysregulated in "Normal" Aging. Rejuv Res 22:121–130.

192. Koning W de, Dam K van. 1992. A method for the determination of changes of glycolytic metabolites in yeast on a subsecond time scale using extraction at neutral pH. Anal Biochem 204:118–123.

193. Faijes M, Mars AE, Smid EJ. 2007. Comparison of quenching and extraction methodologies for metabolome analysis of Lactobacillus plantarum. Microb Cell Fact 6:27–27.

194. Cequier-Sánchez E, Rodríguez C, Ravelo AG, Zárate R. 2008. Dichloromethane as a Solvent for Lipid Extraction and Assessment of Lipid Classes and Fatty Acids from Samples of Different Natures. J Agr Food Chem 56:4297–4303.

195. Neubauer S, Haberhauer-Troyer C, Klavins K, Russmayer H, Steiger MG, Gasser B, Sauer M, Mattanovich D, Hann S, Koellensperger G. 2012. U 13 C cell extract of Pichia pastoris - a powerful tool for evaluation of sample preparation in metabolomics. J Sep Sci 35:3091–3105.

196. Hofmann D, Wirtz A, Santiago-Schübel B, Disko U, Pohl M. 2010. Structure elucidation of the thermal degradation products of the nucleotide cofactors NADH and NADPH by nano-ESI-FTICR-MS and HPLC-MS. Anal Bioanal Chem 398:2803–2811.

197. Hachisuka S, Sato T, Atomi H. 2017. Metabolism Dealing with Thermal Degradation of NAD + in the Hyperthermophilic Archaeon Thermococcus kodakarensis. J Bacteriol 199.

198. USFDA. 2018. Bioanalytical Method Validation Guidance for Industry. Bioanalytical Method Validation Guidance for Industry. https://www.fda.gov/media/70858/download. Retrieved 4 March 2022.

199. Amsterdam P van, Companjen A, Brudny-Kloeppel M, Golob M, Luedtke S, Timmerman P. 2013. The European Bioanalysis Forum communitys evaluation, interpretation and implementation of the European Medicines Agency guideline on Bioanalytical Method Validation. Bioanalysis 5:645–659.

200. Rampler E, Abiead YE, Schoeny H, Rusz M, Hildebrand F, Fitz V, Koellensperger G. 2021. Recurrent Topics in Mass Spectrometry-Based Metabolomics and Lipidomics□Standardization, Coverage, and Throughput. Anal Chem 93:519–545.

201. Bürkle A. 2001. Physiology and pathophysiology of poly(ADP-ribosyl)ation *. Bioessays 23:795–806.

202. Berthelier V, Tixier J-M, Muller-Steffner H, Schuber F, Deterre P. 1998. Human CD38 is an authentic NAD(P)+ glycohydrolase. Biochem J 330:1383–1390.

203. Lee HC, Aarhus R. 1991. ADP-ribosyl cyclase: an enzyme that cyclizes NAD+ into a calcium-mobilizing metabolite. Cell Regul 2:203–209.

204. Lee HC. 1997. Mechanisms of calcium signaling by cyclic ADP-ribose and NAADP. Physiol Rev 77:1133–1164.

205. Grundy SM, Mok HY, Zech L, Berman M. 1981. Influence of nicotinic acid on metabolism of cholesterol and triglycerides in man 1. J Lipid Res 22:24–36.

206. Majamaa K, Rusanen H, Remes AM, Pyhtinen J, Hassinen IE. 1996. Increase of blood NAD+ and attenuation of lactacidemia during nicotinamide treatment of a patient with the melas syndrome. Life Sci 58:691–699.

207. Nejabati HR, Samadi N, Shahnazi V, Mihanfar A, Fattahi A, Latifi Z, Bahrami-asl Z, Roshangar L, Nouri M. 2020. Nicotinamide and its metabolite N1-Methylnicotinamide alleviate endocrine and metabolic abnormalities in adipose and ovarian tissues in rat model of Polycystic Ovary Syndrome. Chem-biol Interact 324:109093.

208. Yang J, Klaidman LK, Nalbandian A, Oliver J, Chang ML, Chan PH, Adams JD. 2002. The effects of nicotinamide on energy metabolism following transient focal cerebral ischemia in Wistar rats. Neurosci Lett 333:91–94.

209. Dali-Youcef N, Lagouge M, Froelich S, Koehl C, Schoonjans K, Auwerx J. 2009. Sirtuins: The ‘magnificent seven’, function, metabolism and longevity. Ann Med 39:335–345.

210. Hwang ES, Song SB. 2017. Nicotinamide is an inhibitor of SIRT1 in vitro, but can be a stimulator in cells. Cell Mol Life Sci 74:3347–3362.

211. Hoffer A. 1967. Biochemistry of Nicotinic Acid and Nico Tinamide. Psychosomatics 8:95–100.

212. Handler P, Dann WJ. 1942. THE INHIBITION OF RAT GROWTH BY NICOTINAMIDE. J Biol Chem 146:357–368.

213. Winter SL, Boyer JL. 1973. Hepatic Toxicity from Large Doses of Vitamin B3 (Nicotinamide). New Engl J Medicine 289:1180–1182.

214. Airhart SE, Shireman LM, Risler LJ, Anderson GD, Gowda GAN, Raftery D, Tian R, Shen DD, O'Brien KD. 2017. An open-label, non-randomized study of the pharmacokinetics of the nutritional supplement nicotinamide riboside (NR) and its effects on blood NAD+ levels in healthy volunteers. Plos One 12:e0186459.

215. Brakedal B, Dölle C, Riemer F, Ma Y, Nido GS, Skeie GO, Craven AR, Schwarzlmüller T, Brekke N, Diab J, Sverkeli L, Skjeie V, Varhaug K, Tysnes O-B, Peng S, Haugarvoll K, Ziegler M, Grüner R, Eidelberg D, Tzoulis C. 2022. The NADPARK study: A randomized phase I trial of nicotinamide riboside supplementation in Parkinson's disease. Cell Metab 34:396-407.e6.

216. Dollerup OL, Chubanava S, Agerholm M, Søndergård SD, Altıntaş A, Møller AB, Høyer KF, Ringgaard S, Stødkilde-Jørgensen H, Lavery GG, Barrès R, Larsen S, Prats C, Jessen N, Treebak JT. 2020. Nicotinamide riboside does not alter mitochondrial respiration, content or morphology in skeletal muscle from obese and insulin-resistant men. J Physiology 598:731–754.

217. Trammell SAJ, Weidemann BJ, Chadda A, Yorek MS, Holmes A, Coppey LJ, Obrosov A, Kardon RH, Yorek MA, Brenner C. 2016. Nicotinamide Riboside Opposes Type 2 Diabetes and Neuropathy in Mice. Sci Rep-uk 6:26933.

218. Cantó C, Houtkooper RH, Pirinen E, Youn DY, Oosterveer MH, Cen Y, Fernandez-Marcos PJ, Yamamoto H, Andreux PA, Cettour-Rose P, Gademann K, Rinsch C, Schoonjans K, Sauve AA, Auwerx J. 2012. The NAD+ Precursor Nicotinamide Riboside Enhances Oxidative Metabolism and Protects against High-Fat Diet-Induced Obesity. Cell Metab 15:838–847.

219. Gariani K, Menzies KJ, Ryu D, Wegner CJ, Wang X, Ropelle ER, Moullan N, Zhang H, Perino A, Lemos V, Kim B, Park Y, Piersigilli A, Pham TX, Yang Y, Ku CS, Koo SI, Fomitchova A, Cantó C, Schoonjans K, Sauve AA, Lee J, Auwerx J. 2016. Eliciting the mitochondrial unfolded protein response by nicotinamide adenine dinucleotide repletion reverses fatty liver disease in mice. Hepatology 63:1190–1204.

220. Stocks B, Ashcroft SP, Joanisse S, Dansereau LC, Koay YC, Elhassan YS, Lavery GG, Quek L, O'Sullivan JF, Philp AM, Wallis GA, Philp A. 2021. Nicotinamide riboside supplementation does not alter whole-body or skeletal muscle metabolic responses to a single bout of endurance exercise. J Physiology 599:1513–1531.

221. Khan NA, Auranen M, Paetau I, Pirinen E, Euro L, Forsström S, Pasila L, Velagapudi V, Carroll CJ, Auwerx J, Suomalainen A. 2014. Effective treatment of mitochondrial myopathy by nicotinamide riboside, a vitamin B3. Embo Mol Med 6:721–731.

222. Conze D, Crespo-Barreto J, Kruger C. 2016. Safety assessment of nicotinamide riboside, a form of vitamin B3. Hum Exp Toxicol 35:1149–1160.

223. USFDA. 2005. Guidance for Industry: Estimating the Maximum Safe Starting Dose in Adult Healthy Volunteer. Rockville, MD: US Food and Drug Administration; 2005. https://www.fda.gov/regulatory-information/search-fda-guidance-documents/estimating-maximum-safe-starting-dose-initial-clinical-trials-therapeutics-adult-healthy-volunteers. Retrieved 13 January 2023.

224. Nair AB, Jacob S. 2016. A simple practice guide for dose conversion between animals and human. J Basic Clin Pharm 7:27–31.

225. Yoshino J, Mills KF, Yoon MJ, Imai S. 2011. Nicotinamide Mononucleotide, a Key NAD+ Intermediate, Treats the Pathophysiology of Diet- and Age-Induced Diabetes in Mice. Cell Metab 14:528–536.

226. Mudd SH, Poole JR. 1975. Labile methyl balances for normal humans on various dietary regimens. Metabolis 24:721–735.

227. Lu SC, Mato JM. 2012. S-adenosylmethionine in Liver Health, Injury, and Cancer. Physiol Rev 92:1515–1542.

228. Saldeen J, Tillmar L, Karlsson E, Welsh N. 2003. Nicotinamide- and caspase-mediated inhibition of poly(ADP-ribose) polymerase are associated with p53-independent cell cycle (G2) arrest and apoptosis. Mol Cell Biochem 243:113–122.

229. Duce AM, Ortíz P, Cabrero C, Mato JM. 1988. S-adenosyl-L-methionine synthetase and phospholipid methyltransferase are inhibited in human cirrhosis. Hepatology 8:65–68.